MATHEMATICAL ANALYSIS OF ELASTIC BELLOWS WITH WELDED CONSTRAINTS

by

NICHOLAS VASILIOS KOUNTOURAS

A dissertation submitted to the Graduate Faculty in Engineering in partial fulfillment of the requirements for the degree of Doctor of Philosophy, The City University of New York

1974

This manuscript has been read and accepted for the Graduate Faculty in Engineering in satisfaction of the dissertation requirement for the degree of Doctor of Philosophy.

Oct. 16, 1974
date

Robert F. Dressler
Chairman of Examining Committee

Oct 16, 1974
date

Jacques E. Benveniste
Executive Officer

Professor R.F. Dressler, Chairman

Professor N.C. Jen

Professor C.A. Miller

Professor M.L. Pei

Supervisory Committee

The City University of New York

Abstract

MATHEMATICAL ANALYSIS OF ELASTIC BELLOWS

WITH WELDED CONSTRAINTS

by

Nicholas Vasilios Kountouras

Advisor: Professor Robert F. Dressler

A method is formulated which may be applied to the analysis of any precision welded bellows.

The method, which involves the direct solution of the full linear shell equations by numerical integration coupled with a theory of the deformation of axisymmetric tori, is used to make an extensive study of precision welded bellows.

Although the method is applicable to any shape bellows, in order to present quantitative results, we have applied the method to a specific shape consisting of cones and plates. Therefore all graphs and quantitative results presented only apply to this one shape. This specific type of precision welded bellows, presently employed in numerous industrial and scientific applications, is analyzed in detail when subject to an axial force. Some of the salient features of this analysis are summarized as follows:

(1) Solutions for all stresses and displacements are presented for three thickness-diameter-ratios over a 10 to 1 range as well as for various weld radius-thickness-ratios.

(2) The effect of thickness-diameter-ratio variation is discussed with respect to three particular cases: 0.01 ("thick" case), 0.003162 ("medium" case), and 0.001 ("thin" case). Throughout the thickness range analyzed, meridional and circumferential stresses are found to be equally important. Bending and membrane stresses are likewise equally important throughout the range.

(3) The effect of weld radius-thickness-ratio variation is discussed with respect to displacement and peak stress. Through a 0.0 to 1.3 range, displacements decrease, and peak stresses increase slightly with increasing weld radius-thickness-ratio.

(4) A boundary layer effect is exhibited and utilized. In conjunction with this boundary layer effect, the concept of an "interior" layer is developed, and a method developed using both in combination which permits analysis of welded bellows having many (e.g. 30 or 40) layers. Therefore a bellows of any very large number of layers can be analyzed by means of one machine calculation for a single interior layer, plus one machine calculation for the boundary layer effect involving between one and three layers depending upon the bellows' thickness-diameter-ratio.

(5) The flexibility of a precision welded bellows having 34 layers is calculated mathematically and compared with a value obtained experimentally. The theoretical and experimental results are found to be in excellent agreement.

ACKNOWLEDGEMENTS

I wish to express my deepest gratitude to my mentor, Professor Robert F. Dressler for suggesting the topic of research and skillfully guiding me through the completion of the thesis. Professor Dressler's expert guidance, insight, knowledge, and inspiration in all phases of the research and preparation of the thesis are gratefully acknowledged.

For their guidance and constructive comments, I extend heartfelt thanks to the members of my Doctoral Committee: Professors N.C. Jen, S.B. Menkes, C.A. Miller, and M.L. Pei. My sincerest thanks also extend to Professor Frederick V. Pohle of Adelphi University and Dean Jacques E. Benveniste for their constructive comments and illuminating discussions.

I would like to thank Mr. William H. Hall for his assistance in the experimental phase of the thesis. Mr. Hall's assistance at many other critical points in the preparation of the thesis is most gratefully acknowledged.

TABLE OF CONTENTS

Abstract			iv
Acknowledgements			vi
List of Symbols			x
List of Illustrations			xii
Chapter 1	INTRODUCTION		1
	1.1	Review of Work Related to the Analysis of Precision Welded Bellows	5
	1.2	The Present Study of Precision Welded Bellows - Some Salient Features	6
	1.3	Summary	7
Chapter 2	GOVERNING EQUATIONS		9
	2.1	Equations of Equilibrium	11
	2.2	Force-Displacement and Moment-Curvature Relations	12
	2.3	Transformation of the Independent Variable From Shell Angle φ to Arc Length s	13
	2.4	Formulation of Governing Equations for Meridians With a Constant Shell Angle	16
	2.5	Transformation of the Basic Equations Into Dimensionless Form	19
	2.6	Boundary Conditions Without Welds	23
	2.7	Matching Conditions Between Cones and Plates	27
	2.8	Formulation of Matching Conditions Involving Welds at Inner and Outer Diameters	32
	2.9	Modification of Boundary Conditions Due to Welds	35

2.10 Formulation of Boundary Conditions for an "Interior" Layer Without Welds 36

2.11 Formulation of Boundary Conditions for an "Interior" Layer Involving Welds 38

Chapter 3 SOLUTION OF GOVERNING EQUATIONS 39

3.1 Solution by Superposition of Four Independent Pure Initial Value Problem Solutions 40

3.2 Analysis of Welded Bellows With Many Layers and the Problem of Loss in Computational Significance 45

Chapter 4 DISCUSSION OF RESULTS 48

4.1 Discussion of Numerical Error 50

4.2 Discussion of Physical Quantities of Interest for Welded Bellows (β = 1.3) 56

1. Displacements 56

2. Transverse Shear 63

3. Membrane Stresses 73

4. Bending Stresses 83

5. Some Other Quantities of Physical Interest 93

4.3 A Boundary Layer Effect 118

1. Definition of an Interior Layer 118

2. Definition of the Boundary Layer 126

3. The Full Problem Decomposed Into a Pure Interior Problem ("A") and a Pure Edge Problem ("B") 128

4.4 Application of the Interior Layer Concept to the Analysis of Welded Bellows Having Many Layers 139

1. Determination of Stresses 140

2. Determination of Displacements 140

4.5 Experimental Corroboration of the Theoretical Method 141

4.6 Conclusions 146

Bibliography 147

Vita 150

LIST OF SYMBOLS

v	Tangential displacement
w	Normal displacement
V	Horizontal displacement
W	Vertical displacement
k	Meridional curvature
r_1	Meridional radius of curvature
r_2	Perpindicular distance from meridian to axis of symmetry
r	Radial distance from axis of symmetry to any point on the shell
s	Arc length
φ	Shell angle
Y	Applied load (force/area) in tangential direction
Z	Applied load (force/area) in normal direction
N_s	Membrane force per unit length in meridional direction
N_θ	Membrane force per unit length in circumferential direction
M_s	Bending moment per unit length acting on a section perpindicular to a meridian
M_θ	Bending moment per unit length acting on a meridional section
Q	Transverse shear force per unit length acting on a section perpindicular to a meridian
E	Young's modulus
ν	Poisson's ratio
t	Shell thickness
$\mathfrak{Z}$	Actual applied transverse shear force per unit length acting on a section perpindicular to a meridian
β	Ratio of weld radius to shell thickness

d	Outside diameter of bellows measured to the rigid clamp
λ	Scalar multiplier
D	Determinant of the normalized coefficient matrix
n	Number of layers counted from the rigid clamp to the bellows' mid-plane of symmetry
n_c	Critical number of layers
σ_s^e	Membrane stress in the meridional direction
σ_θ^e	Membrane stress in the circumferential direction
σ_s^{o+}	Bending stress in the meridional direction at the shell's bottom face
σ_θ^{o+}	Bending stress in the circumferential direction at the shell's bottom face
σ_s^+	Total stress in the meridional direction at the shell's bottom face
σ_s^-	Total stress in the meridional direction at the shell's top face
σ_θ^+	Total stress in the circumferential direction at the shell's bottom face
σ_θ^-	Total stress in the circumferential direction at the shell's top face
σ_z^+	Normal stress at the shell's bottom face
σ_z^-	Normal stress at the shell's top face
δ	Boundary layer thickness
n^*	Number of layers contained within the boundary layer

LIST OF ILLUSTRATIONS

Figure No.		Page
1.1	Cross-sectional View of a Welded Bellows With Twelve Layers	4
2.1	Typical Rotationally Symmetric Shell Element	10
2.2	Arbitrary Meridian	10
2.3a	Even Numbered Layer at Bellows' Mid-plane of Symmetry	26
2.3b	Odd Numbered Layer at Bellows' Mid-plane of Symmetry	26
2.4	Components of Displacement at an Arbitrary Juncture Between Shell Elements	26
2.5a	Cross-sectional View of Forces Acting on an Arbitrary Triangular Torus	29
2.5b	Cross-sectional View of Moments Acting on an Arbitrary Triangular Torus	29
2.6a	"Overlapping" Shell Model	30
2.6b	Characteristic Dimensions of a Triangular Torus	30
2.7a	Membrane Forces Acting on an Inner and Outer Weld	30
2.7b	Moments Acting on an Inner and Outer Weld	30
4.1	Dimensionless Geometry of a Single Layer	50
4.2a	Absolute Value of the Determinant of the Normalized Coefficient Matrix Versus the Number of Layers From the Rigid Clamp to the Mid-plane of Symmetry; Magnitude of the Per Cent Error in the Final Value of Transverse Shear Versus the Number of Layers From the Rigid Clamp to the Mid-plane of Symmetry	53

4.2b	Condition Number of Coefficient Matrix Based Upon the One Norm Versus the Number of Layers From the Rigid Clamp to the Mid-plane of Symmetry	54
4.3	Critical Number of Layers Versus Thickness-Diameter-Ratio	55
4.4a	Tangential Displacement Versus Radius - Thick Case	57
4.4b	Tangential Displacement Versus Radius - Medium Case	58
4.4c	Tangential Displacement Versus Radius - Thin Case	59
4.5a	Normal Displacement Versus Radius - Thick Case	60
4.5b	Normal Displacement Versus Radius - Medium Case	61
4.5c	Normal Displacement Versus Radius - Thin Case	62
4.6a	Horizontal Displacement Versus Radius - Thick Case	64
4.6b	Horizontal Displacement Versus Radius - Medium Case	65
4.6c	Horizontal Displacement Versus Radius - Thin Case	66
4.7a	Vertical Displacement Versus Radius - Thick Case	67
4.7b	Vertical Displacement Versus Radius - Medium Case	68
4.7c	Vertical Displacement Versus Radius - Thin Case	69
4.8a	Transverse Shear Versus Radius - Thick Case	70
4.8b	Transverse Shear Versus Radius - Medium Case	71
4.8c	Transverse Shear Versus Radius - Thin Case	72

4.9a	Meridional Membrane Stress Versus Radius - Thick Case	74
4.9b	Meridional Membrane Stress Versus Radius - Medium Case	75
4.9c	Meridional Membrane Stress Versus Radius - Thin Case	76
4.10a	Circumferential Membrane Stress Versus Radius - Thick Case	77
4.10b	Circumferential Membrane Stress Versus Radius - Medium Case	78
4.10c	Circumferential Membrane Stress Versus Radius - Thin Case	79
4.11a	Magnitude of Peak Meridional Membrane Stress Versus Thickness-Diameter-Ratio	80
4.11b	Magnitude of Peak Circumferential Membrane Stress Versus Thickness-Diameter-Ratio	81
4.12a	Top and Bottom Faces of an Odd Numbered Layer	82
4.12b	Top and Bottom Faces of an Even Numbered Layer	82
4.13a	Meridional Bending Stress at Bottom Face Versus Radius - Thick Case	85
4.13b	Meridional Bending Stress at Bottom Face Versus Radius - Medium Case	86
4.13c	Meridional Bending Stress at Bottom Face Versus Radius - Thin Case	87
4.14a	Circumferential Bending Stress at Bottom Face Versus Radius - Thick Case	88
4.14b	Circumferential Bending Stress at Bottom Face Versus Radius - Medium Case	89
4.14c	Circumferential Bending Stress at Bottom Face Versus Radius - Thin Case	90

4.15a	Magnitude of Peak Meridional Bending Stress at Bottom Face Versus Thickness-Diameter-Ratio	91
4.15b	Magnitude of Peak Circumferential Bending Stress at Bottom Face Versus Thickness-Diameter-Ratio	92
4.16a	Total Meridional Stress at Bottom Face Versus Radius - Thick Case	95
4.16b	Total Meridional Stress at Bottom Face Versus Radius - Medium Case	96
4.16c	Total Meridional Stress at Bottom Face Versus Radius - Thin Case	97
4.17a	Total Meridional Stress at Top Face Versus Radius - Thick Case	98
4.17b	Total Meridional Stress at Top Face Versus Radius - Medium Case	99
4.17c	Total Meridional Stress at Top Face Versus Radius - Thin Case	100
4.18a	Total Circumferential Stress at Bottom Face Versus Radius - Thick Case	101
4.18b	Total Circumferential Stress at Bottom Face Versus Radius - Medium Case	102
4.18c	Total Circumferential Stress at Bottom Face Versus Radius - Thin Case	103
4.19a	Total Circumferential Stress at Top Face Versus Radius - Thick Case	104
4.19b	Total Circumferential Stress at Top Face Versus Radius - Medium Case	105
4.19c	Total Circumferential Stress at Top Face Versus Radius - Thin Case	106
4.20a	Magnitude of Peak Total Meridional Stress Versus Thickness-Diameter-Ratio	107
4.20b	Magnitude of Peak Total Circumferential Stress Versus Thickness-Diameter-Ratio	108

4.21a	Absolute Value of Largest Possible Shearing Stress at Bottom Face Versus Radius - Thick Case	110
4.21b	Absolute Value of Largest Possible Shearing Stress at Bottom Face Versus Radius - Medium Case	111
4.21c	Absolute Value of Largest Possible Shearing Stress at Bottom Face Versus Radius - Thin Case	112
4.22a	Absolute Value of Largest Possible Shearing Stress at Top Face Versus Radius - Thick Case	113
4.22b	Absolute Value of Largest Possible Shearing Stress at Top Face Versus Radius - Medium Case	114
4.22c	Absolute Value of Largest Possible Shearing Stress at Top Face Versus Radius - Thin Case	115
4.23a	Peak Value of Largest Possible Shearing Stress at Bottom Face Versus Thickness-Diameter-Ratio	116
4.23b	Peak Value of Largest Possible Shearing Stress at Top Face Versus Thickness-Diameter-Ratio	117
4.24	Ratio of Peak Stress to Maximum Vertical Deflection Versus Thickness-Diameter-Ratio	119
4.25a	Vertical Deflection of an Interior Layer Versus Radius - Thick Case	120
4.25b	Vertical Deflection of an Interior Layer Versus Radius - Medium Case	121
4.25c	Vertical Deflection of an Interior Layer Versus Radius - Thin Case	122
4.26a	Relative Vertical Deflection of Each Layer Versus Radius - Thick Case	123
4.26b	Relative Vertical Deflection of Each Layer Versus Radius - Medium Case	124
4.26c	Relative Vertical Deflection of Each Layer Versus Radius - Thin Case	125

4.27a	Ratio of Peak Meridional Bending Stress to Peak Meridional Membrane Stress in the Clamped Layer Versus Thickness-Diameter-Ratio; Ratio of Peak Meridional Bending Moment to Peak Meridional Membrane Force in the Clamped Layer Versus Thickness-Diameter-Ratio	129
4.27b	Ratio of Peak Meridional Bending Stress to Peak Meridional Membrane Stress in an Interior Layer Versus Thickness-Diameter-Ratio; Ratio of Peak Meridional Bending Moment to Peak Meridional Membrane Force in an Interior Layer Versus Thickness-Diameter-Ratio	130
4.27c	Ratio of Peak Circumferential Bending Stress to Peak Circumferential Membrane Stress in the Clamped Layer Versus Thickness-Diameter-Ratio; Ratio of Peak Circumferential Bending Moment to Peak Circumferential Membrane Force in the Clamped Layer Versus Thickness-Diameter-Ratio	131
4.27d	Ratio of Peak Circumferential Bending Stress to Peak Circumferential Membrane Stress in an Interior Layer Versus Thickness-Diameter-Ratio; Ratio of Peak Circumferential Bending Moment to Peak Circumferential Membrane Force in an Interior Layer Versus Thickness-Diameter-Ratio	132
4.28a	Relative Vertical Deflection of Each Layer Versus Arc Length - Thick Case	135
4.28b	Relative Vertical Deflection of Each Layer Versus Arc Length - Medium Case	136
4.28c	Relative Vertical Deflection of Each Layer Versus Arc Length - Thin Case	137
4.29	Arc Length Corresponding to 95% of an Interior Layer's Vertical Deflection Versus Thickness-Diameter-Ratio	138
4.30	Overall Deflection of Experimental Bellows Versus Applied Load	143
4.31a	Dimensions of a Single Wafer From the Experimental Bellows	144
4.31b	"Parallel" Weld Design	144
4.31c	"Inclined" Weld Design	144

CHAPTER 1

INTRODUCTION

Due to the extensive use of multi-layered precision welded bellows in a wide range of exacting industrial and scientific applications, reliable information concerning the various characteristics which affect a welded bellows' performance is of considerable interest to engineers and designers.

A multi-layered precision welded bellows may be considered to be an elastic shell structure consisting of any number of rotationally symmetric layers which are joined to each other by means of circular welds having equal cross-sectional area. The shape and size of the constituent layers vary from one manufacturer to the next. For instance, the "nested-convex" shape consists of various cones and arcs of circles. The particular bellows which will be studied in this investigation consists of plates, portions of cones, and toroidal welds, as this shape is one of the most common. The outside diameter of any particular welded bellows may vary from less than one inch to several feet. Another type of bellows which consists of arcs of circles is the "hydraulic" bellows. Hydraulic bellows differ considerably from precision welded bellows in that they have no welds and they are crudely manufactured by extrusion using hydraulic pressure. Because of the manner in which they are made, hydraulic bellows are

not precision devices, hence a very accurate analysis of them would be unnecessary.

The method to be developed in this study will employ the full linear shell equations. Since the usual applications of a welded bellows require a high degree of reliability and precision, the maximum deflection of any layer will be very small, hence a nonlinear theory, e.g. the theory of Reissner[1] or Sanders[2] is unnecessary. In contrast to this, a layer within a hydraulic bellows is usually subjected to comparatively larger deflections and therefore, most useful results for hydraulic bellows would require a nonlinear theory.

Multi-layered precision welded bellows are often used to provide motion in some part of a servomechanism involving a liquid or gaseous medium, while providing a hermetic seal between the servomechanism and its environment. When a welded bellows is calibrated for use in a high precision measuring instrument, knowledge of the bellows' flexibility and various material characteristics which affect the instrument's accuracy, such as hysteresis and creep is required. Also, when used as a flexible coupling in tubing systems, reliable information concerning displacements, peak stresses, flexibility, and fatigue life is likewise of particular interest. In these applications, a welded bellows may be subjected to different combinations of pressure and axial force loading.

To obtain reliable information about the various characteristics which influence the performance of a welded bellows, it is essential to have accurate information concerning the displacement and state of stress at each point within the bellows under the given loading conditions. Some manufacturers have developed approximate experimental methods for predicting peak stresses and deflections. These methods primarily involve various well known experimental techniques for measuring displacements[3], stresses[4], and strains[5], although strain (and stress) measurements are not very accurate. These approximate methods invariably include empirical correction factors which have been determined from tests on sample bellows. Thus empirical formulas can be established to predict the performance of other welded bellows. The major disadvantage of using this approach to analyze welded bellows is that it will not yield accurate information about the displacement and state of stress at every point within the bellows. Specifically, our study will be directed toward the analysis of a particular shape of welded bellows of which many have been made. This specific shape, which consists of plates, conical frusta, and elastic toroidal welds having equal cross-sectional areas, is depicted in Fig. 1.1. Nevertheless, the method to be developed in this investigation will be completely general, and hence immediately applicable to precision welded bellows having any arbitrary meridional shape whatsoever.

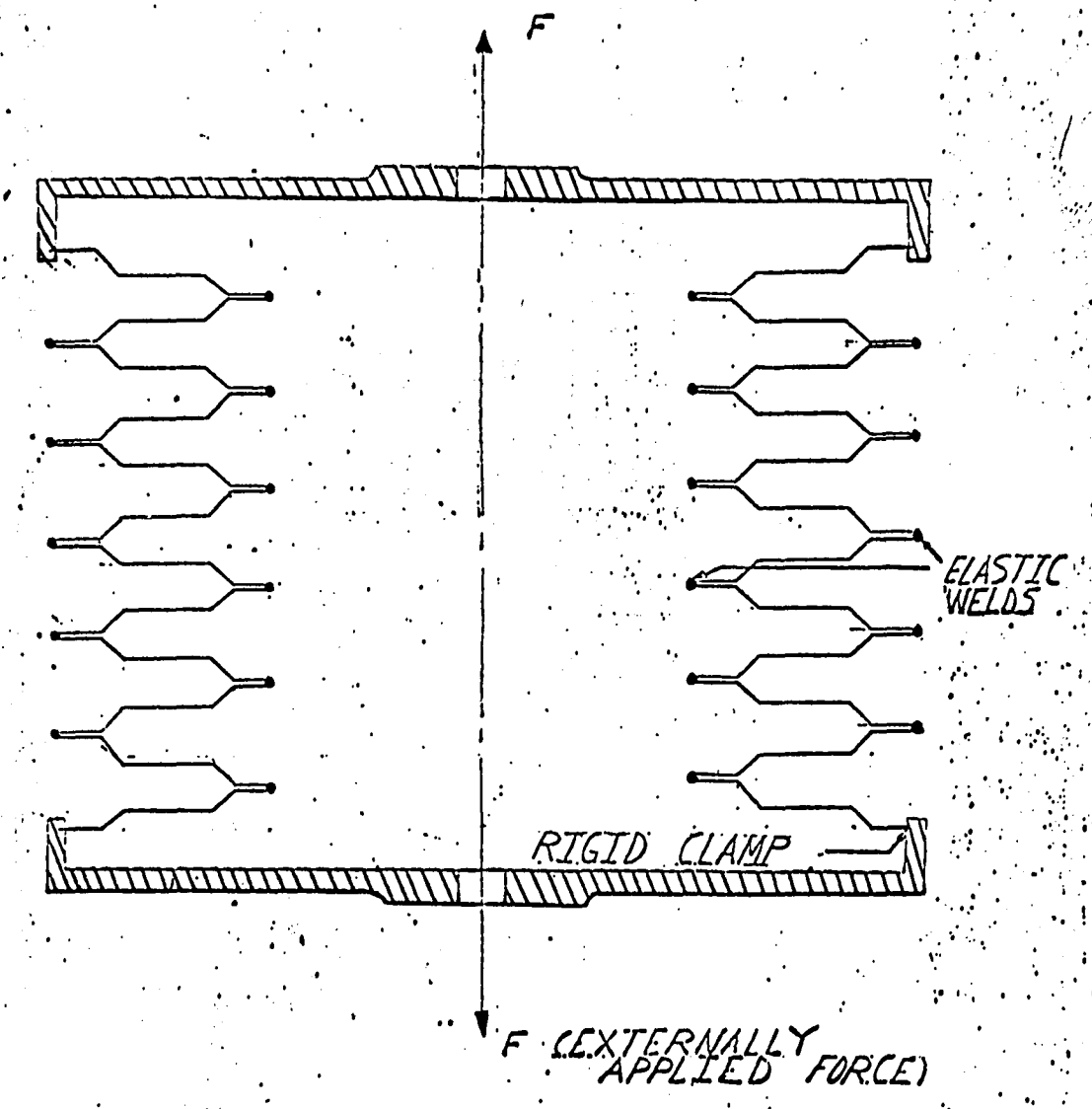

FIGURE 1.1 CROSS-SECTIONAL VIEW OF A WELDED BELLOWS WITH TWELVE LAYERS.

1.1 REVIEW OF WORK RELATED TO THE ANALYSIS OF PRECISION WELDED BELLOWS

Since the early 1900's, investigators have been interested in the analysis of various pressure elements which can be considered to be the precursors of the present-day precision welded bellows. In the work by Wissler[6], the analysis of "ringed" shells (i.e., a shell in the form of a torus) is considered. Stange[7] extended the work of Wissler to treat the problem of the compression of thin walled pipes with circular corrugations, while in the work by Clark, Gilroy, and Reissner[8], the problem of the compression of thin walled pipes with elliptical corrugations is considered. Final mention is made of the work by Clark and Reissner[9], in which the analysis of corrugated pipes is made by considering them to be "nearly" cylindrical shells.

In addition to the various studies on corrugated pipes, mention should be made of the various work on another important predecessor of the precision welded bellows - the corrugated diaphragm. In the work by Haringx[10], the diaphragm is referred back to plate behavior by smearing out the effects of the corrugations over a wave length. This leads to the consideration of a plate with variable elastic constants which, on the average, approximate the elastic constants of the diaphragm. By contrast, Grover and Bell[11] analyzed more accurately the stresses in a specific corrugated by fitting together known solutions.

In all of these analyses, the emphasis has been placed upon fitting together known solutions. In contrast to this approach, Dressler[12] applied numerical integration techniques to the full linear shell equations to obtain information about the displacement-stress behavior of corrugated diaphragms. More recently, Kalnins[13], Cohen[14], and Bushnell[15] have considered more general computer analyses of shell structures. For the analysis of large deflections, Kalnins and Lestingi[16] have incorporated Sanders' theory into a computer code. Lestingi and Brown[17] discuss the merits of applying multisegment numerical integration, finite difference, and finite element techniques to the analysis of various shell structures. Specifically, they use the method of [16] to analyze a hydraulic bellows. In the study by Lestingi and Hulbert[18], the methods of [15] and [16] are compared with regard to the analysis of a nested-convex bellows. However, their analysis of the bellows is confined to only one particular layer which is far removed from the bellows' outermost layer, i.e., an "interior" layer. Furthermore, no provision was made for the analysis of the welds. Thus their analysis is actually on a single non-welded diaphragm.

1.2 THE PRESENT STUDY OF PRECISION WELDED BELLOWS - SOME SALIENT FEATURES

In addition to utilizing the full linear shell equations, theory of the deformation of axisymmetric tori will be used to take into account the important effects of the welds.

Since precision welded bellows are deflected in a cyclical manner where peak stresses should never exceed the proportional limit, information concerning peak stresses is important for estimating fatigue life. Furthermore, various aspects of the overall displacement-stress behavior needed for the determination of those characteristics which govern the satisfactory performance of a welded bellows, such as flexibility will be presented.

The problem of analyzing welded bellows with many layers is of special interest. The direct application of any numerical (or analytical) method of analysis will lead to an excessive loss in computational significance due to accumulated roundoff error or increase in matrix order as the number of layers in the bellows increases. We will show that this loss in computational significance is highly dependent upon the bellows' thickness-diameter-ratio. That is to say, as the thickness-diameter-ratio decreases, fewer layers can be analyzed before excessive loss in computational significance occurs. It will also be shown that welded bellows exhibit a boundary layer effect. By means of this boundary layer effect, the concept of an "interior" layer will be developed in full detail and applied to the analysis of precision welded bellows having as many layers as desired.

1.3 SUMMARY

In the following sections, Chapter 2 gives the mathematical formulation of the governing equations,

boundary conditions, and matching conditions. Chapter 3 describes the actual method of solution. Discussion of the solutions along with a description of an experiment performed on a precision welded bellows having 34 layers appear in Chapter 4.

CHAPTER 2

GOVERNING EQUATIONS

A precision welded bellows consists of two entirely different elastic elements: shells and toroidal welds. Consequently a different set of governing equations must be formulated for each.

The analysis of the shell portions of the bellows will be based upon the full linear shell equations. These must be transformed so that arc length becomes the independent variable rather than the shell angle, which is normally used. This choice of independent variable will greatly facilitate the application of the shell equations to any shape of welded bellows no matter how complicated the meridian. Also, our independent and dependent variables will be transformed into dimensionless form for more general applicability. To ensure the continuity of any solution at the junctures between shell elements, the matching conditions involving displacement, force, moment, and meridional rotation will be derived.

Since the toroidal welds are not "shells", we shall employ a mechanics of materials approach to the analysis of the welds. In view of the fact that the effect of the welds is small (but nevertheless very important for the precise determination of displacements), the use of exact elasticity solutions for a torus is clearly not necessary. The radius

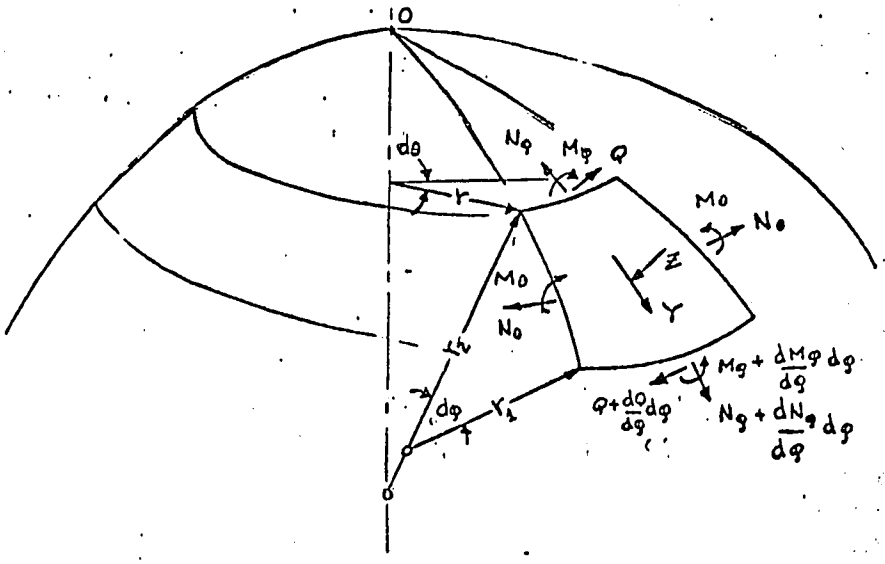

FIGURE 2.1 TYPICAL ROTATIONALLY SYMMETRIC SHELL ELEMENT

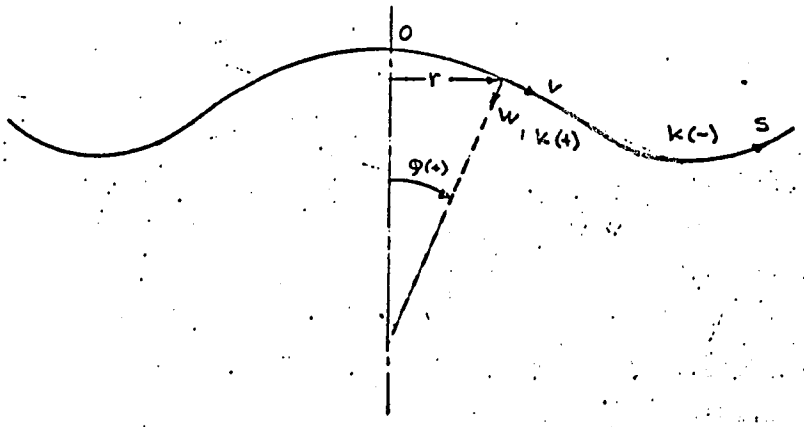

FIGURE 2.2 ARBITRARY MERIDIAN

of the circular cross-section of a weld is denoted as βt, where t is the thickness of the shell, hence β measures the size of the welds. Using both theories, we can formulate the appropriate boundary conditions and matching conditions that involve the welds.

2.1 EQUATIONS OF EQUILIBRIUM

The equations governing the equilibrium of the rotationally symmetric shell element shown in Fig. 2.1 are[19]:

$$\frac{d(rN_\varphi)}{d\varphi} - r_1 N_\theta \cos\varphi - rQ = -rr_1 Y \qquad (2.1\text{-}1a)$$

$$rN_\varphi + r_1 N_\theta \sin\varphi + \frac{d(rQ)}{d\varphi} = -rr_1 Z \qquad (2.1\text{-}1b)$$

$$\frac{d(rM_\varphi)}{d\varphi} - r_1 M_\theta \cos\varphi - rr_1 Q = 0 \qquad (2.1\text{-}1c)$$

where Y and Z are externally applied loads (see Fig. 2.2); Q is the transverse shear; the N's and M's are membrane forces and bending moments, respectively.

2.2 FORCE-DISPLACEMENT AND MOMENT-CURVATURE RELATIONS

Considerations of displacement and change in curvature of the middle surface of a rotationally symmetric shell element lead to the well-known[20] relations:

$$N_\varphi = \frac{Et}{(1-\nu^2)}\left[\frac{1}{r_1}\left(\frac{dv}{d\varphi} - w\right) + \frac{\nu}{r}(\cos\varphi\, v - \sin\varphi\, w)\right] \qquad (2.2\text{-}1a)$$

$$N_\theta = \frac{Et}{(1-\nu^2)}\left[\frac{\cos\varphi}{r} v - \frac{\sin\varphi}{r} w + \frac{\nu}{r_1}\left(\frac{dv}{d\varphi} - w\right)\right] \qquad (2.2\text{-}1b)$$

$$M_\varphi = \frac{-Et^3}{12(1-\nu^2)}\left[\frac{1}{r_1}\frac{d}{d\varphi}\left(\frac{v}{r_1} + \frac{1}{r_1}\frac{dw}{d\varphi}\right) + \frac{\nu}{r}\left(\frac{v}{r_1} + \frac{1}{r_1}\frac{dw}{d\varphi}\right)\cos\varphi\right] \qquad (2.2\text{-}1c)$$

$$M_\theta = \frac{-Et^3}{12(1-\nu^2)}\left[\left(\frac{v}{r_1} + \frac{1}{r_1}\frac{dw}{d\varphi}\right)\frac{\cos\varphi}{r} + \frac{\nu}{r_1}\frac{d}{d\varphi}\left(\frac{v}{r_1} + \frac{1}{r_1}\frac{dw}{d\varphi}\right)\right] \qquad (2.2\text{-}1d)$$

where E and ν are Young's modulus and Poisson's ratio, respectively.

2.3 TRANSFORMATION OF INDEPENDENT VARIABLE FROM SHELL ANGLE φ TO ARC LENGTH s

In equations (2.1-1a-c) and (2.2-1a-d), the shell angle φ is employed as the independent variable. Use of the shell angle, however, would lead to multi-valued functions for any complicated meridional shape as is the case for any multi-layered welded bellows. Consequently, we must introduce an independent variable which will keep all functions single-valued, thus we choose arc length s. To accomplish this, we note that:

$$k = \frac{1}{r_1} \tag{2.3-1}$$

and

$$\frac{d}{ds} = k \frac{d}{d\varphi} \tag{2.3-2}$$

If we introduce equations (2.3-1) and (2.3-2) into equations (2.1-1a-c) and (2.2-1a-d), expand, and make use of the fact that:

$$\frac{dr}{ds} = \cos\varphi \tag{2.3-3}$$

equations (2.1-1a-c) and (2.2-1a-d) become respectively, after changing the subscript φ to s:

$$\frac{dN_s}{ds} + (N_s - N_\theta)\frac{\cos\varphi}{r} - kQ = -Y \qquad (2.3\text{-}4a)$$

$$\frac{dQ}{ds} + kN_s + N_\theta \frac{\sin\varphi}{r} + \frac{\cos\varphi}{r} Q = -Z \qquad (2.3\text{-}4b)$$

$$\frac{dM_s}{ds} + (M_s - M_\theta)\frac{\cos\varphi}{r} - Q = 0 \qquad (2.3\text{-}4c)$$

$$N_s = \frac{Et}{(1-\nu^2)}\left[\frac{dv}{ds} - kw + \frac{\nu}{r}(\cos\varphi\, v - \sin\varphi\, w)\right] \qquad (2.3\text{-}5a)$$

$$N_\theta = \frac{Et}{(1-\nu^2)}\left[\frac{\cos\varphi}{r} v - \frac{\sin\varphi}{r} w + \nu\left(\frac{dv}{ds} - kw\right)\right] \qquad (2.3\text{-}5b)$$

$$M_s = \frac{-Et^3}{12(1-\nu^2)}\left[v\frac{dk}{ds} + k\frac{dv}{ds} + \frac{d^2w}{ds^2} + \frac{\nu}{r}\left(kv + \frac{dw}{ds}\right)\cos\varphi\right] \qquad (2.3\text{-}5c)$$

$$M_\theta = \frac{-Et^3}{12(1-\nu^2)}\left[\left(kv + \frac{dw}{ds}\right)\frac{\cos\varphi}{r} + \nu\left(v\frac{dk}{ds} + k\frac{dv}{ds} + \frac{d^2w}{ds^2}\right)\right] \qquad (2.3\text{-}5d)$$

If we introduce equations (2.3-5a-d) into equations (2.3-4a-c) and make use of the relation:

$$k = \frac{d\varphi}{ds} \tag{2.3-6}$$

equations (2.3-4a-c) will take the form:

$$(rk + \nu \sin\varphi)\frac{dw}{ds} - (\frac{\sin\varphi\cos\varphi}{r} - k\cos\varphi - r\frac{dk}{ds})w$$

$$- r\frac{d^2v}{ds^2} - \cos\varphi\frac{dv}{ds} + (\frac{\cos^2\varphi}{r} + \nu k\sin\varphi)v$$

$$+ \frac{rk(1-\nu^2)Q}{Et} = \frac{r(1-\nu^2)Y}{Et} \tag{2.3-7a}$$

$$(\frac{\sin^2\varphi}{r} + rk^2 + 2\nu k\sin\varphi)w - (rk + \nu\sin\varphi)\frac{dv}{ds}$$

$$- (\frac{\sin\varphi\cos\varphi}{r} + \nu k\cos\varphi)v - \frac{r(1-\nu^2)}{Et}\frac{dQ}{ds}$$

$$- \frac{(1-\nu^2)}{Et}\cos\varphi Q = \frac{r(1-\nu^2)Z}{Et} \tag{2.3-7b}$$

$$r\frac{d^3w}{ds^3} + \cos\varphi\frac{d^2w}{ds^2} - \left(\frac{\cos^2\varphi}{r} + \nu k\sin\varphi\right)\frac{dw}{ds}$$

$$+ rk\frac{d^2v}{ds^2} + \left(k\cos\varphi + 2r\frac{dk}{ds}\right)\frac{dv}{ds}$$

$$+ \left(\frac{dk}{ds}\cos\varphi + r\frac{d^2k}{ds^2} - k\frac{\cos^2\varphi}{r}\right.$$

$$\left. - \nu k^2\sin\varphi\right)v + \frac{12(1-\nu^2)rQ}{Et^3} = 0 \qquad (2.3\text{-}7c)$$

The variable signs of k and φ are chosen as indicated in Fig. 2.2. The radial distance r and arc length s are always taken with positive sign.

Equations (2.3-7a-c) represent the form of the exact linear shell equations (which include all bending and stretching effects and the coupling between them) found to be best adapted to the computational requirements for an arbitrary meridional shape and for multi-layered precision welded bellows.

2.4 FORMULATION OF GOVERNING EQUATIONS FOR MERIDIANS WITH A CONSTANT SHELL ANGLE

In Chapter 1, it was pointed out that precision welded bellows are fabricated in many meridional shapes.

The welded bellows which we have chosen here to

analyze in detail has a shape which may be described in the following manner: each layer within the bellows is composed of three circular plates, two conical frusta with equal vertex angles, and toroidal welds with circular cross-sections joining the innermost and outermost plates. A typical welded bellows with this shape, and having twelve layers, is depicted in Fig. 1.1.

In view of the fact that all plates and conical shells are characterized by a constant (though different) shell angle, equations (2.3-7a-c), by virtue of equation (2.3-6) become:

$$\nu \sin\varphi \frac{dw}{ds} - \frac{\sin\varphi\cos\varphi}{r} w - r \frac{d^2v}{ds^2} - \cos\varphi \frac{dv}{ds} + \frac{\cos^2\varphi}{r} v = \frac{r(1-\nu^2)}{Et} Y \qquad (2.4\text{-}1a)$$

$$\frac{\sin^2\varphi}{r} w - \nu \sin\varphi \frac{dv}{ds} - \frac{\sin\varphi\cos\varphi}{r} v - \frac{r(1-\nu^2)}{Et} \frac{dQ}{ds} - \frac{(1-\nu^2)}{Et} \cos\varphi Q = \frac{r(1-\nu^2)}{Et} Z \qquad (2.4\text{-}1b)$$

$$r \frac{d^3w}{ds^3} + \cos\varphi \frac{d^2w}{ds^2} - \frac{\cos^2\varphi}{r} \frac{dw}{ds} + \frac{12(1-\nu^2)}{Et^3} rQ = 0 \qquad (2.4\text{-}1c)$$

Equations (2.4-1a-c) represent the governing differential equations for our specific analysis. In addition to the necessity of using arc length as the independent variable mentioned in Section 2.3, our choice of v, w, and Q as the basic independent variables (rather than those suggested by Timoshenko[21], namely the angle of meridional rotation and modified shear) leads to two additional computational advantages. They may be summarized as follows:

i) Our set of dependent variables is better suited for shells of arbitrary shape rather than the variables chosen in [21].

ii) Our set of dependent variables does not require a separate machine integration to obtain the normal displacement w.

Likewise for piece-wise constant shell angles, equations (2.3-5a-d) take the form:

$$N_s = \frac{Et}{(1-\nu^2)}\left[\frac{dv}{ds} + \frac{\nu}{r}(\cos\varphi\, v - \sin\varphi\, w)\right] \quad (2.4\text{-}2a)$$

$$N_\theta = \frac{Et}{(1-\nu^2)}\left[\frac{\cos\varphi}{r}v - \frac{\sin\varphi}{r}w + \nu\frac{dv}{ds}\right] \quad (2.4\text{-}2b)$$

$$M_s = \frac{-Et^3}{12(1-\nu^2)}\left[\frac{d^2w}{ds^2} + \frac{\nu}{r}\cos\varphi\frac{dw}{ds}\right] \qquad (2.4\text{-}2c)$$

$$M_\theta = \frac{-Et^3}{12(1-\nu^2)}\left[\frac{\cos\varphi}{r}\frac{dw}{ds} + \nu\frac{d^2w}{ds^2}\right] \qquad (2.4\text{-}2d)$$

2.5 TRANSFORMATION OF THE BASIC EQUATIONS INTO DIMENSIONLESS FORM

Although the most general application of a welded bellows may consist of axial force loading with internal fluid (or gas) pressure, this may be split in linear applications into two cases, wherein each loading is considered separately. The mathematical principles and difficulties involved in solving either case are identical. Therefore, for brevity, we will confine our analysis here to the axial load case only. An external axial force applied to the rigid mounting, which is free to move in the axial direction, will result in a prescribed value δ of transverse shear Q (force/length) at the rigid clamp boundary. The outside diameter of the bellows measured to the rigid clamp is denoted by d.

We next transform to dimensionless variables for the case of axial loading.

Inspection of equations (2.4-1a-c) and the associated boundary conditions shows that for a fixed meridional pattern, there are exactly eight dimensional quantities

involved directly plus the two dimensionless parameters β and ν. Using the two fundamental dimensions of force and length, application of the Buckingham pi theorem leads to six dimensionless groups. One such set of dimensionless groups is defined as follows:

$$\bar{v} = \frac{Ev}{(1-\nu^2)\mathcal{Q}} \tag{2.5-1a}$$

$$\bar{w} = \frac{Ew}{(1-\nu^2)\mathcal{Q}} \tag{2.5-1b}$$

$$\bar{Q} = \frac{Q}{\mathcal{Q}} \tag{2.5-1c}$$

$$\bar{r} = \frac{r}{d} \tag{2.5-1d}$$

$$\bar{s} = \frac{s}{d} \tag{2.5-1e}$$

$$\bar{t} = \frac{t}{d} \tag{2.5-1f}$$

plus the dimensionless parameters β and ν. In equations (2.5-1a-f), every quantity with a bar is dimensionless.

In a similar manner, the dimensionless membrane forces, bending moments, and stresses follow as:

$$\bar{N} = \frac{N}{\mathcal{E}} \tag{2.5-2a}$$

$$\bar{M} = \frac{M}{\mathcal{E}d} \tag{2.5-2b}$$

$$\bar{\sigma} = \frac{\sigma d}{\mathcal{E}} \tag{2.5-2c}$$

Substitution of equations (2.5-1a-f) into equations (2.4-1a-c) results in the following system of dimensionless ordinary differential equations:

$$\nu \sin\varphi \frac{d\bar{w}}{d\bar{s}} - \frac{\sin\varphi\cos\varphi}{\bar{r}}\bar{w} - \bar{r}\frac{d^2\bar{v}}{d\bar{s}^2} - \cos\varphi\frac{d\bar{v}}{d\bar{s}}$$

$$+ \frac{\cos^2\varphi}{\bar{r}}\bar{v} = 0 \tag{2.5-3a}$$

$$\frac{\sin^2\varphi}{\bar{r}}\bar{w} - \nu\sin\varphi\frac{d\bar{v}}{d\bar{s}} - \frac{\sin\varphi\cos\varphi}{\bar{r}}\bar{v} - \frac{\bar{r}}{\bar{t}}\frac{d\bar{Q}}{d\bar{s}}$$

$$- \frac{\cos\varphi}{\bar{t}}\bar{Q} = 0 \tag{2.5-3b}$$

$$\bar{r}\,\frac{d^3\bar{w}}{d\bar{s}^3} + \cos\varphi\,\frac{d^2\bar{w}}{d\bar{s}^2} - \frac{\cos^2\varphi}{\bar{r}}\,\frac{d\bar{w}}{d\bar{s}} + \frac{12\bar{r}\bar{Q}}{\bar{t}^3} = 0 \qquad (2.5\text{-}3c)$$

Equations (2.5-3a-c) represent the governing dimensionless differential equations for the axial load application of the welded bellows under consideration. Clearly, the total order of equations (2.5-3a-c) is six, thus requiring a total of six boundary conditions. These boundary conditions may be specified in either of the following ways:

i) Three boundary conditions at the rigid clamp and three at the mid-plane of symmetry.

ii) Six initial conditions at the rigid clamp.

Clearly, only case (i) can be formulated directly from the physical problem. The complete discussion of cases (i) and (ii) will be presented in Sections 2.10 and 3.1, respectively.

In a similar manner, substitution of equations (2.5-1a-b,d,f) into equations (2.4-2a-d) results in the following set of dimensionless force-displacement and moment-curvature relations:

$$\bar{N}_s = \bar{t}\left[\frac{d\bar{v}}{d\bar{s}} + \frac{\nu}{\bar{r}}\,(\cos\varphi\,\bar{v} - \sin\varphi\,\bar{w})\right] \qquad (2.5\text{-}4a)$$

$$\bar{N}_\theta = \bar{t}\left[\frac{\cos\varphi}{\bar{r}}\,\bar{v} - \frac{\sin\varphi}{\bar{r}}\,\bar{w} + \nu\,\frac{d\bar{v}}{d\bar{s}}\right] \qquad (2.5\text{-}4b)$$

$$M_s = \frac{-\bar{t}^3}{12}\left[\frac{d^2\bar{w}}{d\bar{s}^2} + \nu\frac{\cos\varphi}{\bar{r}}\frac{d\bar{w}}{d\bar{s}}\right] \qquad (2.5\text{-}4c)$$

$$M_\theta = \frac{-\bar{t}^3}{12}\left[\frac{\cos\varphi}{\bar{r}}\frac{d\bar{w}}{d\bar{s}} + \nu\frac{d^2\bar{w}}{d\bar{s}^2}\right] \qquad (2.5\text{-}4d)$$

2.6 BOUNDARY CONDITIONS WITHOUT WELDS

In general, any solution for the three unknowns $\bar{v}$, $\bar{w}$, and $\bar{Q}$ will require the solution of a two point boundary value problem or a one point initial value problem.

The mathematical formulation of the two point boundary value problem requires a total of six boundary conditions. In stating these six boundary conditions, we will first consider the case of no welds. The modification of the boundary conditions from welds will be considered separately in Section 2.9.

The first three boundary conditions are specified at the rigid clamp shown in Fig. 1.1. They are:

$$\bar{v} = 0 \qquad (2.6\text{-}1a)$$

$$\frac{d\bar{w}}{d\bar{s}} = 0 \qquad (2.6\text{-}1b)$$

$$\bar{Q} = \text{PRESCRIBED BY EXTERNAL FORCE} \qquad (2.6\text{-}1c)$$

The remaining three boundary conditions are imposed at the bellows' mid-plane of symmetry.

The bellows' symmetry about its mid-plane leads to the remaining boundary conditions which will be imposed at either the bellows' inner or outer diameter depending upon whether the layer which terminates at the mid-plane is odd or even numbered. These boundary conditions are:

$$\bar{w} = 0 \qquad (2.6\text{-}2a)$$

$$\frac{d\bar{w}}{d\bar{s}} = 0 \qquad (2.6\text{-}2b)$$

$$\bar{N}_s = 0 \qquad (2.6\text{-}2c)$$

Introducing the expression for $\bar{N}_s$ from equation (2.5-4a), equation (2.6-2c) becomes:

$$\frac{d\bar{v}}{d\bar{s}} + \frac{\nu}{\bar{r}} (\cos\varphi\,\bar{v} - \sin\varphi\,\bar{w}) = 0 \qquad (2.6\text{-}3)$$

From Figs. 2.3a-b, we note that for any layer which terminates at the mid-plane of symmetry, the shell angle φ is defined as:

$$\varphi = \begin{cases} 180^{\circ} \; ; \; n = 1,3,\ldots, \\ \\ 0 \quad ; \; n = 2,4,\ldots, \end{cases} \tag{2.6-4}$$

where n is the number of layers counted from the rigid clamp to the mid-plane of symmetry. Hence equation (2.6-3) will take the form:

$$\frac{d\bar{v}}{d\bar{s}} + (-1)^{n} \nu \frac{\bar{v}}{\bar{r}} \tag{2.6-5}$$

Thus, the final three boundary conditions to be imposed at the bellows' mid-plane of symmetry are:

$$\bar{w} = 0 \tag{2.6-6a}$$

$$\frac{d\bar{w}}{d\bar{s}} = 0 \tag{2.6-6b}$$

$$\frac{d\bar{v}}{d\bar{s}} + (-1)^{n} \nu \frac{\bar{v}}{\bar{r}} = 0 \tag{2.6-6c}$$

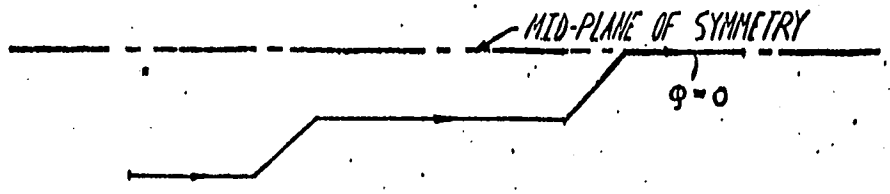

FIGURE 2.3a EVEN NUMBERED LAYER AT BELLOWS' MID-PLANE OF SYMMETRY

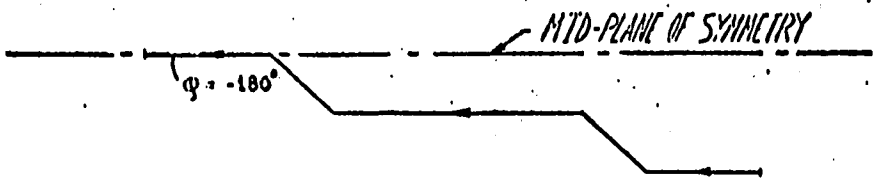

FIGURE 2.3b ODD NUMBERED LAYER AT BELLOWS' MID-PLANE OF SYMMETRY

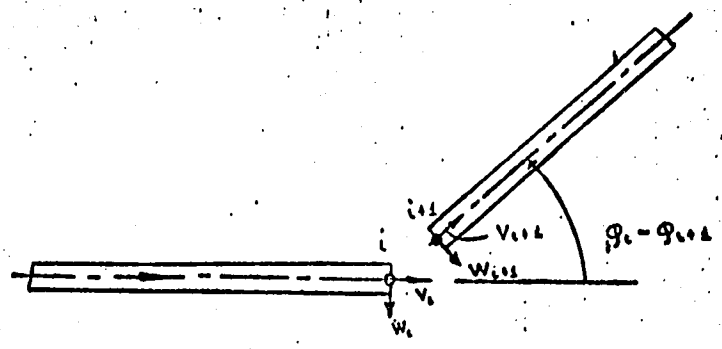

FIGURE 2.4 COMPONENTS OF DISPLACEMENT AT AN ARBITRARY JUNCTURE BETWEEN SHELL ELEMENTS

2.7 MATCHING CONDITIONS BETWEEN CONES AND PLATES

Since the total order of equations (2.5-3a-c) is six, any general solution will involve six arbitrary parameters. These six arbitrary parameters will be determined by imposing a set of six matching conditions at every juncture between shell elements. These matching conditions evolve from the requirements of:

i) Continuity of displacement

ii) Continuity of meridional rotation

iii) Force equilibrium

iv) Meridional moment equilibrium

The requirement of continuous displacement between the two arbitrary shell elements shown in Fig. 2.4, along with equations (2.5-1a-b), yields the relations:

$$\bar{v}_{i+1} = [\cos\varphi_i\cos\varphi_{i+1} + \sin\varphi_i\sin\varphi_{i+1}]\bar{v}_i - [\sin\varphi_i\cos\varphi_{i+1} - \cos\varphi_i\sin\varphi_{i+1}]\bar{w}_i \qquad (2.7\text{-}1a)$$

$$\bar{w}_{i+1} = [\sin\varphi_i\cos\varphi_{i+1} - \cos\varphi_i\sin\varphi_{i+1}]\bar{v}_i + [\cos\varphi_i\cos\varphi_{i+1} + \sin\varphi_i\sin\varphi_{i+1}]\bar{w}_i \qquad (2.7\text{-}1b)$$

The requirement of continuous meridional rotation, along with equations (2.5-1b,e), leads to the relation:

$$\frac{d\bar{w}_{i+1}}{d\bar{s}} = \frac{d\bar{w}_i}{d\bar{s}} \qquad (2.7\text{-}2)$$

since the meridional curvature for cones and plates is zero.

In order to obtain the force and meridional moment matching conditions appropriate to the "overlapping" shell model shown in Fig. 2.6a, we consider the forces and meridional moments acting on the small triangular torus which exists between any cone and plate. This small triangular torus is indicated in Fig. 2.6a by the heavy dot.

Force equilibrium for the small triangular torus which exists between an arbitrary cone and plate as shown in Fig. 2.5a, along with equations (2.5-1c) and (2.5-2a), leads to the relations:

$$\bar{N}_s^{i+1} = [\cos\varphi_i\cos\varphi_{i+1} + \sin\varphi_i\sin\varphi_{i+1}]\bar{N}_s^i - [\sin\varphi_i\cos\varphi_{i+1} - \cos\varphi_i\sin\varphi_{i+1}]\bar{Q}^i \qquad (2.7\text{-}3a)$$

$$\bar{Q}^{i+1} = [\sin\varphi_i\cos\varphi_{i+1} - \cos\varphi_i\sin\varphi_{i+1}]\bar{N}_s^i + [\cos\varphi_i\cos\varphi_{i+1} + \sin\varphi_i\sin\varphi_{i+1}]\bar{Q}^i \qquad (2.7\text{-}3b)$$

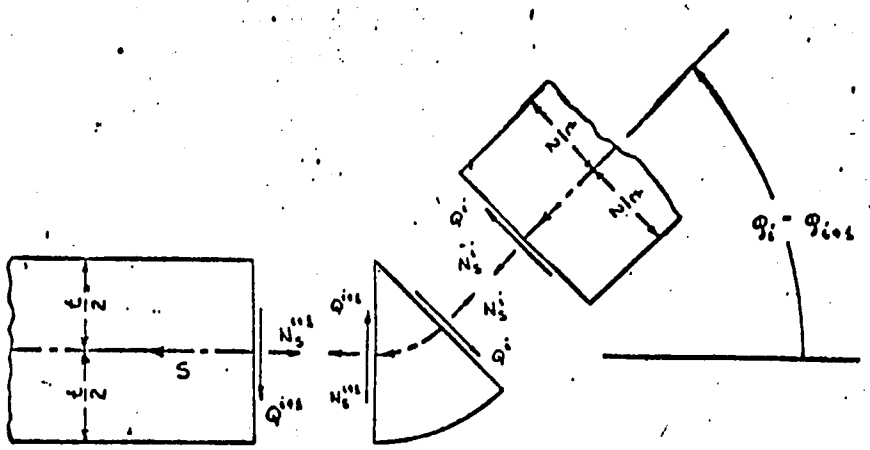

FIGURE 2.5a CROSS-SECTIONAL VIEW OF FORCES ACTING ON AN ARBITRARY TRIANGULAR TORUS

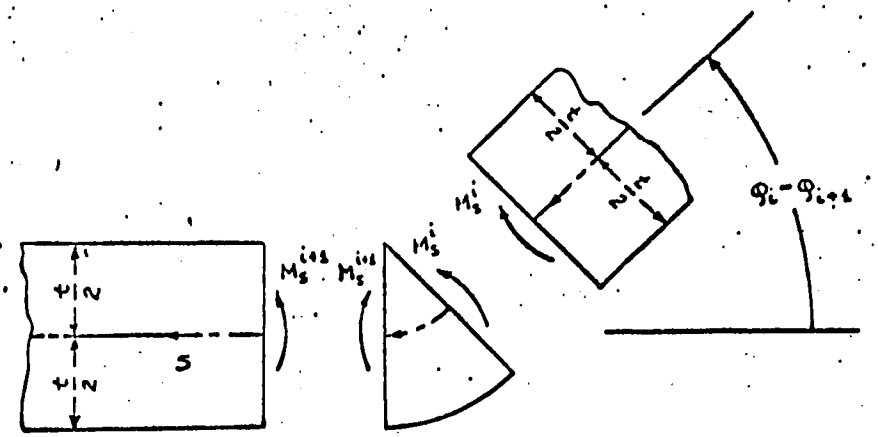

FIGURE 2.5b CROSS-SECTIONAL VIEW OF MOMENTS ACTING ON AN ARBITRARY TRIANGULAR TORUS

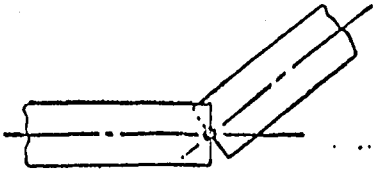

FIGURE 2.6a "OVERLAPPING" SHELL MODEL

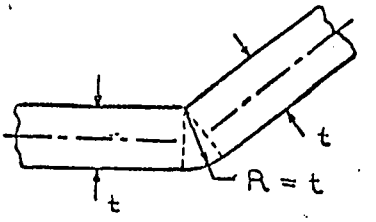

FIGURE 2.6b CHARACTERISTIC DIMENSIONS OF A TRIANGULAR TORUS

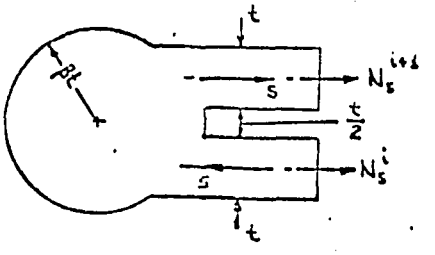

"A"- INNER WELD

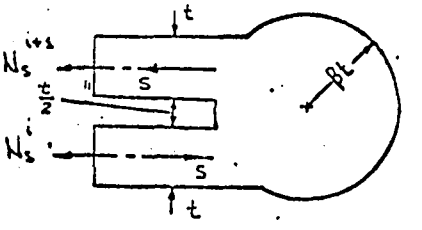

"B"- OUTER WELD

FIGURE 2.7a MEMBRANE FORCES ACTING ON AN INNER AND OUTER WELD

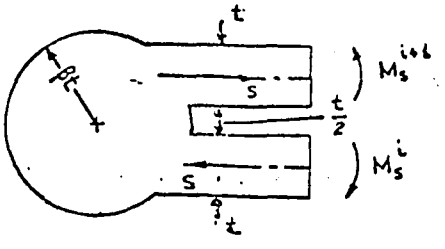

"A"- INNER WELD

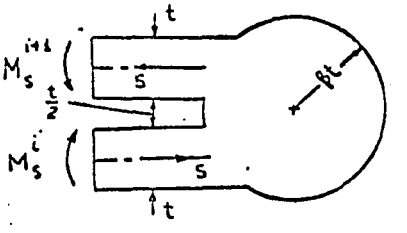

"B"- OUTER WELD

FIGURE 2.7b MOMENTS ACTING ON AN INNER AND OUTER WELD

Considerations of moment equilibrium in the circumferential direction for the small triangular torus which exists between an arbitrary cone and plate as shown in Fig. 2.5b, along with equation (2.5-2b), lead to the relation:

$$\bar{M}_s^{i+1} = \bar{M}_s^i \qquad (2.7\text{-}4)$$

Equations (2.7-1a-b), (2.7-2), (2.7-3a-b), and (2.7-4) express the six basic matching conditions that must be imposed between any combination of plates and conical shells, provided that no welds exist and the model of Fig. 2.6a is used.

It should be noted, that any attempt to consider any triangular torus to be a curved shell element, so that the shell equations can be applied directly, will necessarily lead to error; the reason for this can be seen from Fig. 2.6b, i.e., the meridional radius of curvature, R, is of the same order of magnitude as the thickness t of the curved shell, hence the shell equations become inapplicable. Thus, any attempt to apply the shell equations will necessarily lead to error.

2.8 FORMULATION OF MATCHING CONDITIONS INVOLVING WELDS AT INNER AND OUTER DIAMETERS

From Fig. 1.1, it can be seen that with the exception of the plates at the two rigid clamps, there exist small circular welds of equal cross-sectional area at the inner and outer junctures between plates.

Every weld is considered to be an elastic axisymmetric torus with a circular cross-section. This toroidal weld is subjected to the effects of the two meridional membrane forces from the two plates which it joins, namely N_s^i and N_s^{i+1}, and the corresponding meridional bending moments M_s^i and M_s^{i+1}. These are shown in Figs. 2.7a-b, respectively. The two membrane forces stretch the weld in the radial direction and also cause the weld to rotate in the circumferential direction. The two meridional bending moments only cause the weld to rotate in the circumferential direction.

Application of the theory[22] of axisymmetric in-plane stretching of rings, along with equations (2.5-1a,d,f) and (2.5-2a), lead to the relation:

$$\bar{N}_s^{i+1} = -\bar{N}_s^i - \frac{\pi \beta^2 (1-\nu^2)\bar{t}^2}{\bar{r}(\bar{r} - \beta\bar{t})} \bar{v}_i \qquad (2.8\text{-}1)$$

Equation (2.8-1) is used instead of equation (2.7-3a) at <u>any inner weld</u>.

In a similar manner, for <u>any outer weld</u>, the relation:

$$\bar{N}_s^{i+1} = -\bar{N}_s^i - \frac{\pi \beta^2 (1-\nu^2)\bar{t}^2}{\bar{r}(\bar{r}+\beta\bar{t})}\,\bar{v}_i \qquad (2.8\text{-}2)$$

is used instead of equation (2.7-3a). Equations (2.8-1) and (2.8-2) may be written in the following unified form:

$$\bar{N}_s^{i+1} = -\bar{N}_s^i - \frac{\pi \beta^2 (1-\nu^2)\bar{t}^2}{\bar{r}(\bar{r}+(-1)^i\beta\bar{t})}\,\bar{v}_i \qquad (2.8\text{-}3)$$

$$; \; i = 5,10,\ldots,$$

Here, the values of i which correspond to odd multiples of five are associated with inner welds, while those values of i which correspond to even multiples of five are associated with outer welds.

By considering the theory[23] of the circumferential rotation of axisymmetric tori, we can relate the total applied meridional bending moment (see Figs. 2.7a-b) to the amount that the weld rotates in the circumferential direction. Use of this theory, along with equations (2.5-1a,b,d-f), leads to the relation:

$$\bar{M}_s^{i+1} = \bar{M}_s^i + \frac{3}{4}(\bar{N}_s^{i+1} - \bar{N}_s^i)\bar{t}$$

$$- \frac{\pi \beta^4 (1 - \nu^2)\bar{t}^4}{4\bar{r}(\bar{r} - \beta\bar{t})} \frac{d\bar{w}_i}{d\bar{s}} \qquad (2.8\text{-}4)$$

In equation (2.8-4), the only significant parameters are the cross-sectional area of the weld ($\pi \beta^2 \bar{t}^2$) and its moment of inertia ($\frac{1}{4}\pi \beta^4 \bar{t}^4$). Substitution of equation (2.8-1) into equation (2.8-4) leads to the result:

$$\bar{M}_s^{i+1} = \bar{M}_s^i - \frac{3}{2}\bar{N}_s^i\bar{t} - \frac{3\pi \beta^2 (1 - \nu^2)\bar{t}^3}{4\bar{r}(\bar{r} - \beta\bar{t})} \bar{v}_i$$

$$- \frac{\pi \beta^4 (1 - \nu^2)\bar{t}^4}{4\bar{r}(\bar{r} - \beta\bar{t})} \frac{d\bar{w}_i}{d\bar{s}} \qquad (2.8\text{-}5)$$

Equation (2.8-5) is used instead of equation (2.7-4) at <u>any inner weld</u>.

In a similar manner, for <u>any outer weld</u>, the relation:

$$\bar{M}_s^{i+1} = \bar{M}_s^i + \frac{3}{2}\bar{N}_s^i\bar{t} + \frac{3\pi \beta^2 (1 - \nu^2)\bar{t}^3}{4\bar{r}(\bar{r} + \beta\bar{t})} \bar{v}_i$$

$$- \frac{\pi \beta^4 (1 - \nu^2)\bar{t}^4}{4\bar{r}(\bar{r} + \beta\bar{t})} \frac{d\bar{w}_i}{d\bar{s}} \qquad (2.8\text{-}6)$$

is used instead of equation (2.7-4).

Equations (2.8-5) and (2.8-6) may be written in the following unified form:

$$\bar{M}_s^{i+1} = \bar{M}_s^i + (-1)^i \frac{3}{2} \bar{N}_s^i \bar{t}$$

$$+ \frac{(-1)^i 3\pi \beta^2 (1-\nu^2) \bar{t}^3}{4\bar{r}(\bar{r} + (-1)^i \beta \bar{t})} \bar{v}_i$$

$$- \frac{\pi \beta^4 (1-\nu^2) \bar{t}^4}{4\bar{r}(\bar{r} + (-1)^i \beta \bar{t})} \frac{d\bar{w}_i}{d\bar{s}} \qquad (2.8\text{-}7)$$

$$; \; i = 5, 10, \ldots,$$

Thus equations (2.7-1a-b), (2.7-2), and (2.7-3b) are valid at any inner or outer diameter whether a weld is present or not. When a weld exists, then equations (2.7-3a) and (2.7-4) must be replaced by the more general expressions given by equations (2.8-3) and (2.8-7), respectively.

2.9 MODIFICATION OF BOUNDARY CONDITIONS DUE TO WELDS

Since no weld exists at the rigid clamp, it follows that the presence of welds can only affect the boundary conditions at the bellows' mid-plane of symmetry. Specifically, equations (2.6-2a-b) will be unaffected by the presence of a weld. However, equation (2.6-2c) must be modified to take into account the effect of a weld. In order to do this, we

notice that at the bellows' mid-plane of symmetry, the following condition must hold:

$$\bar{N}_s^{i+1} = \bar{N}_s^i \qquad (2.9\text{-}1)$$

Substitution of equation (2.9-1) into equation (2.8-3) leads to the result:

$$\bar{N}_s^i + \frac{\pi \beta^2 (1-\nu^2)\bar{t}^2}{2\bar{r}(\bar{r} + (-1)^i \beta \bar{t})} \bar{v}_i = 0 \qquad (2.9\text{-}2)$$

$$; \; i = 5,10,\ldots,$$

Equation (2.9-2) replaces equation (2.6-2c) as the third boundary condition in the remaining set of three boundary conditions that must be imposed at the bellows' mid-plane of symmetry. As equation (2.9-2) appears, it is completely general, i.e., equation (2.9-2) may be applied at an inner or outer weld.

2.10 FORMULATION OF BOUNDARY CONDITIONS FOR AN "INTERIOR" LAYER WITHOUT WELDS

An "interior" layer is defined as any layer which is so far removed from the rigid clamp (or any other type of outer support), that the boundary conditions associated with

the rigid clamp have lost their effect on the layer. Furthermore, as far as the layer is concerned, it is impossible to determine its position with respect to the bellows' mid-plane of symmetry. Consequently, an interior layer will have associated with it a displacement-stress response which is exactly the same as the displacement-stress response of a layer which terminates at the mid-plane of symmetry. Two interior layers without welds are shown in Figs. 2.3a-b.

The first two boundary conditions at the outermost point ($\bar{r} = 0.5$) of an interior layer are given explicitly by equations (2.6-1b-c). The third boundary condition is, by symmetry:

$$\bar{N}_s = 0 \qquad (2.10\text{-}1)$$

If we set n = 1 in equation (2.6-5), equation (2.10-1) may be written as:

$$\frac{d\bar{v}}{d\bar{s}} - \nu \frac{\bar{v}}{\bar{r}} = 0 \qquad (2.10\text{-}2)$$

The final three boundary conditions to be imposed at the innermost point ($\bar{r} = 0.25$) of an interior layer are then given explicitly by equations (2.6-2a-b) and (2.10-2).

2.11 FORMULATION OF BOUNDARY CONDITIONS FOR AN "INTERIOR" LAYER INVOLVING WELDS

The presence of welds in an interior layer will only affect the boundary conditions given by equation (2.10-2). The welds associated with an interior layer are depicted in Figs. 2.7a-b. The requirement of compatibility between the radial displacement of the outer weld (point "B", Fig. 2.7a) and the membrane force which causes the displacement, leads to the relation:

$$\frac{d\bar{v}}{d\bar{s}} - \left[\frac{\nu}{\bar{r}} + \frac{\pi \beta^2 (1 - \nu^2) \bar{t}}{2\bar{r}(\bar{r} + \beta \bar{t})} \right] \bar{v} = 0 \qquad (2.11\text{-}1)$$

which is used instead of equation (2.10-2) at <u>any outer weld</u>.

In a similar manner, at an inner weld (point "A", Fig. 2.7a), we obtain the relation:

$$\frac{d\bar{v}}{d\bar{s}} - \left[\frac{\nu}{\bar{r}} - \frac{\pi \beta^2 (1 - \nu^2) \bar{t}}{2\bar{r}(\bar{r} - \beta \bar{t})} \right] \bar{v} = 0 \qquad (2.11\text{-}2)$$

which is used instead of equation (2.10-2) at <u>any inner weld</u>.

CHAPTER 3

SOLUTION OF GOVERNING EQUATIONS

In Chapter 2, it was indicated that the determination of $\bar{v}$, $\bar{w}$, and $\bar{Q}$ at every point within the bellows requires the solution of a two point boundary value problem.

One possible method of solution of this two point boundary value problem would consist of piecing together exact solutions for plates, conical frusta, and toroidal welds. This approach to the analysis of a welded bellows will always require the inversion of a very large banded matrix for the various sets of six arbitrary parameters obtained with each general solution of equations (2.5-3a-c).

The size of this banded matrix will, of course, depend upon the number of layers in the bellows. For any given layer, there are five constituent shell elements. Since there will be six arbitrary parameters from each general solution for any constituent shell element, it follows that for a welded bellows having n layers counted from the rigid clamp to the mid-plane of symmetry, a banded matrix of order 30n would have to be inverted. In order to analyze a welded bellows having a total of forty layers, which is quite common, a banded matrix of order 600 (and a band width of 18) would have to be inverted. While this method has been applied to much simpler problems, namely corrugated diaphragms by Grover and Bell in [11], the size of the resulting matrix was only 44.

We decided not to use this method of solution, not only because it involves inversion of a very large banded matrix (which as we shall show later, will also be nearly singular, thus greatly increasing the resulting overall numerical errors), but primarily because this method will obviously not be applicable to arbitrary meridional shapes, for which exact shell solutions are unknown. Therefore, the following alternate method of solution is developed, which does not involve inversion of a large matrix, and which is applicable to any meridional shape.

3.1 SOLUTION BY SUPERPOSITION OF FOUR INDEPENDENT PURE INITIAL VALUE PROBLEM SOLUTIONS

We seek solutions to equations (2.5-3a-c) which satisfy all of the boundary conditions given by equations (2.6-1a-c), (2.6-2a-b), and (2.9-2) and the various matching conditions described in Chapter 2.

To this end, we introduce a total solution vector $\bar{G}(\bar{s})$ defined as follows:

$$\bar{G}(\bar{s}) = \lambda_1\bar{G}_1(\bar{s}) + \lambda_2\bar{G}_2(\bar{s}) + \lambda_3\bar{G}_3(\bar{s}) + \bar{G}_p(\bar{s}) \qquad (3.1\text{-}1)$$

where λ_1, λ_2, and λ_3 are scalar multipliers which are determined by imposing the final three boundary conditions on $\bar{G}(\bar{s})$ at the bellows' mid-plane of symmetry.

$\bar{G}(\bar{s})$ will contain the following set of variables as its elements:

$$\bar{G}(\bar{s}) = \begin{bmatrix} \bar{v} \\ \bar{w} \\ \bar{Q} \\ \frac{d\bar{v}}{d\bar{s}} \\ \frac{d\bar{w}}{d\bar{s}} \\ \frac{d^2\bar{w}}{d\bar{s}^2} \end{bmatrix} \qquad (3.1\text{-}2)$$

Each $\bar{G}_i(\bar{s})$ is a solution determined by its six initial conditions:

$$\bar{G}_1^T(0) = [\,0,\ 0,\ 0,\ 1,\ 0,\ 0\,] \qquad (3.1\text{-}3a)$$

$$\bar{G}_2^T(0) = [\,0,\ 1,\ 0,\ 0,\ 0,\ 0\,] \qquad (3.1\text{-}3b)$$

$$\bar{G}_3^T(0) = [\,0,\ 0,\ 0,\ 0,\ 0,\ 1\,] \qquad (3.1\text{-}3c)$$

Thus we see that all three of the $\bar{G}_i(\bar{s})$ satisfy the homogeneous boundary conditions $\bar{v} = 0$, $\frac{d\bar{w}}{d\bar{s}} = 0$, and $\bar{Q} = 0$ at the rigid clamp.

$\bar{G}_p(\bar{s})$ represents a particular solution to equations (2.5-3a-c) which is chosen in such a way that it satisfies the third non-homogeneous boundary condition at the rigid clamp, namely equation (2.6-1c) with $\bar{Q} = 1$. The initial conditions for $\bar{G}_p(\bar{s})$ at the rigid clamp are then given as:

$$\bar{G}_p^T(0) = [\, 0, \quad 0, \quad 1, \quad 0, \quad 0, \quad 0 \,] \qquad (3.1\text{-}4)$$

The choice of $\bar{Q} = 1$ in equation (3.1-4) is obviously not significant, since all quantities in the linear theory are directly proportional to $\bar{Q}$ and can be obtained for any value of $\bar{Q}$ once a solution using $\bar{Q} = 1$ has been generated.

Obviously, the total solution vector (3.1-1) will therefore satisfy all three boundary conditions at the rigid clamp, and it also contains three arbitrary parameters which can be chosen to satisfy the other three boundary conditions at the end of the range of $\bar{s}$.

Separately for each of the four sets of initial conditions, equations (2.5-3a-c) are then integrated numerically as a pure initial value problem. This will lead to a set of four independent solution vectors at each integration step within the bellows.

The actual numerical integration of equations (2.5-3a-c) using these four sets of initial conditions was performed by means of a standard[24] fourth-order Runge-Kutta method. In view of the accuracy (a detailed discussion of

the numerical results along with a discussion of the resulting computational error will be presented in Chapter 4) obtained with a fourth-order Runge-Kutta method, higher order[25] Runge-Kutta methods and self-correcting[26] Runge-Kutta methods were deemed unnecessary.

We employed an integration step size which varied with each shell element in the bellows. The actual value of the integration step size used in the numerical integrations was determined by a procedure of trial and error. Specifically, we chose a trial integration step size and then computed the resulting error in $\bar{Q}$ at the end of the range of $\bar{s}$ (the method for computing the error in $\bar{Q}$ will be discussed in Section 4.1) obtained from each of the four pure initial value problem solutions as well as the value of $\bar{Q}$ obtained for the total solution vector. The step size was then halved, and the corresponding error in $\bar{Q}$ was computed. The final integration step size was obtained when the error in $\bar{Q}$ was made[27] as small as possible. Using this method, we arrived at a final value for an average integration step size of $\Delta\bar{s} = 0.0005$. For one layer, we required 545 increments for each of the four pure initial value problem solutions. Using single precision on an IBM 360 computer, this resulted in an approximate execution time of two minutes for the solution of a single layer.

In order to obtain the total solution vector as defined by equation (3.1-1), we must determine the scalar multipliers λ_1, λ_2, and λ_3. This is accomplished by imposing the final three boundary conditions on $\bar{G}(\bar{s})$ at the end of the range of $\bar{s}$. The final three boundary conditions are given by equations (2.6-2a-b) and (2.9-2). This leads to a linear system of order three in the unknowns λ_1, λ_2, and λ_3. This linear system is then solved by Gaussian elimination for the three scalar multipliers. Having determined λ_1, λ_2, and λ_3, $\bar{G}(\bar{s})$ can then be determined at each step within the bellows. Hence various quantities of physical interest (e.g. displacements, components of stress) can also be computed at each integration step within the bellows. An extensive discussion of the numerical results will be presented in Chapter 4. In contrast to the exact-solution method which leads to a banded matrix of order 600 (with a corresponding band width of 18) or more to be inverted, the numerical method just developed requires only that we invert a matrix of order three at the far boundary. Furthermore, the use of equations (2.3-7a-c) which introduce the curvature of shell's meridian in the most general form, makes this method immediately applicable to welded bellows with <u>any</u> meridional shape whatsoever. This is not true for the other method whenever exact solutions are not available (e.g. cicular[28] meridians, elliptic[29] meridians, etc.).

The total machine program consisted essentially of four parts:

i) A code which applies the matching conditions to obtain the required set of six initial conditions at any juncture between shell elements.

ii) A code for the Runge-Kutta method applied four times to generate $\bar{G}_1(\bar{s})$, $\bar{G}_2(\bar{s})$, $\bar{G}_3(\bar{s})$, and $\bar{G}_p(\bar{s})$.

iii) A code to form the appropriate linear combination of the solutions for the quantities $\bar{v}$, $\bar{w}$, $\bar{Q}$, $\frac{d\bar{v}}{d\bar{s}}$, $\frac{d\bar{w}}{d\bar{s}}$, and $\frac{d^2\bar{w}}{d\bar{s}^2}$ obtained from (ii) to solve the specific boundary value problem defined by the farther edge conditions.

iv) A code to compute the various quantities of physical interest from the solutions for the six unknowns. A variety of different boundary value problems can be solved for a welded bellows with a given geometry using codes (iii) and (iv) after the four basic solutions have been obtained from codes (i) and (ii).

3.2 ANALYSIS OF WELDED BELLOWS WITH MANY LAYERS AND THE PROBLEM OF LOSS IN COMPUTATIONAL SIGNIFICANCE

Due to the accumulation of roundoff error, the application of any method of solution to equations (2.4-1a-c) will, for a welded bellows with a sufficiently large number of layers, lead to a loss in computational significance. The limit to the number of layers which can be analyzed without this loss in computational significance depends upon such

factors as integration step size, word length of the computing machine, thickness-diameter-ratio, and boundary conditions at the point where the initial conditions are specified. Of all these factors, we find the most important to be the thickness-diameter-ratio. As the thickness-diameter-ratio decreases, the maximum number of layers that can be analyzed without this loss in computational significance also decreases.

The accumulation of roundoff error causes each of the four independent pure initial value problem solutions to become increasingly inaccurate as $\bar{s}$ increases. Furthermore, the increasing distance away from the initial point causes each solution to "lose" the effect from the initial conditions; this results in the determinant of the coefficient matrix of the linear system involving the λ's tending to zero. Consequently, a sufficiently accurate solution for the λ's eventually cannot be obtained. It should be emphasized that the contribution to the overall error in the total solution vector $\bar{G}(\bar{s})$ from accumulated roundoff error is very small. The bulk of the overall error arises from the effect of the boundary conditions being "lost" which leads to a nearly singular matrix which must be inverted to obtain the three scalar multipliers. This inversion of a nearly singular matrix leads to a set of scalar multipliers which contain a substantial amount of error. Consequently, when the total solution vector $\bar{G}(\bar{s})$ is computed in accordance with equation (3.1-1), the small numerical error in the four independent solutions $\bar{G}_1(\bar{s})$,

$\bar{G}_2(\bar{s})$, $\bar{G}_3(\bar{s})$, and $\bar{G}_p(\bar{s})$ which is the outgrowth of accumulated roundoff error, is magnified considerably by the scalar multipliers which contain a large amount of error; hence a resultant error in $\bar{G}(\bar{s})$ which is large.

The physical interpretation of the near-singular coefficient matrix for the λ's is that as the integration process extends through more layers, the initial conditions specified at the rigid clamp (or any other type of outer support) become less significant. In essence, the boundary conditions at the rigid clamp have been "lost". This "loss" of the boundary conditions at the rigid clamp is manifested mathematically by an inaccurate solution for the λ's. One indication that the solution for the λ's is inaccurate, is that the "residuals" (the difference between the left and right hand sides of the linear system) are large. Another is that one of the solved scalar multipliers is large in comparison to the other two.

A reliable check on the accuracy of any solution can easily be made by comparing the computed value of $\bar{Q}$ along any horizontal section with the exact value of $\bar{Q}$ obtained from the requirement of overall static equilibrium.

In order to analyze welded bellows with many layers without this eventual loss in computational significance, we shall develop an alternate method of analysis which is based upon the concepts of a "boundary layer" and an "interior layer". The discussion of this method will be presented in Section 4.4.

CHAPTER 4

DISCUSSION OF RESULTS

The various physical quantities of interest such as displacement, stress variation, and peak stress will be presented for three basic thickness-diameter-ratios. These three basic thickness-diameter-ratios range from 0.01 which characterizes a "thick" bellows to 0.001 which characterizes a "thin" bellows. An intermediate value of 0.003162 is included to correspond to a "medium" bellows. Bellows are not normally manufactured with thickness-diameter-ratios outside this range. For the purposes of investigating the various effects of the welds, a range of values of β from 0.0 up to 1.3 will be used. A boundary layer effect will be described and the concept of an interior layer developed. The concept of an interior layer will be used to calculate the flexibility of a welded bellows with 34 layers, which has also been measured experimentally. The calculated value of flexibility will be found to compare favorably with the value obtained experimentally.

The results which follow are based upon the analysis of a welded bellows which is subjected to an axial force (i.e., Y = 0, Z = 0 in equations (2.4-1a-c)). The bellows is not prestressed and its weight is neglected. The other solution for loading from an internal pressure p can readily be obtained by setting Y = 0, Z = p in equations (2.4-1a-c)

and applying the method of solution described in Chapter 3. In formulating the solution for an internal pressure, the set of dimensionless variables given by equations (2.5-1a-f) must be replaced by another appropriate set of dimensionless variables. This is necessitated by the fact that in the internal pressure application of a welded bellows $\mathcal{Y} = 0$; hence equations (2.5-1a-c) and (2.5-2a-c) become invalid. Consequently, we must set $\mathcal{Y} = pd$ in equations (2.5-1a-c) and (2.5-2a-c) and retain the other dimensionless variables as they appear in equations (2.5-1d-f) in order to obtain a set of dimensionless variables which is appropriate to the internal pressure application of a welded bellows. Then, any problem which involves loading by both an axial force and an internal pressure can be solved by superimposing the solutions for each respective problem. It should be noted that since we have a different set of dimensionless variables associated with the axial force and internal pressure loading problem, we must transform all solutions to dimensional form before superimposing. The specific shape which we used in this investigation consisted of three flat plates, two cones with equal vertex angles, and toroidal welds with circular cross-sections. Except for one particular set of dimensions that correspond to a particular welded bellows which was used to experimentally confirm (see Section 4.5) the theoretical method, <u>all</u> of the results which follow are based upon the dimensionless geometry of one layer shown in Fig. 4.1.

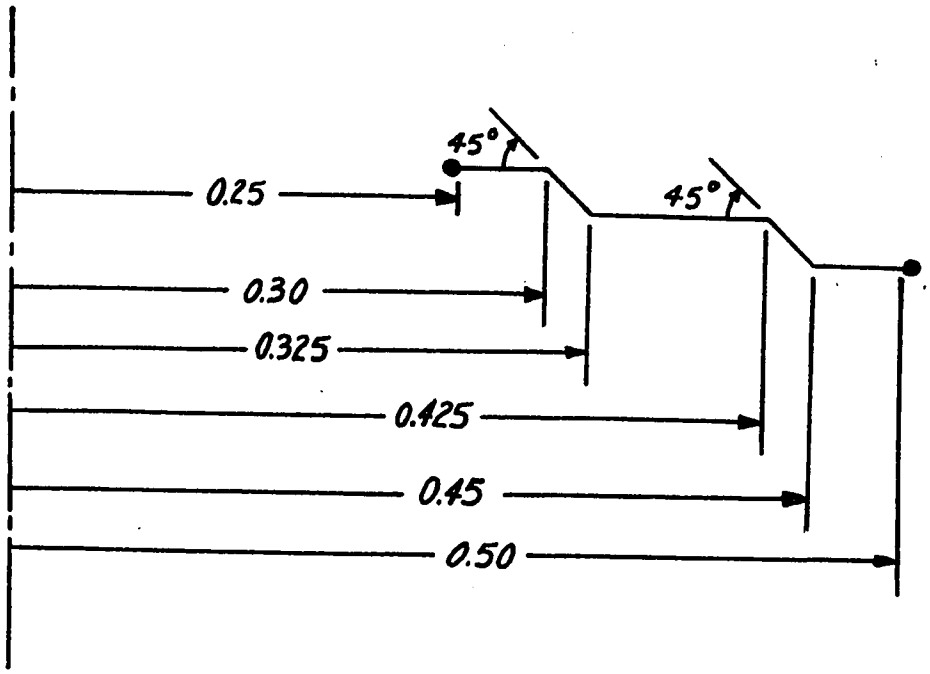

Figure 4.1 Dimensionless Geometry of One Layer

With the exception of one solution in which we set $\nu = 0.409$ for the purpose of confirming certain experimental measurements, all of the results presented here have been calculated with $\nu = 0.28$, corresponding to normal stainless steel. However, all results showed a great insensitivity to large variations in ν.

4.1 DISCUSSION OF NUMERICAL ERROR

In Section 3.2, we indicated that the error at the end of the numerical integration process for any of the four independent pure initial value solutions could be measured by checking the value of $\bar{Q}$ obtained at the end of the integration process. Since the exact value of $\bar{Q}$ at any point on the

meridian where the line of action of $\bar{Q}$ and the normal to the meridian are parallel is, by virtue of static equilibrium (Green's Theorem):

$$\bar{Q}_{exact} = \bar{Q}^* \frac{\bar{r}^*}{\bar{r}} \qquad (4.1\text{-}1)$$

where $\bar{Q}^*$ is the actual value of applied transverse shear and $\bar{r}^*$ is the radial location of its point of application. Since the value of $\bar{Q}^*$ and $\bar{r}^*$ is known for each of the four pure initial value problem solutions, the error in $\bar{Q}$ may be determined exactly at the end of each machine integration merely by comparing the value of $\bar{Q}$ obtained numerically with the exact value given by equation (4.1-1).

For the combined solution, as given by equation (3.1-1), the magnitude of the per cent error in the final value of $\bar{Q}$ is plotted as a function of the number of layers from the rigid clamp to the bellows' mid-plane of symmetry and is presented in Fig. 4.2a. Another quantity which describes how quickly the boundary conditions at the rigid clamp are being "lost" is the determinant of the normalized coefficient matrix in the linear system which is solved for the scalar multipliers λ_1, λ_2, and λ_3. This normalized coefficient matrix is formed by scaling each row so that the first column of the scaled coefficient matrix consists solely of unit values. The magnitude of this matrix's determinant $|D|$ is plotted on the same set of axes with the

magnitude of the per cent error in $\bar{Q}$ obtained at the end of the integration process. These results are indicated in Fig. 4.2a. From Fig. 4.2a, one might be tempted to conclude that the linear system involving the λ's is becoming more poorly conditioned for a fixed number of layers as $\frac{t}{d}$ decreases. However, it should be noted that a small determinant does not necessarily imply that a linear system is poorly conditioned; rather, the condition of a linear system is determined by its condition number. Nevertheless, the fact that in our computations the value of $|D|$ is decreasing, while the associated error in $\bar{Q}$ is increasing, tends to indicate that for a fixed number of layers, as $\frac{t}{d}$ decreases, the resulting linear system at the end of the range of $\bar{s}$ is becoming more poorly conditioned. In order to show this conclusively, we calculated the condition number of each linear system which was solved. The calculation of a condition number requires the use of a matrix "norm". Specifically, using a given matrix norm, the condition number of a linear system is calculated by forming the product of the particular norm of the coefficient matrix with the corresponding norm of the inverse of the coefficient matrix. The most common condition number (for a symmetric matrix) uses the "two norm" (magnitude of largest eigenvalue) and is equal to the absolute value of the largest eigenvalue to the smallest eigenvalue. The "one norm" (maximum absolute column sum) and the "maximum norm" (maximum absolute row sum) are also used to compute condition numbers. Since all matrix norms are related to each other, if one condition number

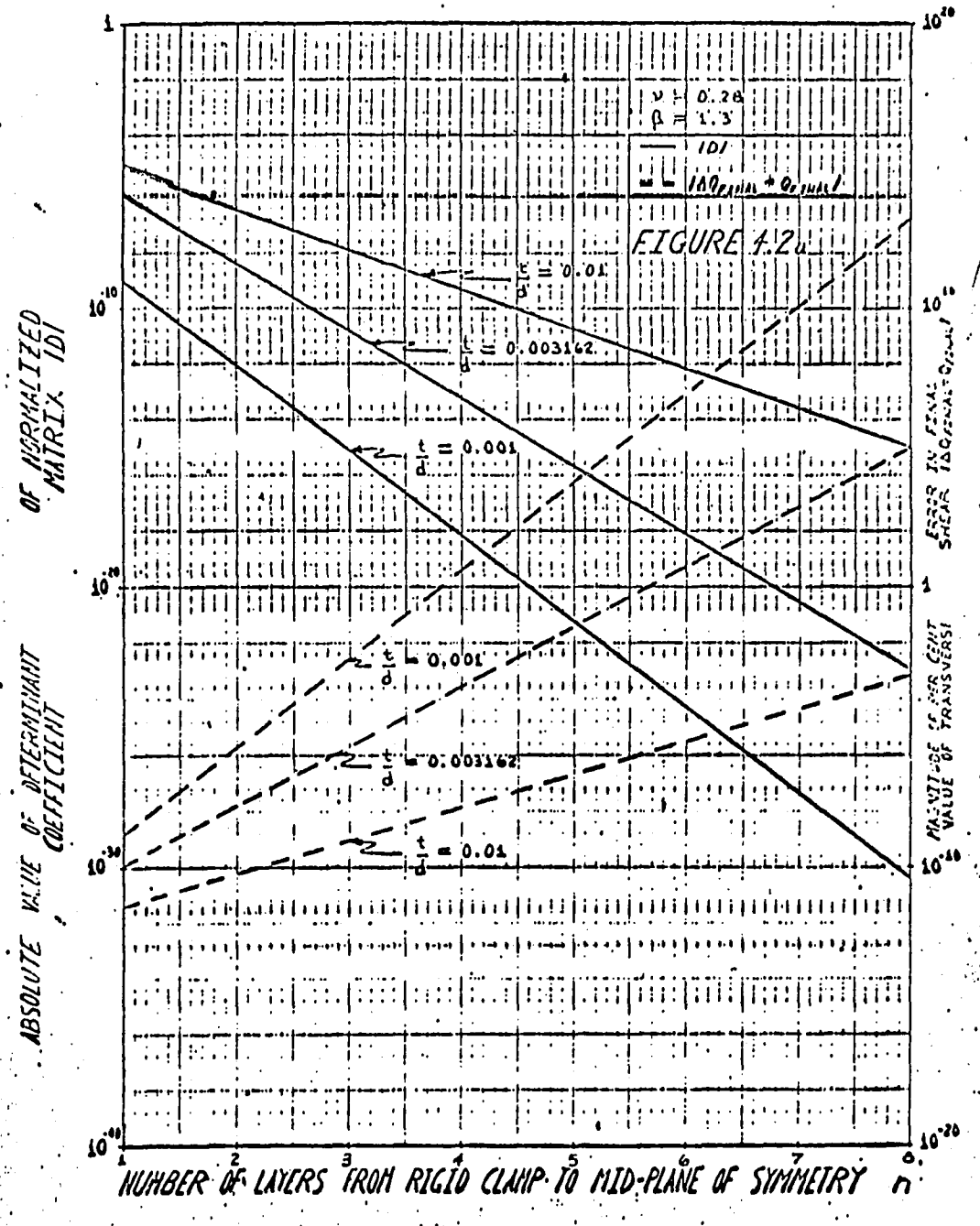
ABSOLUTE VALUE OF DETERMINANT OF NORMALIZED MATRIX |D|
COEFFICIENT
ERROR IN FINAL SHEAR ORDINATE
MAGNITUDE OF ERROR IN SHEAR VALUE OF TRANSVERSE
NUMBER OF LAYERS FROM RIGID CLAMP TO MID-PLANE OF SYMMETRY n
ν = 0.28
β = 1.3
|D|
|D|FINAL + |D|INITIAL
t/d = 0.01
t/d = 0.003162
t/d = 0.001
t/d = 0.001
t/d = 0.003162
t/d = 0.01
1
10^-10
10^-20
10^-30
10^-40
10^-20
10^-10
1
10^-10
10^-20
1
2
3
4
5
6
7
8

FIGURE 4.2a

FIGURE 4.2b

CRITICAL NUMBER OF THE COEFFICIENT WHICH BEGIN THE LOCAL BUCKLING

FIGURE 4.3

indicates ill conditioning, any other condition number will do the same. Consequently, for the sake of convenience (the coefficient matrices of our linear systems were not symmetric), we used the one norm to calculate a condition number. The corresponding results are shown in Fig. 4.2b. Fig. 4.2b clearly indicates that for a fixed number of layers, as the $\frac{t}{d}$ ratio decreases, the resulting linear system at the end of the range of $\bar{s}$ does indeed become more poorly conditioned. Furthermore, from Fig. 4.2a it is evident that the $\frac{t}{d}$ ratio plays a very important role in the growth of computational error. Employing a maximum error tolerance for $\bar{Q}$ of 1%, we were able to analyze three layers for the thin bellows, five layers for the medium bellows, and ten layers for the thick bellows; hence using symmetry, six, ten, and twenty layers respectively. The maximum ("critical") number of layers for a half-bellows which can be analyzed with a maximum error in $\bar{Q}$ of less than 1% as a function of $\frac{t}{d}$ is presented in Fig. 4.3. The analysis of welded bellows having more than the critical number of layers will described in Section 4.4.

4.2 DISCUSSION OF PHYSICAL QUANTITIES OF INTEREST FOR WELDED BELLOWS ($\beta = 1.3$)

4.2.1 DISPLACEMENTS

The results shown in Figs. 4.4a-c and 4.5a-c indicate the differences between the tangential component of displacement $\bar{v}$ and the normal component of displacement $\bar{w}$ for a clamped layer and an interior layer. Both $\bar{v}$ and $\bar{w}$ are

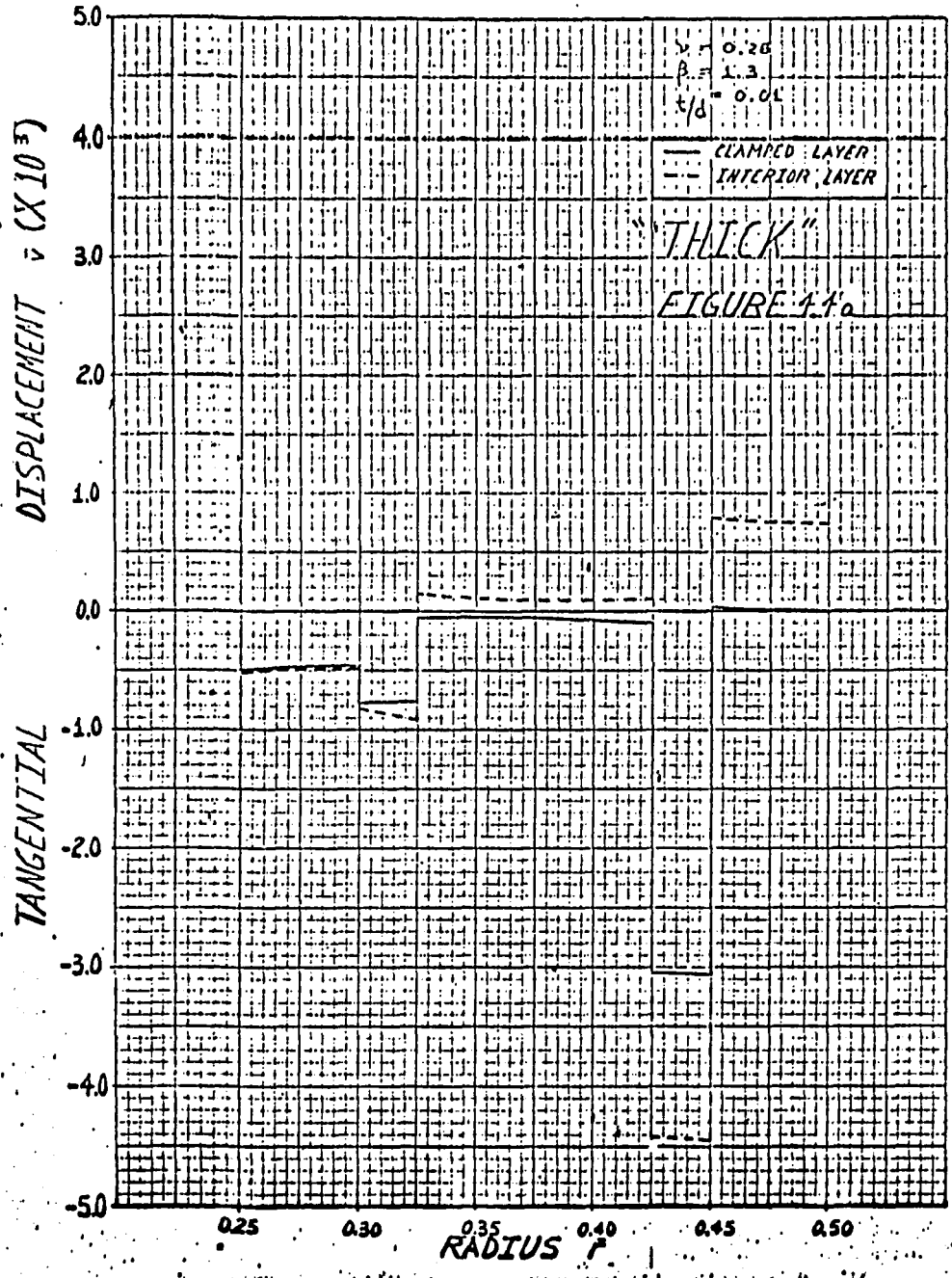
TANGENTIAL DISPLACEMENT v (X 10³)
5.0
4.0
3.0
2.0
1.0
0.0
-1.0
-2.0
-3.0
-4.0
-5.0
0.25
0.30
0.35
0.40
0.45
0.50
RADIUS r
ν = 0.28
β = 1.3
t/d = 0.01
CLAMPED LAYER
INTERIOR LAYER
"THICK"

FIGURE 44a

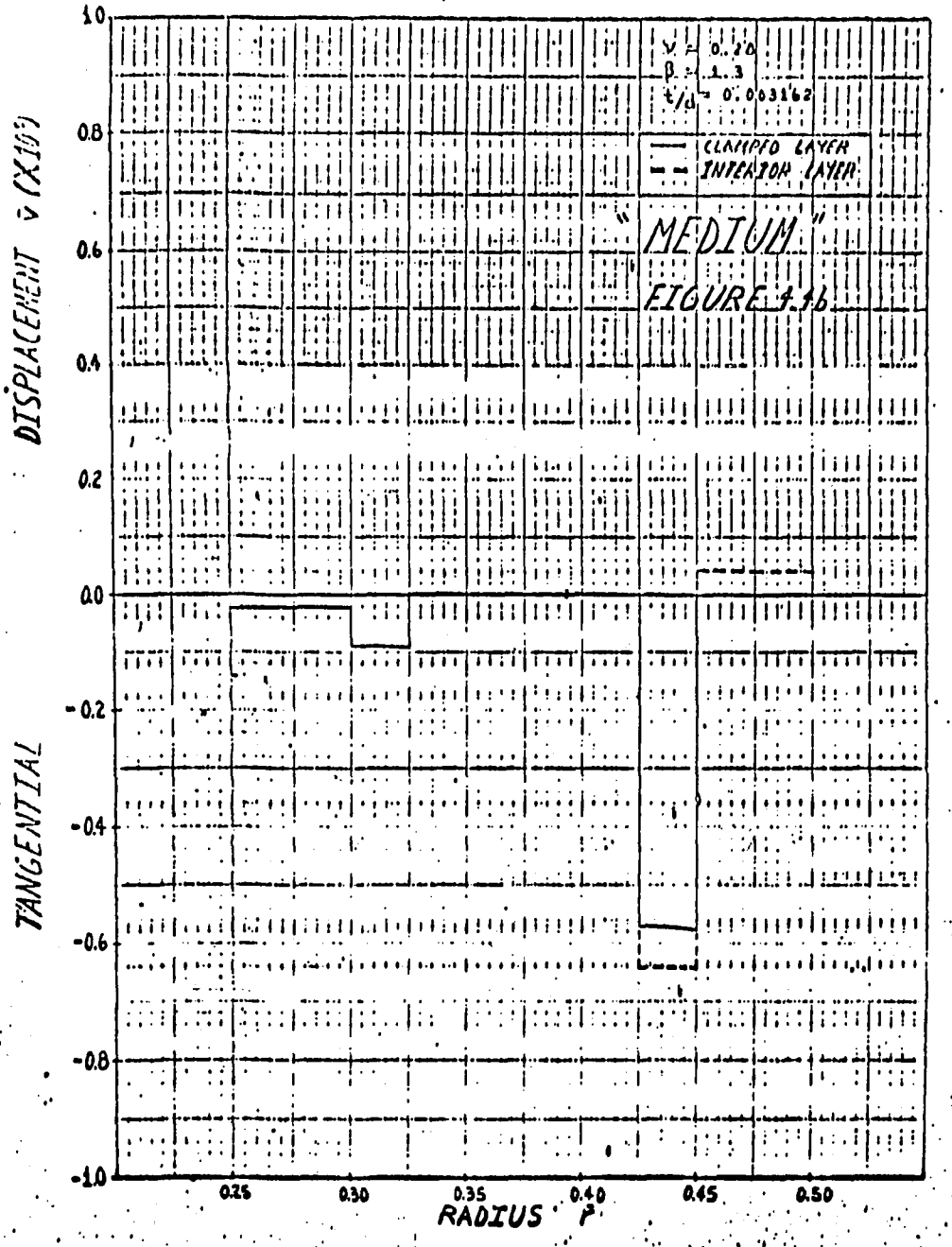
DISPLACEMENT v (X10⁵)
TANGENTIAL
RADIUS r
ν = 0.20
β = 1.3
t/d = 0.063162
CLAMPED LAYER
INTERIOR LAYER
"MEDIUM"
FIGURE 4.4b
1.0
0.8
0.6
0.4
0.2
0.0
-0.2
-0.4
-0.6
-0.8
-1.0
0.25
0.30
0.35
0.40
0.45
0.50

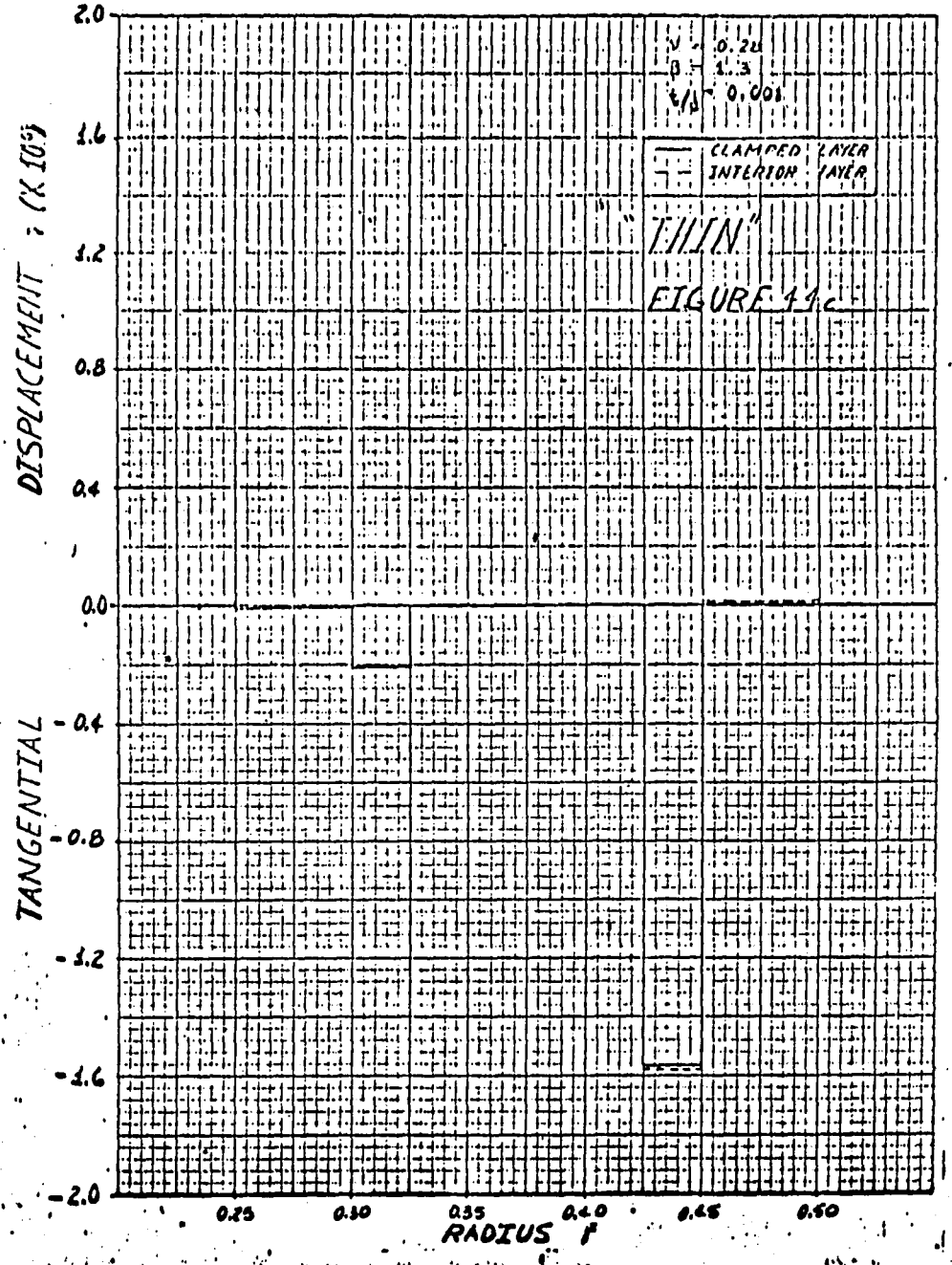
2.0
1.6
1.2
0.8
0.4
0.0
- 0.4
- 0.8
- 1.2
- 1.6
- 2.0
DISPLACEMENT = (X 10⁵)
TANGENTIAL
0.25
0.30
0.35
0.40
0.45
0.50
RADIUS r
ν = 0.28
β = 1.3
t/l = 0.001
CLAMPED
INTERIOR
LAYER
LAYER
"THIN"
FIGURE 11c

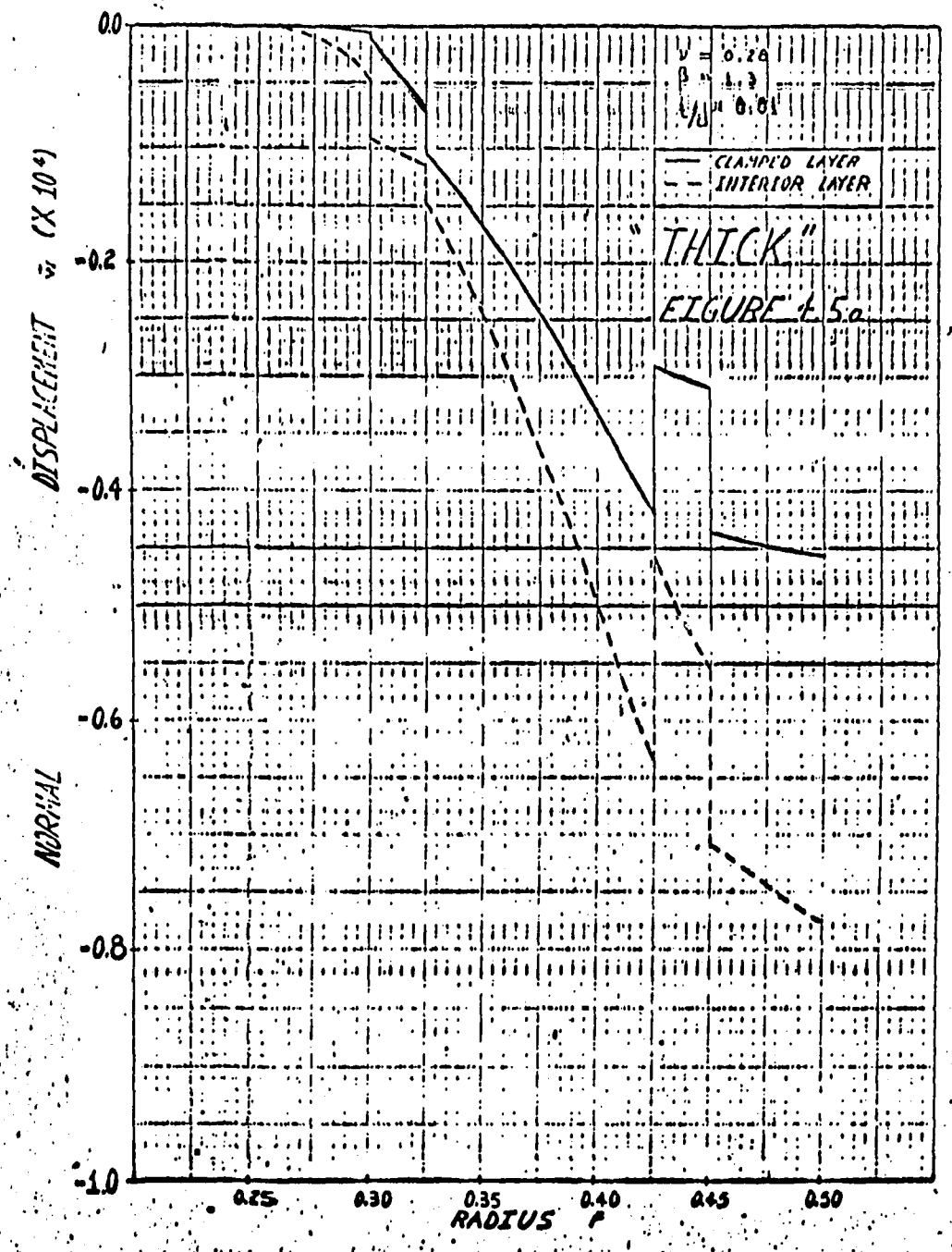
0.0
-0.2
-0.4
-0.6
-0.8
-1.0
NORMAL DISPLACEMENT w (X 10⁻⁴)
0.25
0.30
0.35
0.40
0.45
0.50
RADIUS r
ν = 0.29
β = 1.3
t/a = 0.01
CLAMPED LAYER
INTERIOR LAYER
"THICK"
FIGURE 4.5a

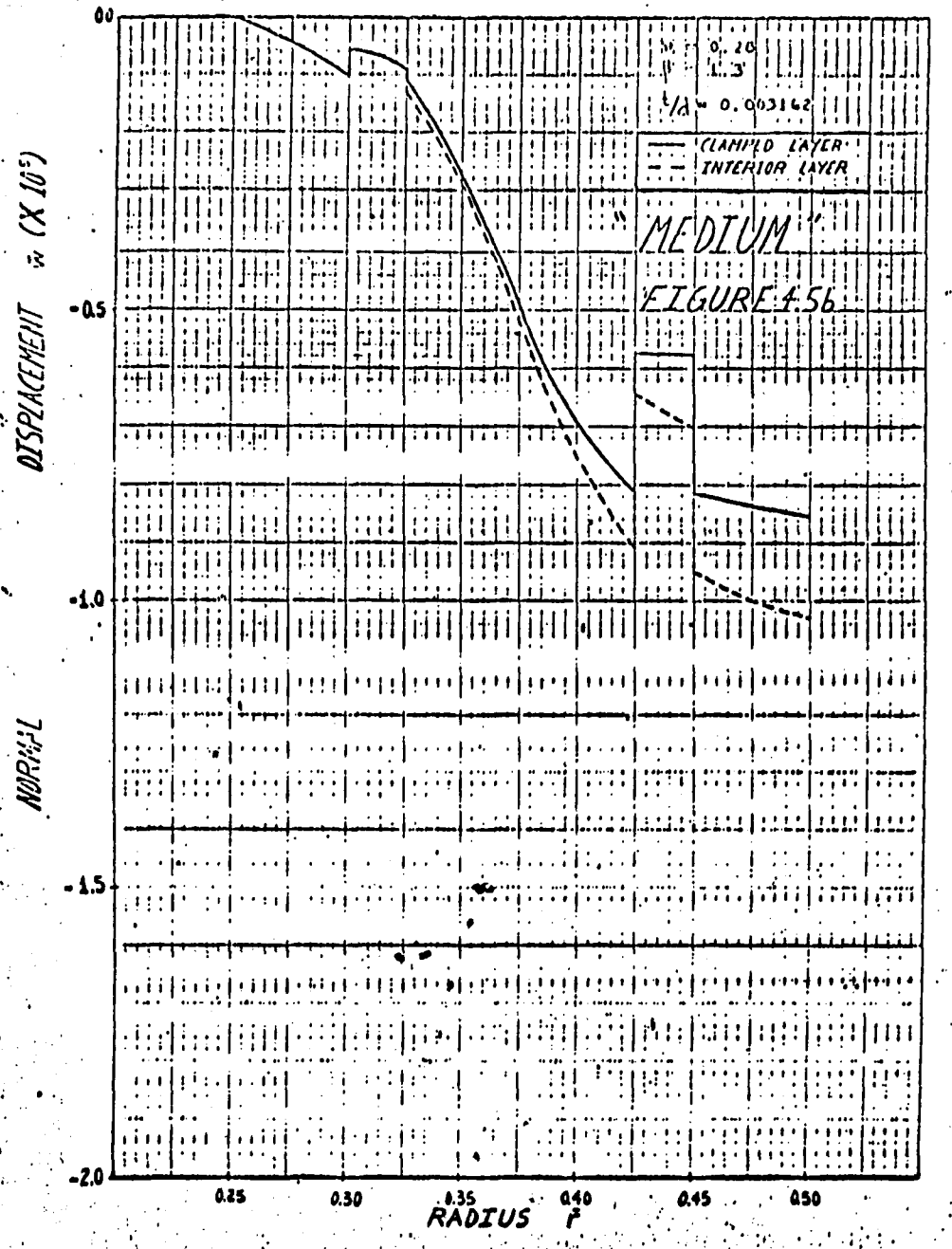
0.0
-0.5
-1.0
-1.5
-2.0
0.25
0.30
0.35
0.40
0.45
0.50
RADIUS r
NORMAL DISPLACEMENT w (X 10⁵)
ν = 0.20
L/a = 3
1/λ = 0.003162
CLAMPED LAYER
INTERIOR LAYER
"MEDIUM"
FIGURE 4.56

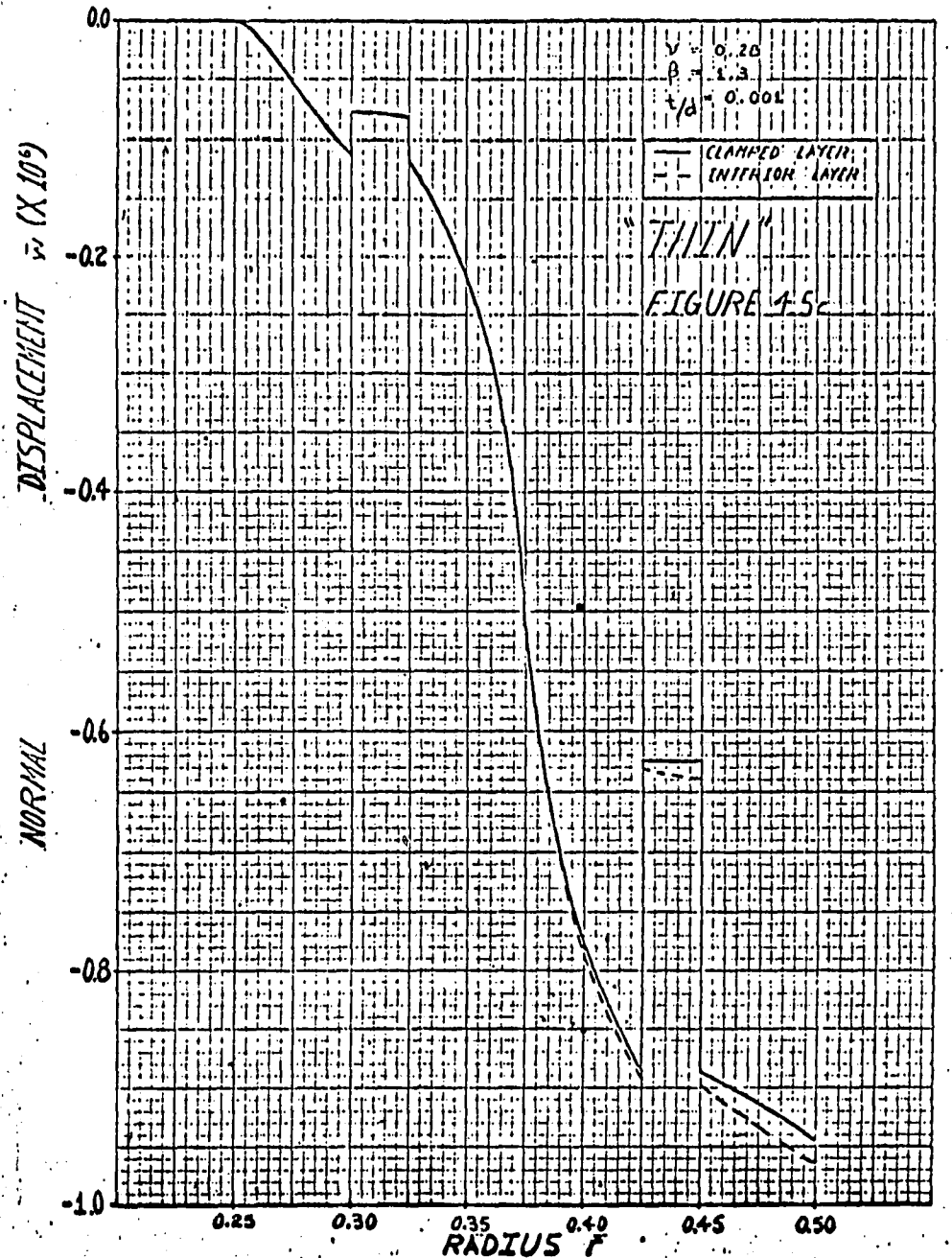
0.0
-0.2
-0.4
-0.6
-0.8
-1.0
NORMAL DISPLACEMENT w (X 10⁶)
0.25
0.30
0.35
0.40
0.45
0.50
RADIUS r
ν = 0.20
β = 1.3
t/d = 0.001
CLAMPED LAYER
INTERIOR LAYER
"THIN"

FIGURE 4.5c

discontinuous at every juncture between shell elements; these discontinuities are caused by the fact that the meridian does not have a continuous tangent at these junctures. As should be expected, the interior layer deflects more than the clamped layer. Except for magnitude, the patterns for $\bar{v}$ and $\bar{w}$ remain largely unchanged over the wide range of thickness-diameter-ratio variation.

By means of the appropriate linear combination of $\bar{v}$ and $\bar{w}$ at each point within the clamped and interior layers, we obtain $\bar{V}$ and $\bar{W}$, the components of displacement measured perpendicular and parallel to the bellows' axis, respectively. They are given by means of the relations:

$$\bar{V} = \cos\varphi\,\bar{v} - \sin\varphi\,\bar{w} \qquad (4.2.1\text{-}1a)$$

$$\bar{W} = \sin\varphi\,\bar{v} + \cos\varphi\,\bar{w} \qquad (4.2.1\text{-}1b)$$

The positive directions for $\bar{V}$ and $\bar{W}$ are to the right and down, respectively. These displacements are presented in Figs. 4.6a-c and 4.7a-c. Since $\bar{V}$ and $\bar{W}$ are measured with respect to a fixed coordinate system, they must be continuous. The apparent rapid variation in $\bar{V}$ which appears in Fig. 4.6c is not due to any abnormality in the numerical solution, but rather to a reduction of two orders of magnitude which results when two large numbers which are almost equal are combined in accordance with equations (4.2.1-1a-b).

4.2.2 TRANSVERSE SHEAR

Figs. 4.8a-c show the variation of the transverse

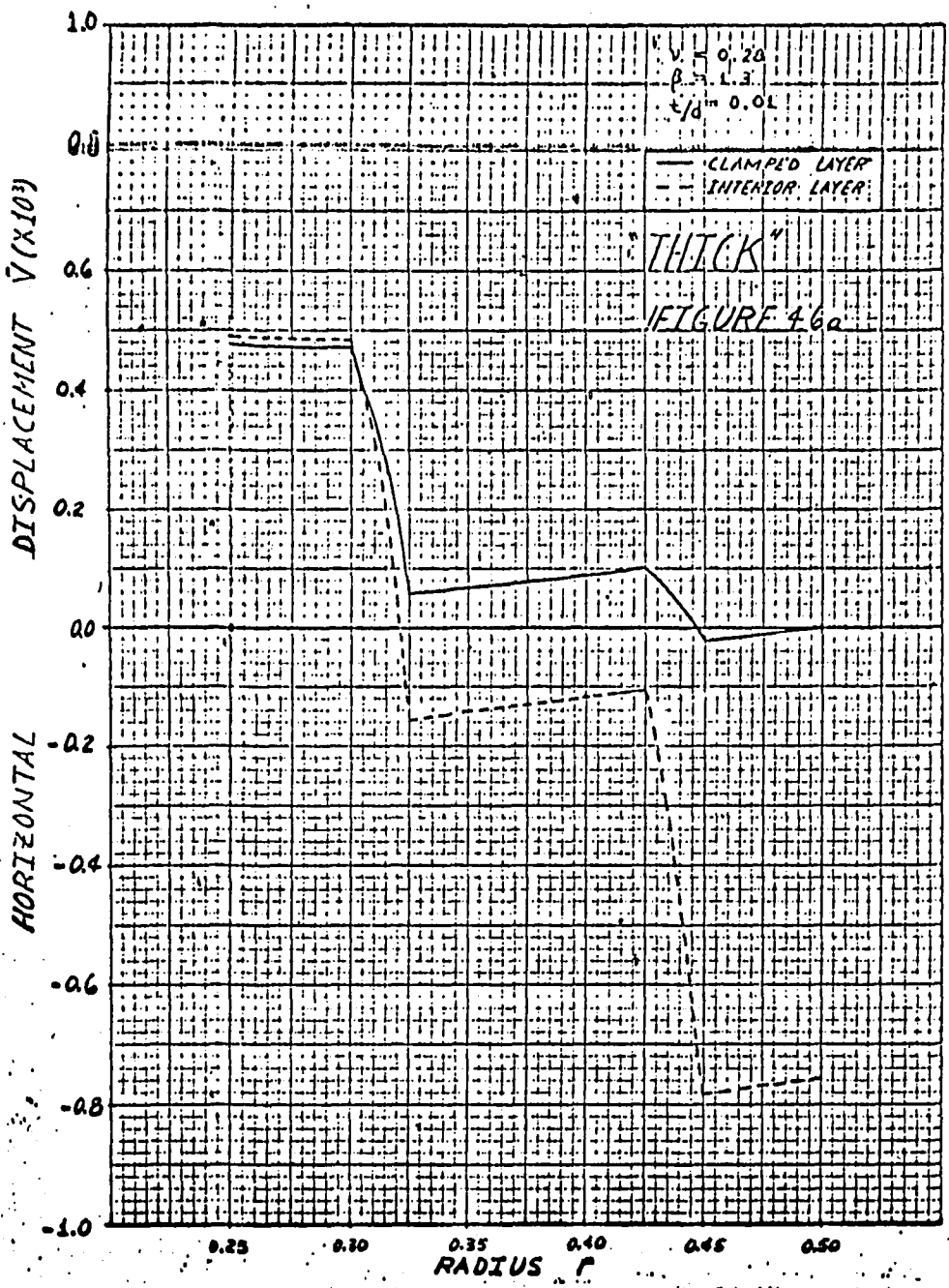
1.0
0.8
0.6
0.4
0.2
0.0
-0.2
-0.4
-0.6
-0.8
-1.0
DISPLACEMENT V (X10³)
HORIZONTAL
0.25
0.30
0.35
0.40
0.45
0.50
RADIUS r
ν = 0.20
β = 1.3
t/a = 0.01
CLAMPED LAYER
INTERIOR LAYER
THICK
FIGURE 46a

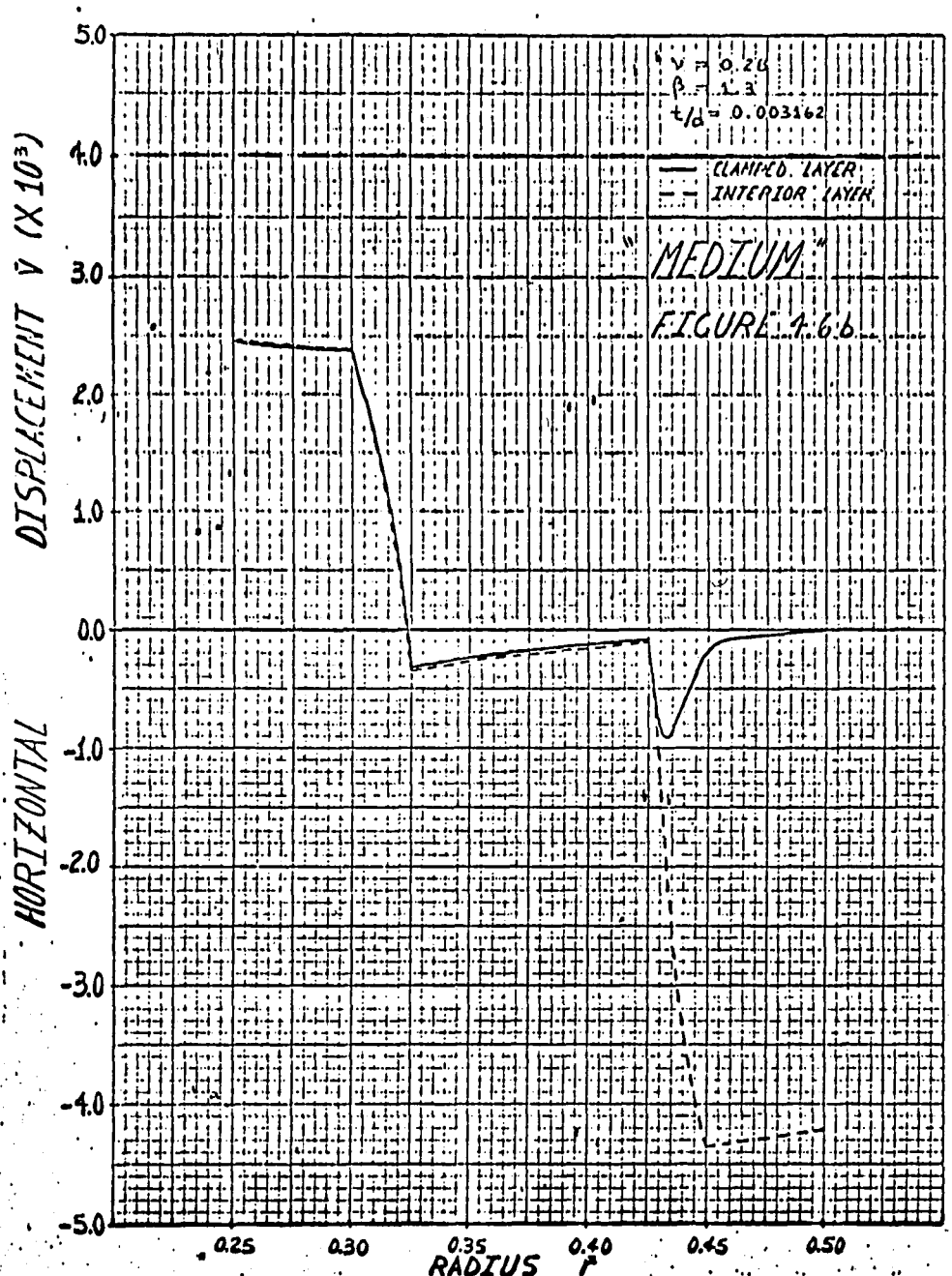
ν = 0.24
β = 1.3
t/d = 0.003162
CLAMPED LAYER
INTERIOR LAYER
"MEDIUM"
FIGURE 4.6b
DISPLACEMENT V (X 10³)
HORIZONTAL
5.0
4.0
3.0
2.0
1.0
0.0
-1.0
-2.0
-3.0
-4.0
-5.0
0.25
0.30
0.35
0.40
0.45
0.50
RADIUS r*

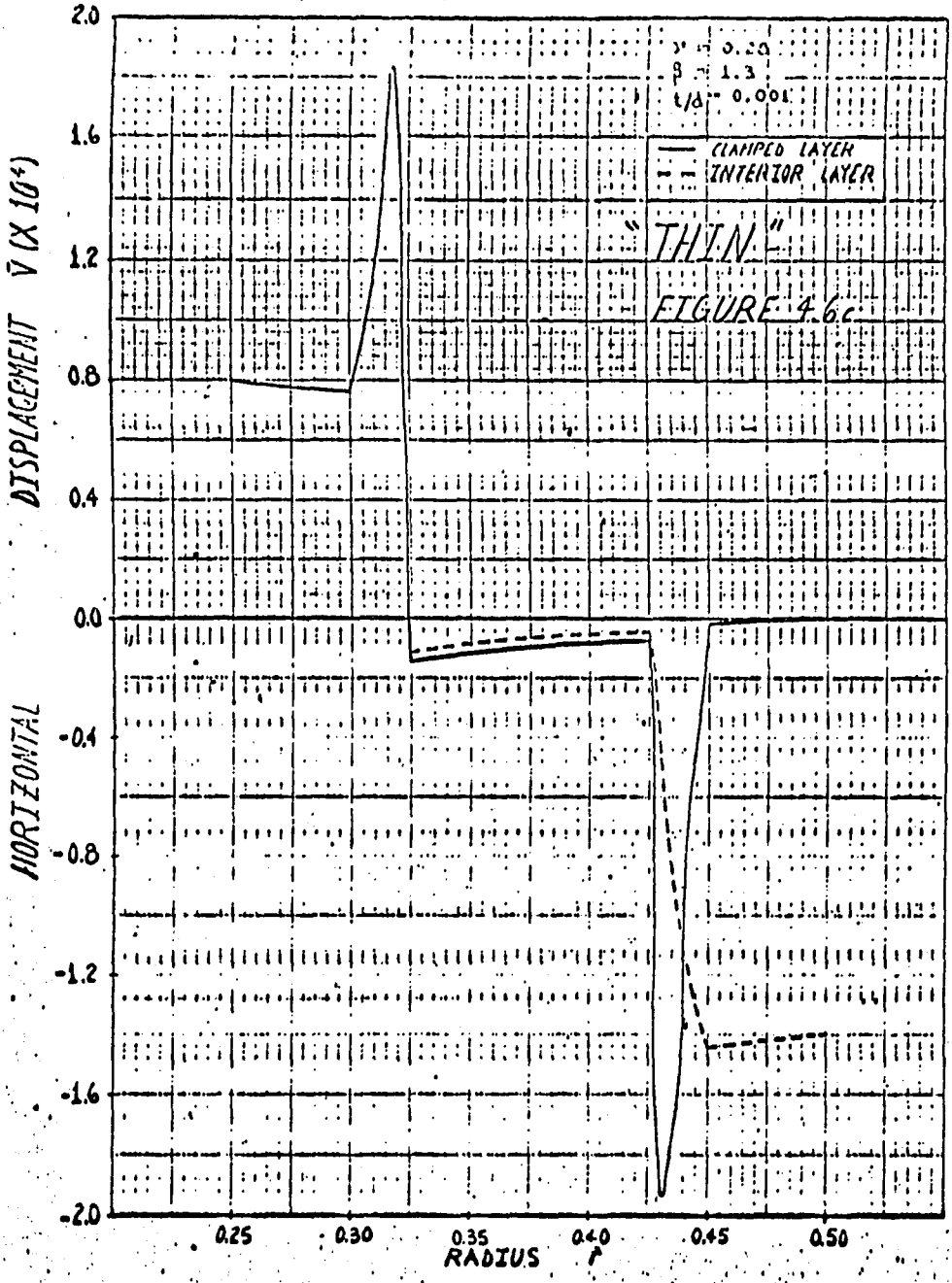
HORIZONTAL DISPLACEMENT $\bar{V}$ (X 10^{-4})
2.0
1.6
1.2
0.8
0.4
0.0
-0.4
-0.8
-1.2
-1.6
-2.0
0.25
0.30
0.35
0.40
0.45
0.50
RADIUS r
γ = 0.20
β = 1.3
t/a = 0.001
CLAMPED LAYER
INTERIOR LAYER
"THIN"

FIGURE 4.6c

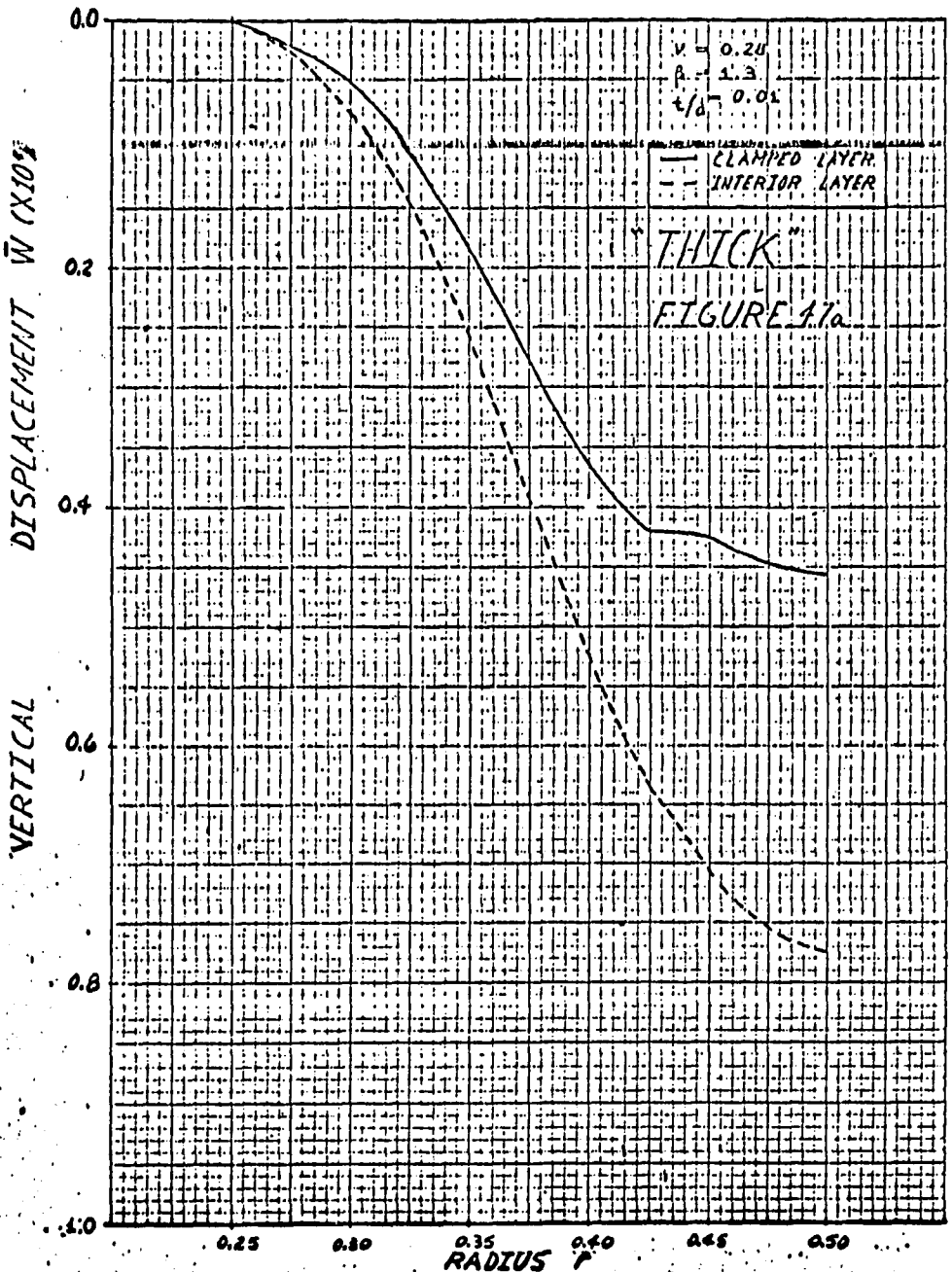
0.0
0.2
0.4
0.6
0.8
1.0
VERTICAL DISPLACEMENT $\bar{W}$ (X10³)
0.25
0.30
0.35
0.40
0.45
0.50
RADIUS r
ν = 0.20
β = 1.3
t/a = 0.01
CLAMPED LAYER
INTERIOR LAYER
"THICK"

FIGURE 17a

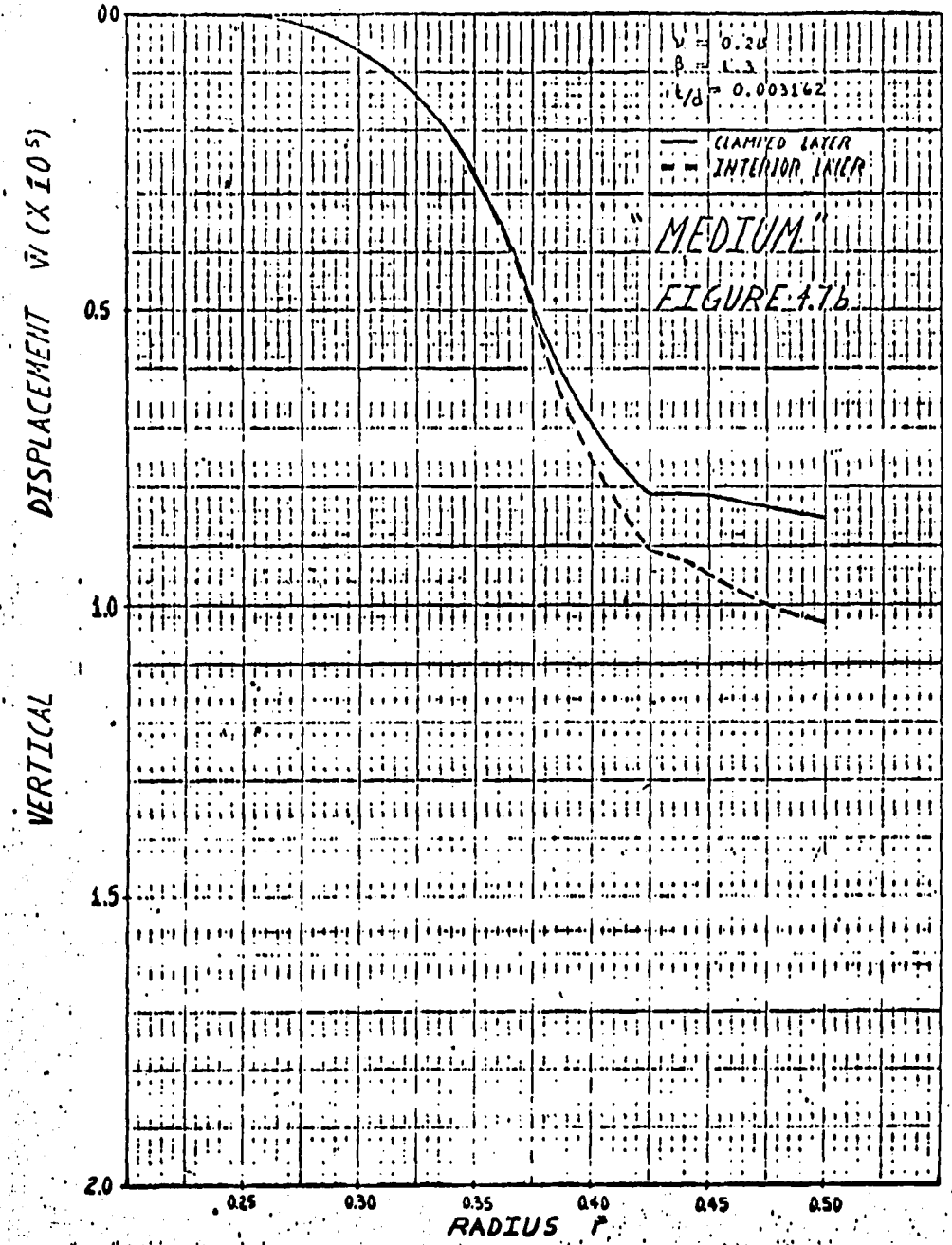
0.0
0.5
1.0
1.5
2.0
0.25
0.30
0.35
0.40
0.45
0.50
VERTICAL DISPLACEMENT $\bar{w}_i$ (X 10^5)
RADIUS r
ν = 0.20
β = 1.3
t/d = 0.003162
CLAMPED LAYER
INTERIOR LAYER
"MEDIUM"
FIGURE 4.7b

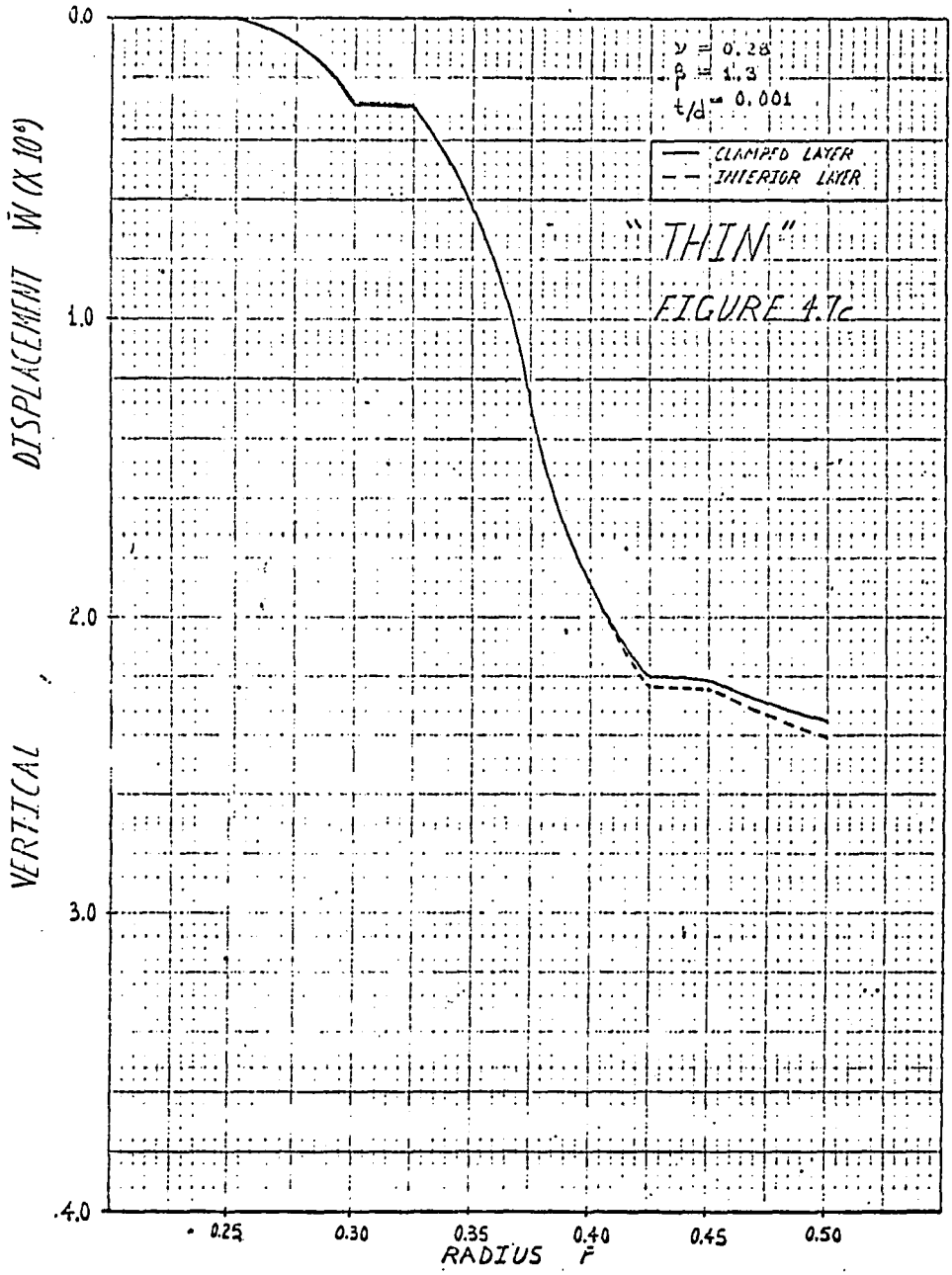
0.0
1.0
2.0
3.0
4.0
VERTICAL DISPLACEMENT $\bar{W}$ (X 10^6)
0.25
0.30
0.35
0.40
0.45
0.50
RADIUS $\bar{r}$
ν = 0.28
β = 1.3
t/d = 0.001
CLAMPED LAYER
INTERIOR LAYER
"THIN"

FIGURE 4.7c

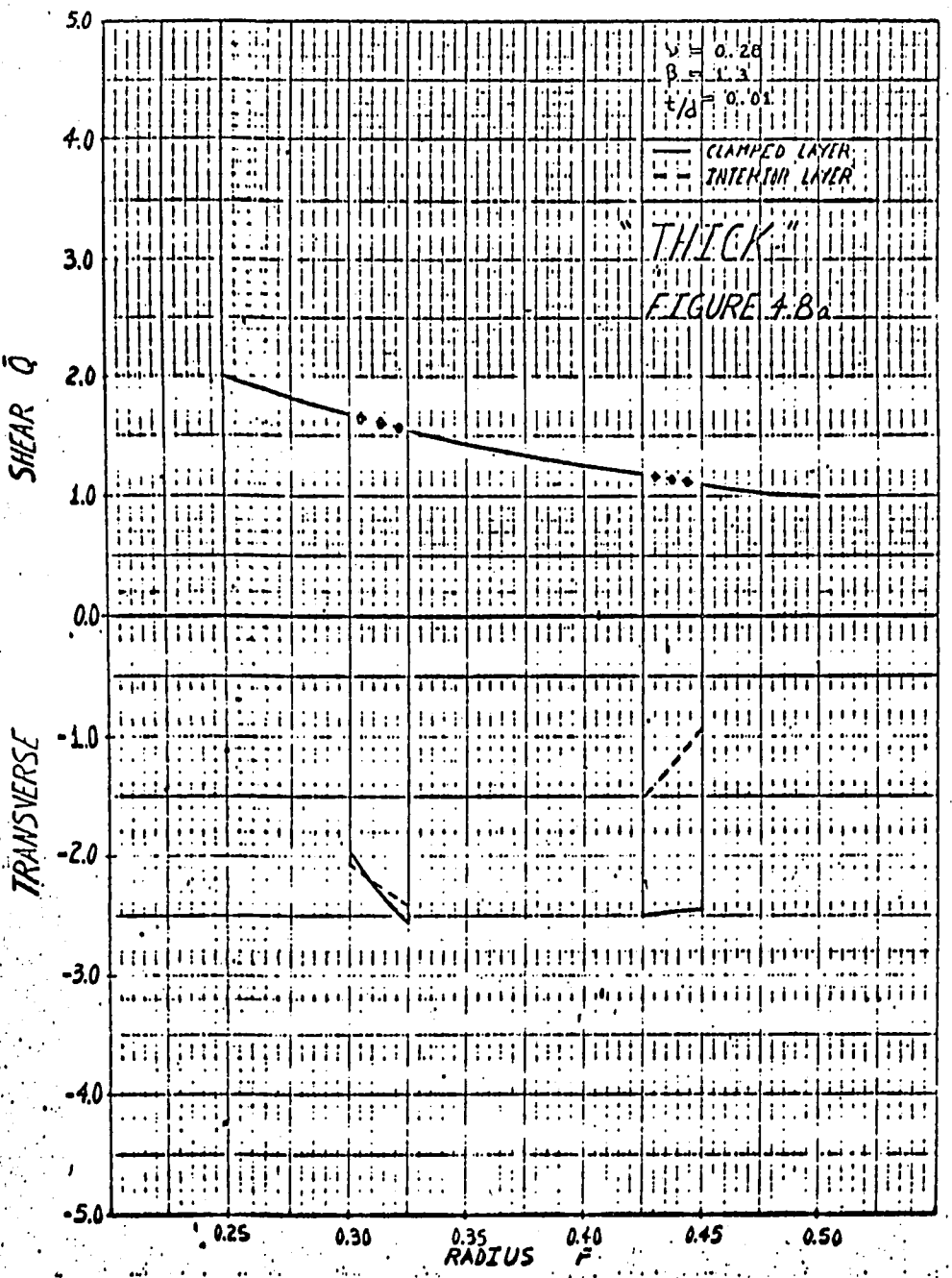
5.0
4.0
3.0
2.0
1.0
0.0
-1.0
-2.0
-3.0
-4.0
-5.0
SHEAR Q
TRANSVERSE
0.25
0.30
0.35
0.40
0.45
0.50
RADIUS r
ν = 0.28
β = 1.3
t/d = 0.01
CLAMPED LAYER
INTERFACE LAYER
"THICK"
FIGURE 4.8a

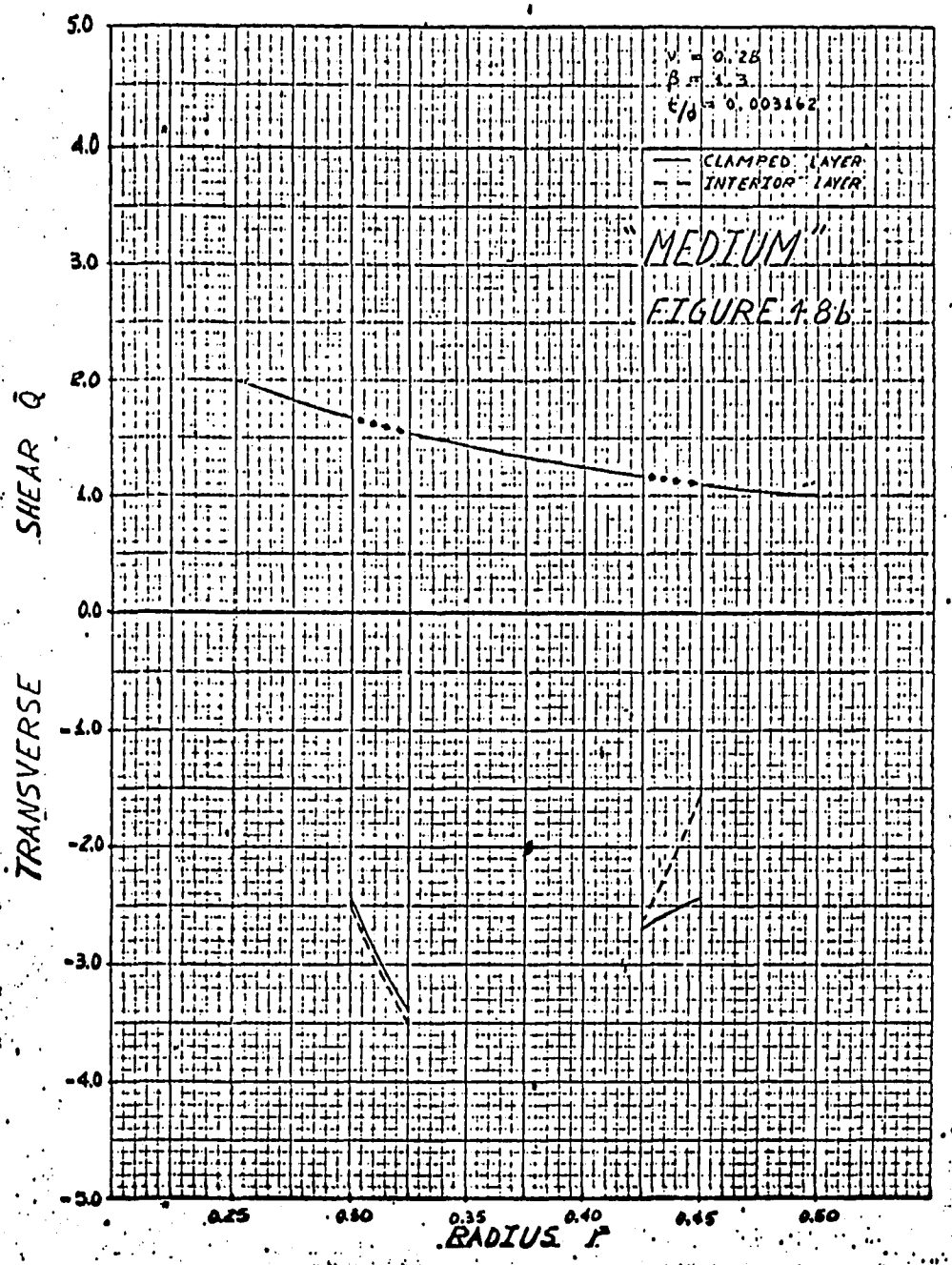
5.0
4.0
3.0
2.0
1.0
0.0
-1.0
-2.0
-3.0
-4.0
-5.0
0.25
0.30
0.35
0.40
0.45
0.50
TRANSVERSE SHEAR Q
RADIUS r
ν = 0.28
β = 1.3
t/a = 0.003162
CLAMPED LAYER
INTERIOR LAYER
"MEDIUM"
FIGURE 4.8b

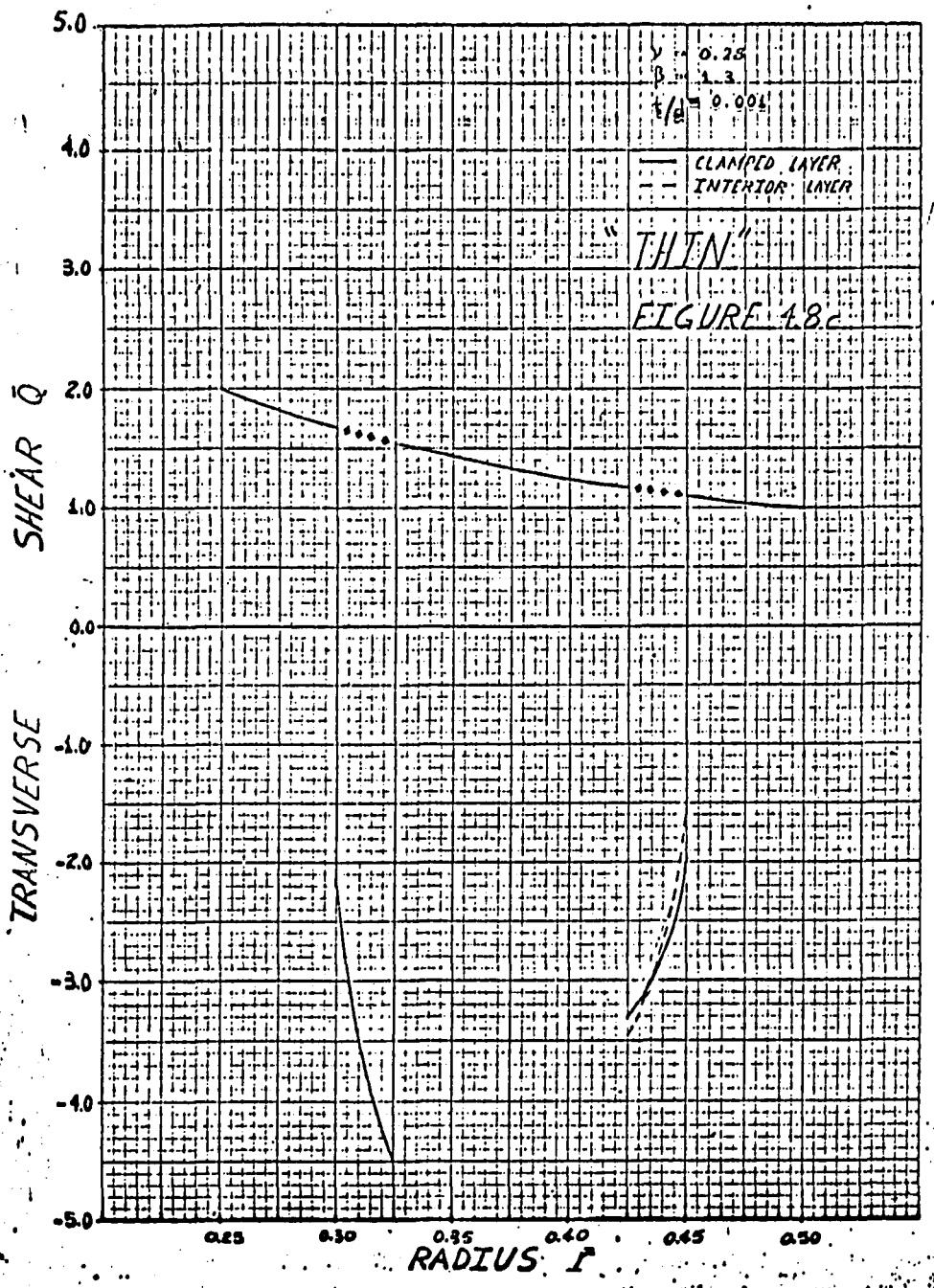
5.0
4.0
3.0
2.0
1.0
0.0
-1.0
-2.0
-3.0
-4.0
-5.0
TRANSVERSE SHEAR Q
0.25
0.30
0.35
0.40
0.45
0.50
RADIUS r
ν = 0.28
β = 1.3
t/ℓ = 0.001
CLAMPED LAYER
INTERIOR LAYER
"THIN"
FIGURE 4.8c

shear $\bar{Q}$. If we set $\bar{Q}^* = 1.0$ and $\bar{r}^* = 0.5$ in equation (4.1-1), then at any point on any plate, $\bar{Q}$ must satisfy the relation:

$$\bar{Q}(\bar{r}) = \frac{1}{2\bar{r}} \qquad (4.2.2\text{-}1)$$

This equilateral hyperbola is indicated on Figs. 4.8a-c by means of the dotted curve with the circles. Since $\bar{Q}$ is governed by equation (4.2.2-1) on any plate, $\bar{Q}$ must have the same value on the plates in both the clamped and interior layers, for any thickness-diameter-ratio.

4.2.3 MEMBRANE STRESSES

The results in Figs. 4.9a-c and 4.10a-c illustrate the effects of the $\frac{t}{d}$ ratio upon the meridional membrane stress $\overline{\sigma}^{\,e}_{s}$ and the circumferential membrane stress $\overline{\sigma}^{\,e}_{\theta}$. These stresses are calculated by means of the relations:

$$\overline{\sigma}^{\,e}_{s} = \frac{\bar{N}_s}{\bar{t}} \qquad (4.2.3\text{-}1a)$$

$$\overline{\sigma}^{\,e}_{\theta} = \frac{\bar{N}_\theta}{\bar{t}} \qquad (4.2.3\text{-}1b)$$

For the whole range of $\frac{t}{d}$ ratios, for clamped and interior layer, $\overline{\sigma}^{\,e}_{s}$ is always tensile. Also, the peak value of $\overline{\sigma}^{\,e}_{s}$ always occurs in the plate at $\bar{r} = 0.325$. As the $\frac{t}{d}$ ratio decreases, the peak value of $\overline{\sigma}^{\,e}_{s}$ increases, with the peak value for the interior layer slightly exceeding that for

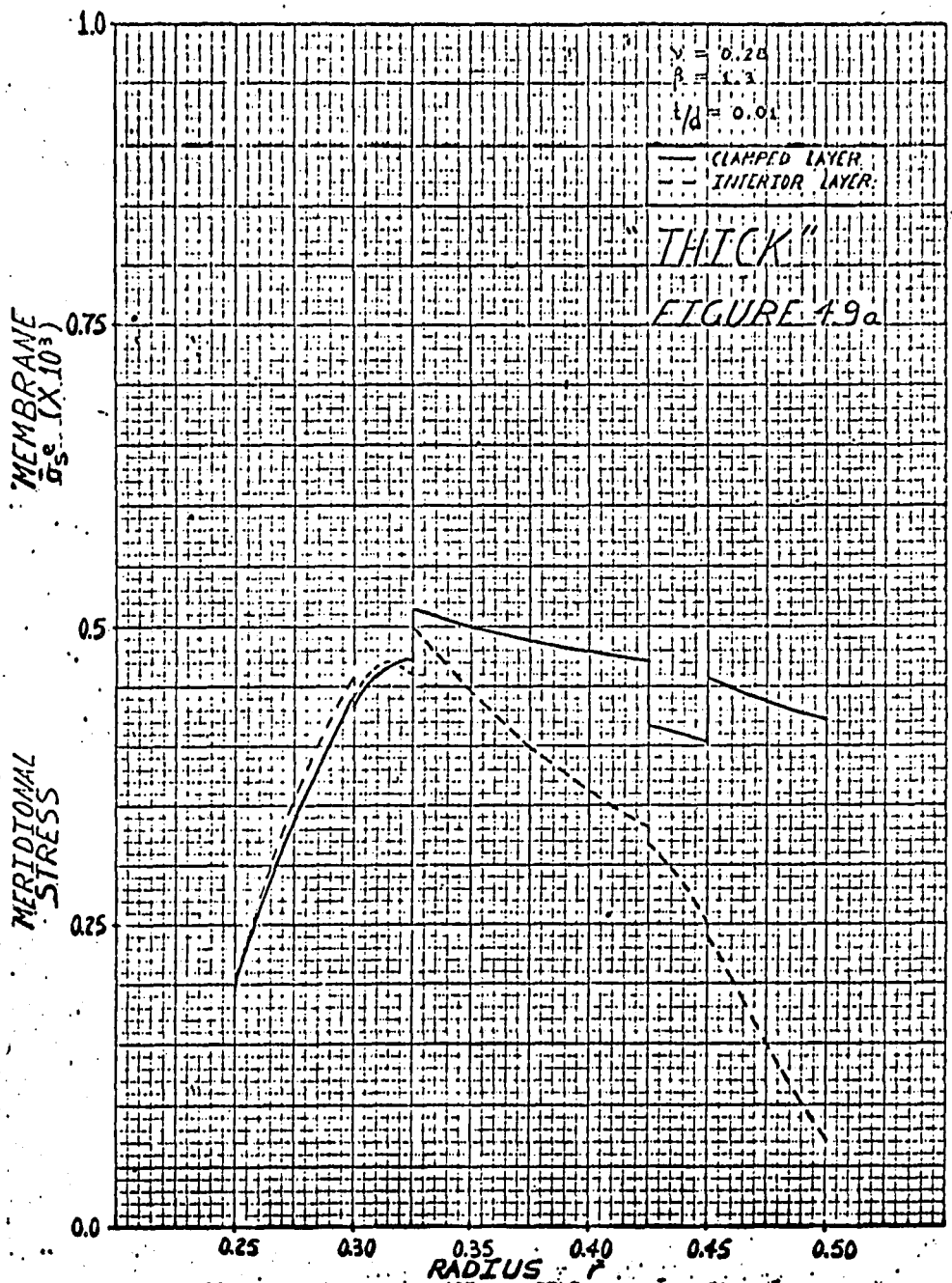
1.0
0.75
0.5
0.25
0.0
MERIDIONAL STRESS
MEMBRANE $\bar{\sigma}_s^e$ (X 10^3)
0.25
0.30
0.35
0.40
0.45
0.50
RADIUS r
ν = 0.25
β = 1.3
t/a = 0.01
CLAMPED LAYER
INTERIOR LAYER
THICK

FIGURE 4.9a

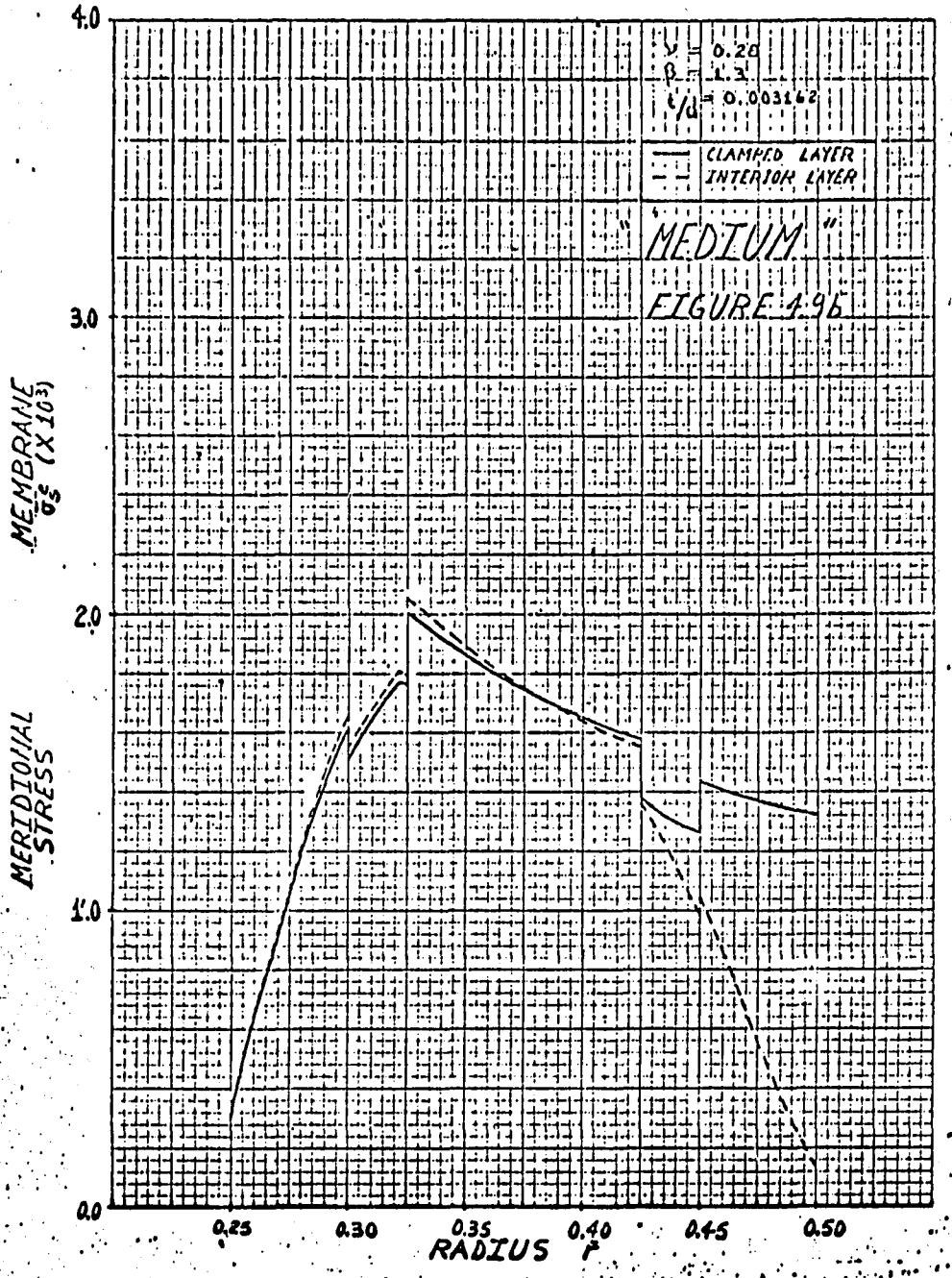
4.0
3.0
2.0
1.0
0.0
MERIDIONAL MEMBRANE STRESS σ_s (X 10^3)
0.25
0.30
0.35
0.40
0.45
0.50
RADIUS r
ν = 0.28
β = 1.3
t/a = 0.003162
CLAMPED LAYER
INTERIOR LAYER
"MEDIUM"

FIGURE 4.96

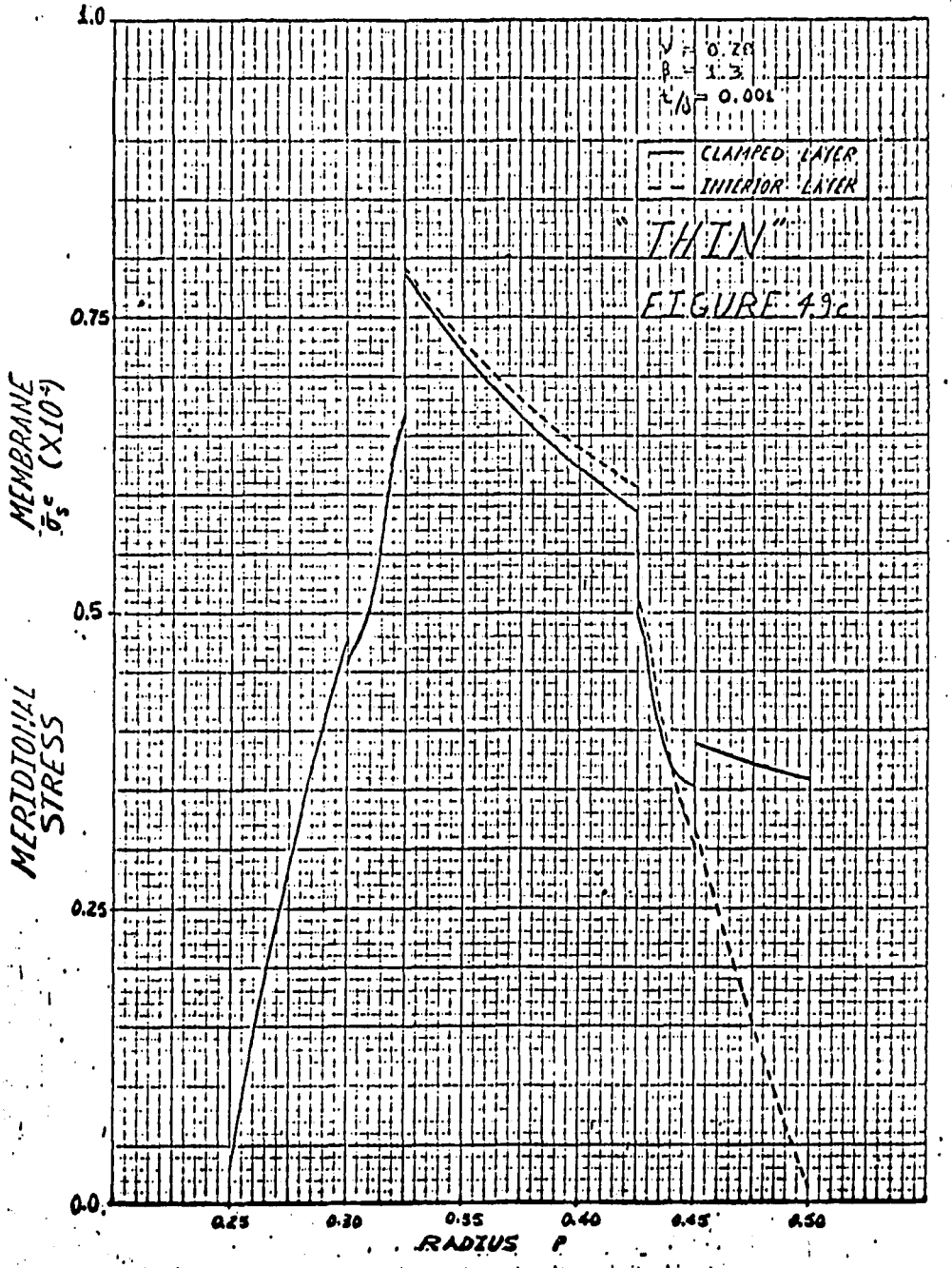
1.0
0.75
0.5
0.25
0.0
0.25
0.30
0.35
0.40
0.45
0.50
RADIUS ρ
MERIDIONAL STRESS
MEMBRANE $\bar{\sigma}_s^c$ (X10⁻¹)
ν = 0.20
β = 1.3
t/δ = 0.001
CLAMPED LAYER
INTERIOR LAYER
"THIN"
FIGURE 4.9c

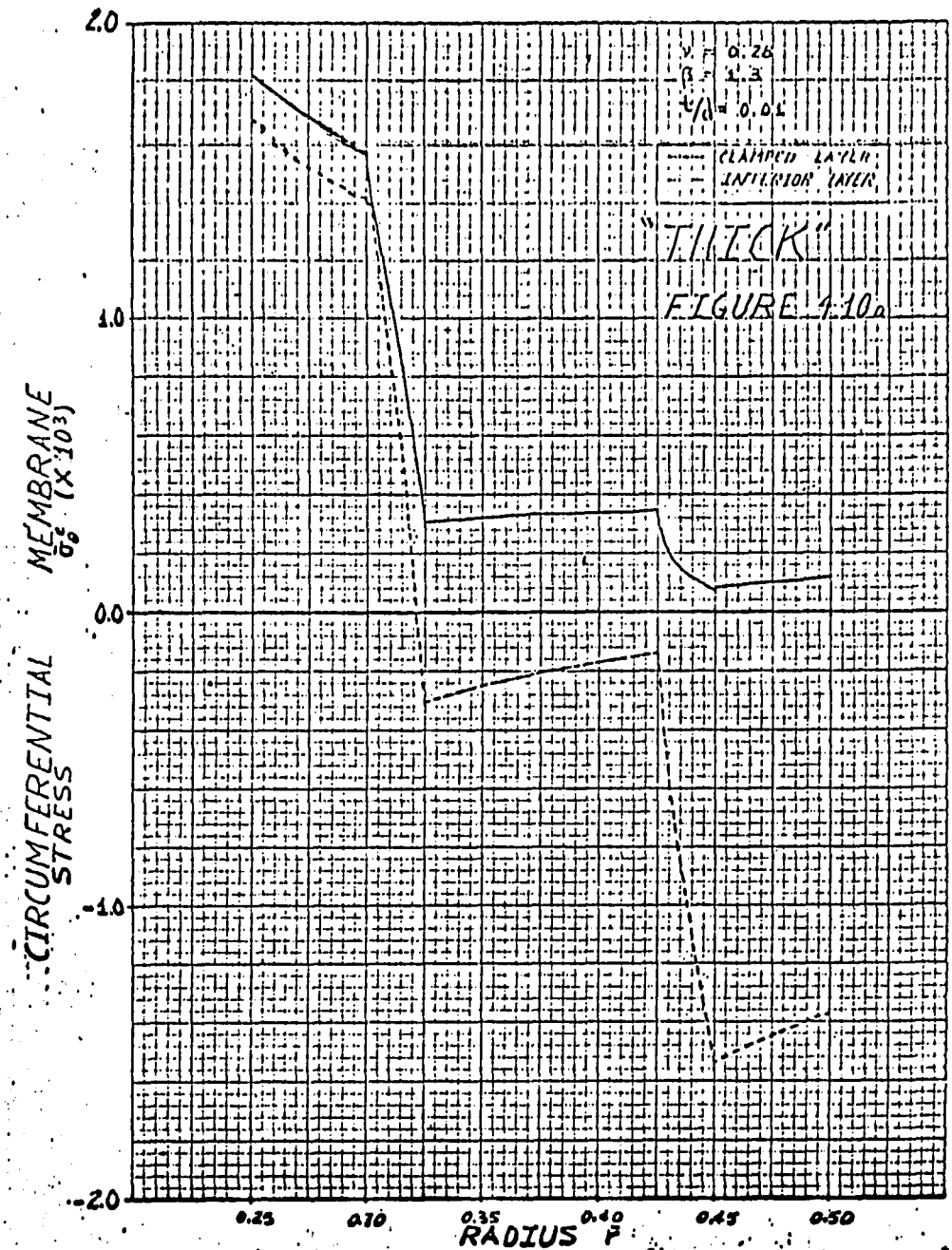
2.0
1.0
0.0
-1.0
-2.0
0.25
0.30
0.35
0.40
0.45
0.50
RADIUS r
CIRCUMFERENTIAL MEMBRANE STRESS σ_θ^* (X 10³)
ν = 0.28
β = 1.3
t/a = 0.05
CLAMPED LAYER
INTERIOR LAYER
"THICK"
FIGURE 4.10a

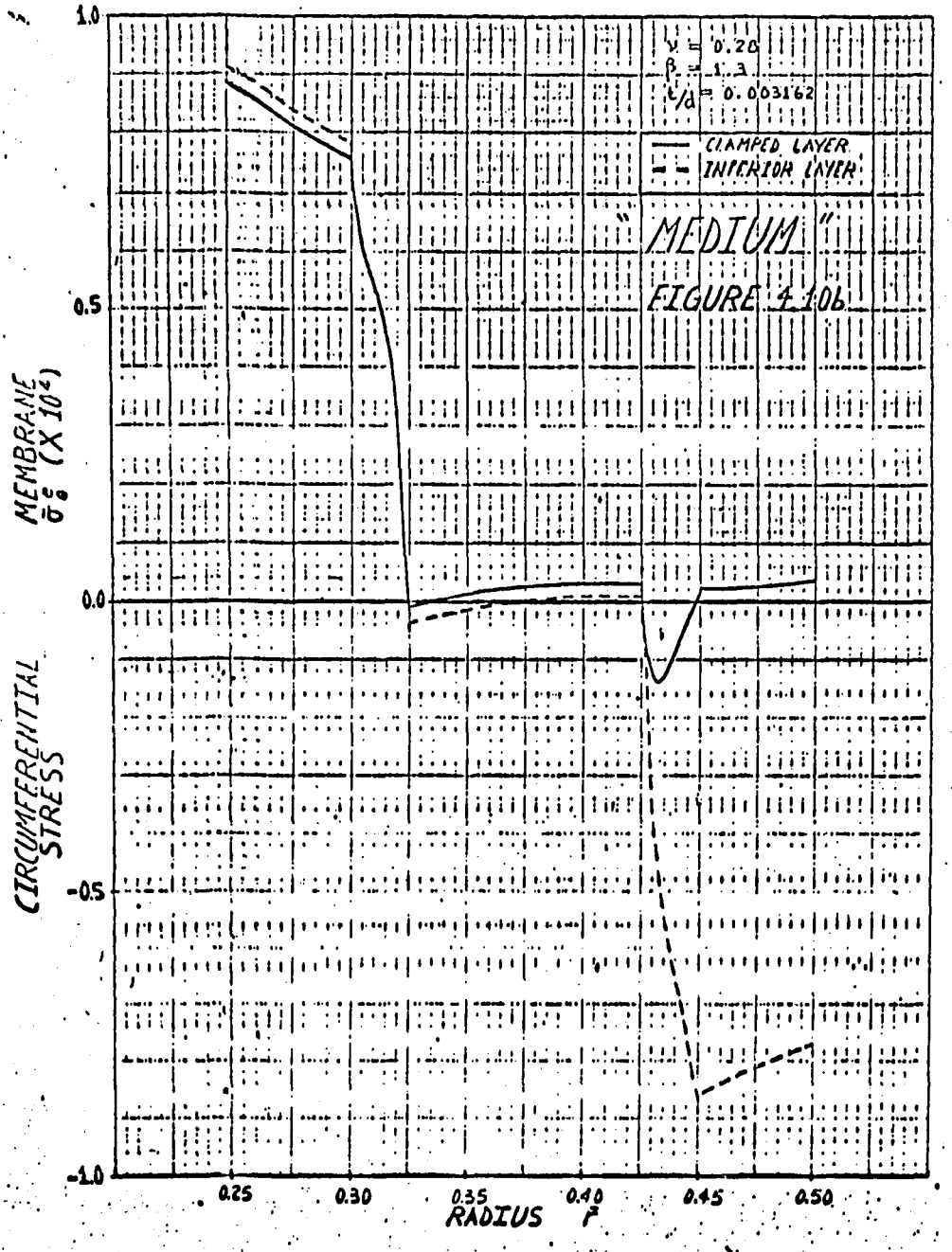
1.0
0.5
0.0
-0.5
-1.0
0.25
0.30
0.35
0.40
0.45
0.50
RADIUS r
MEMBRANE CIRCUMFERENTIAL STRESS σθ (X 10⁴)
ν = 0.28
β = 1.3
t/d = 0.003162
CLAMPED LAYER
INTERIOR LAYER
"MEDIUM"
FIGURE 4.10b

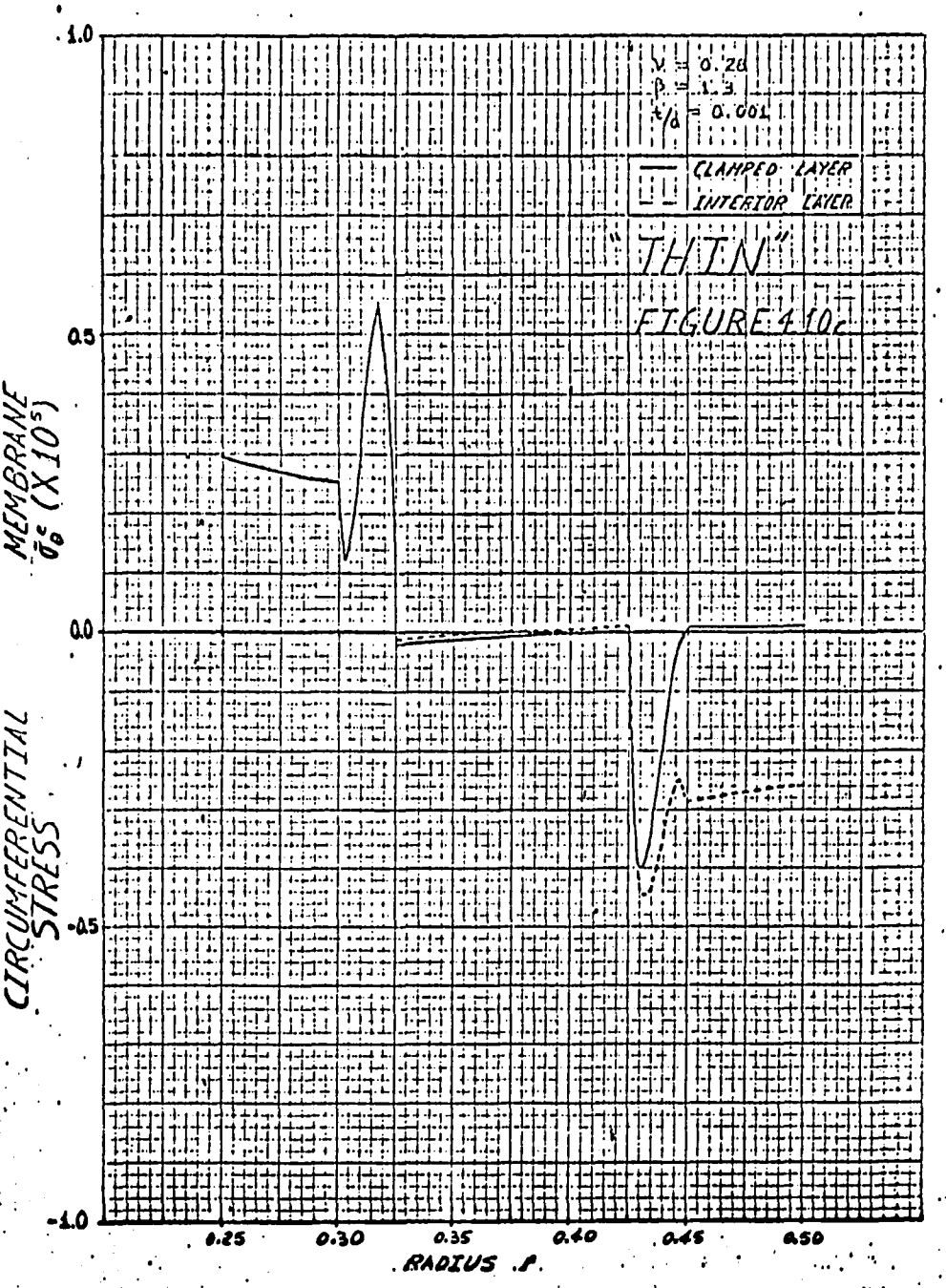
1.0
0.5
0.0
-0.5
-1.0
0.25
0.30
0.35
0.40
0.45
0.50
RADIUS ρ
CIRCUMFERENTIAL STRESS
MEMBRANE $\bar{\sigma}_\theta^c$ (X 10^5)
ν = 0.28
β = 1.3
t/a = 0.001
CLAMPED LAYER
INTERIOR LAYER
"THIN"
FIGURE 4.10c

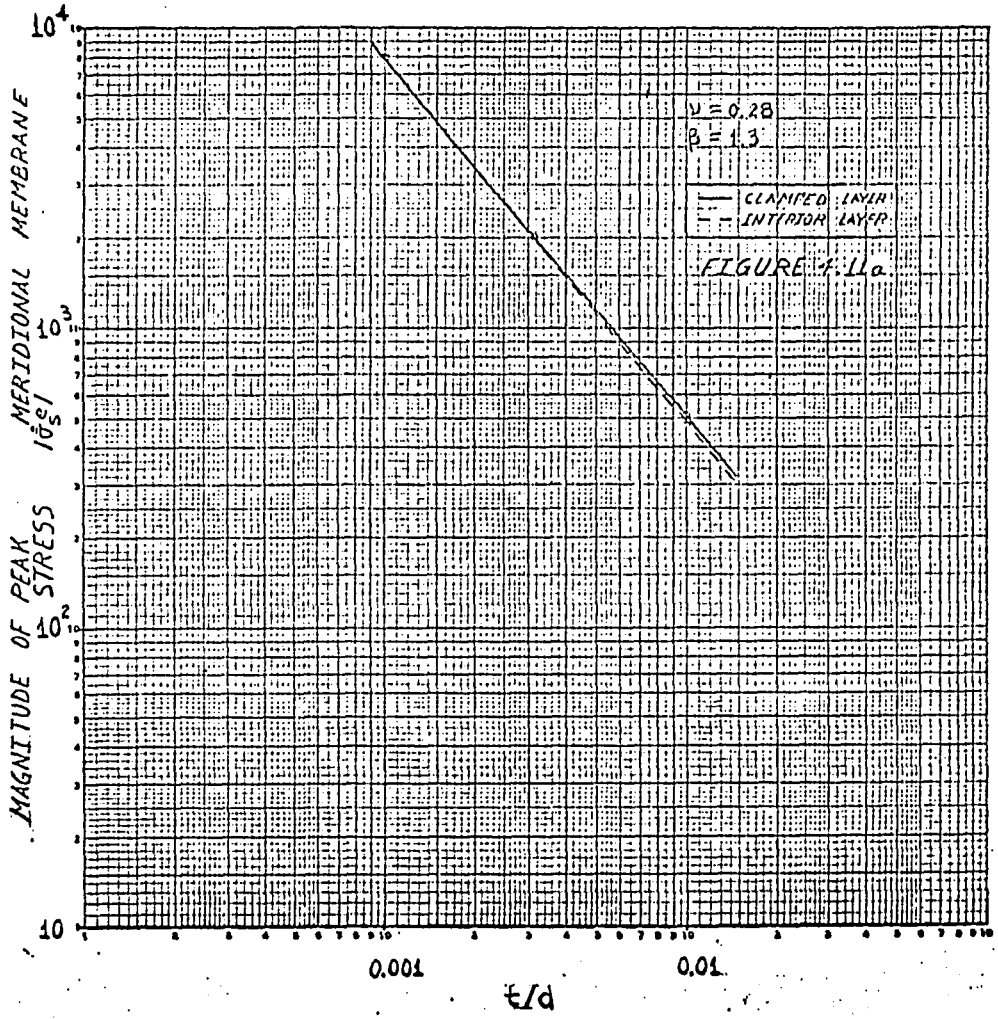
MAGNITUDE OF PEAK MERIDIONAL MEMBRANE STRESS $10^{-3}\sigma_s/l$
10^4
10^3
10^2
10
0.001
0.01
t/d
ν = 0.28
β = 1.3
CLAMPED LAYER
INTERIOR LAYER
FIGURE 4.11a.

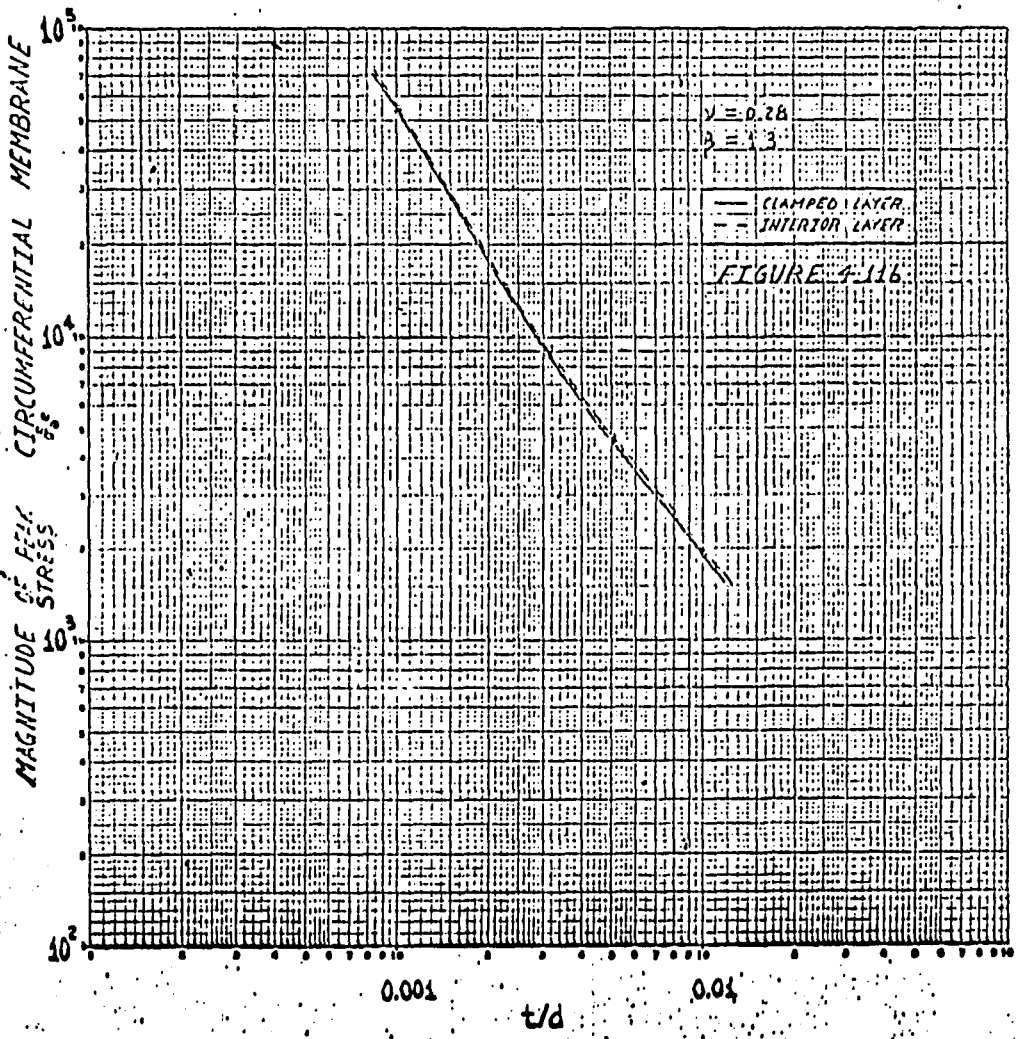
MAGNITUDE OF PEAK CIRCUMFERENTIAL MEMBRANE STRESS
10^5
10^4
10^3
10^2
σ_θ
$\nu = 0.28$
$\beta = 13$
CLAMPED EDGE LAYER
INTERIOR LAYER
0.001
0.01
t/d

FIGURE 4-116

the clamped layer. Except for magnitude, $\overline{\sigma}^{e}_{s}$ exhibits the same type of variation throughout the $\frac{t}{d}$ range, namely that of a "single-frequency" behavior.

The results for $\overline{\sigma}^{e}_{\theta}$ are presented in Figs. 4.10a-c. In contrast to $\overline{\sigma}^{e}_{s}$ which is tensile throughout the $\frac{t}{d}$ range, $\overline{\sigma}^{e}_{\theta}$ is tensile for approximately half the radial length of both the clamped and interior layer. As $\frac{t}{d}$ decreases from the thick value to the medium value, $\overline{\sigma}^{e}_{\theta}$ begins to oscillate in the first conical segment (section BC, Fig. 4.12a). As $\frac{t}{d}$ continues to decrease to the thin value, these oscillations appear in the second conical segment (section DE, Fig. 4.12a) as their amplitudes increase. Throughout the $\frac{t}{d}$ range, the peak value of $\overline{\sigma}^{e}_{s}$ exceeds the peak value of $\overline{\sigma}^{e}_{\theta}$. In this case, the peak values of $\overline{\sigma}^{e}_{\theta}$ occur at the innermost point ($\bar{r} = 0.25$) of the clamped and interior layer. Whether the peak value occurs in the clamped or interior layer depends upon the particular value of $\frac{t}{d}$. The variation of the peak values of $\overline{\sigma}^{e}_{s}$ and $\overline{\sigma}^{e}_{\theta}$ (in absolute value) with respect to $\frac{t}{d}$ for a clamped and interior layer is presented in Figs. 4.11a-b.

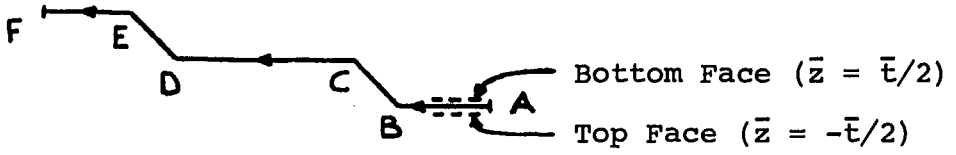

Figure 4.12a Top and Bottom Faces of an Odd Numbered Layer

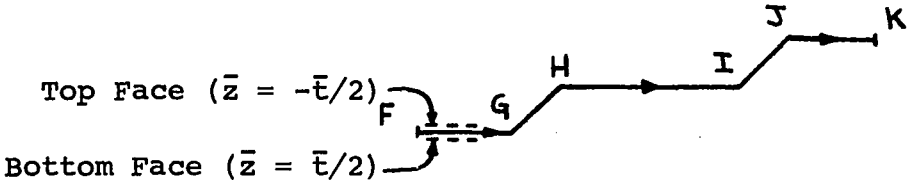

Figure 4.12b Top and Bottom Faces of an Even Numbered Layer

4.2.4 BENDING STRESSES

The meridional and circumferential bending stresses $\bar{\sigma}^{\,o}_{s}$ and $\bar{\sigma}^{\,o}_{\theta}$ are calculated by means of the relations:

$$\bar{\sigma}^{\,o}_{s} = \frac{12\bar{M}_{s}\bar{z}}{\bar{t}^{3}} \qquad (4.2.4\text{-}1a)$$

$$\bar{\sigma}^{\,o}_{\theta} = \frac{12\bar{M}_{\theta}\bar{z}}{\bar{t}^{3}} \qquad (4.2.4\text{-}1b)$$

The various bending stresses at the "top" ($\bar{z} = -\bar{t}/2$) and "bottom" ($\bar{z} = \bar{t}/2$) face of an odd or even numbered layer shown in Figs. 4.12a-b may, by virtue of equations (4.2.4-1a-b), be calculated by means of the following relations:

$$\bar{\sigma}^{\,o-}_{s} = \frac{-6\bar{M}_{s}}{\bar{t}^{2}} \qquad (4.2.4\text{-}2a)$$

$$\bar{\sigma}^{\,o-}_{\theta} = \frac{-6\bar{M}_{\theta}}{\bar{t}^{2}} \qquad (4.2.4\text{-}2b)$$

$$\bar{\sigma}^{\,o+}_{s} = \frac{6\bar{M}_{s}}{\bar{t}^{2}} \qquad (4.2.4\text{-}2c)$$

$$\bar{\sigma}^{\,o+}_{\theta} = \frac{6\bar{M}_{\theta}}{\bar{t}^{2}} \qquad (4.2.4\text{-}2d)$$

The results for the various bending stresses are presented in Figs. 4.13a-c and 4.14a-c. The bending stresses exhibit a "double-frequency" behavior. For all values of $\frac{t}{d}$ in the range studied, the peak bending stresses occur in the interior layer, with the peak meridional bending stress exceeding the peak circumferential bending stress. For both the meridional and circumferential directions, the peak bending stresses tend to occur in the plate at point "D" in Fig. 4.12a. The only exception to this is the meridional bending stress at the bottom face for the thick case. Here, the peak values for the clamped and interior layer occur at point "F" in Fig. 4.12a. The variation of the peak values (in absolute value) of $\overline{\sigma}_{s}^{o+}$ and $\overline{\sigma}_{\theta}^{o+}$ with respect to $\frac{t}{d}$ for the clamped and interior layer is presented in Figs. 4.15a-b. It is noteworthy, that as $\frac{t}{d}$ decreases to the case of a "thin" welded bellows ($\frac{t}{d} = 0.001$), the bending stresses clearly do <u>not</u> become negligible in comparison to the membrane stresses. In fact, as $\frac{t}{d}$ decreases, the peak bending stresses <u>increase</u> in relation to the peak membrane stresses; i.e., the contribution of the bending stresses in "thin" welded bellows is as important if not more important than the membrane stresses. Various ratios (in absolute value) of peak bending stress to peak membrane stress along with the corresponding bending moment to membrane force ratios (in absolute value) for a thick, medium, and thin value of $\frac{t}{d}$ are presented in Figs. 4.27a-d. Obviously as $\frac{t}{d}$ decreases, the ratio of the bending moment to the membrane

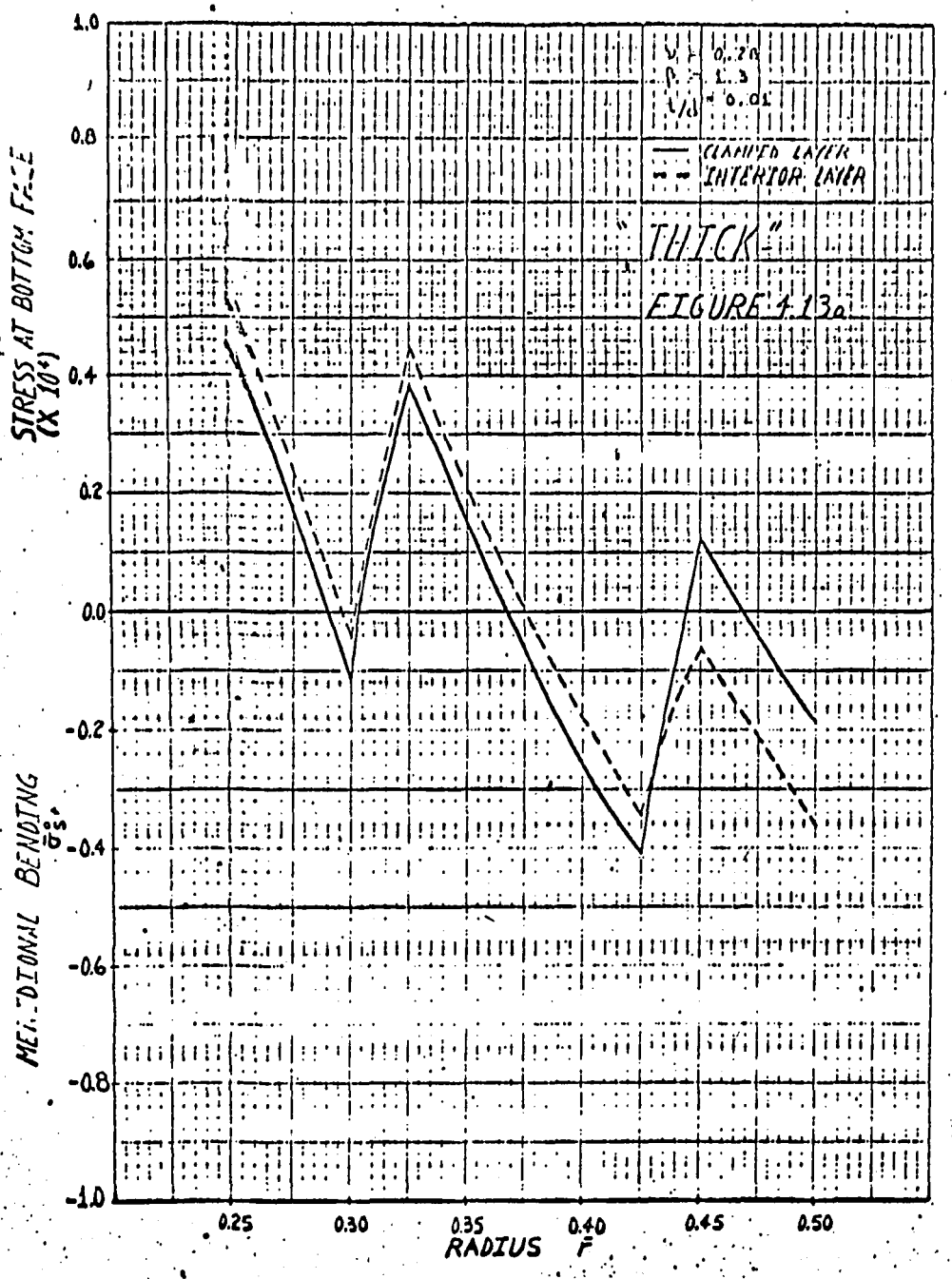
1.0
0.8
0.6
0.4
0.2
0.0
-0.2
-0.4
-0.6
-0.8
-1.0
0.25
0.30
0.35
0.40
0.45
0.50
RADIUS r
MERIDIONAL BENDING σs*
STRESS AT BOTTOM FACE (X 10⁴)
CLAMPED LAYER
INTERIOR LAYER
"THICK"
FIGURE 4.13a

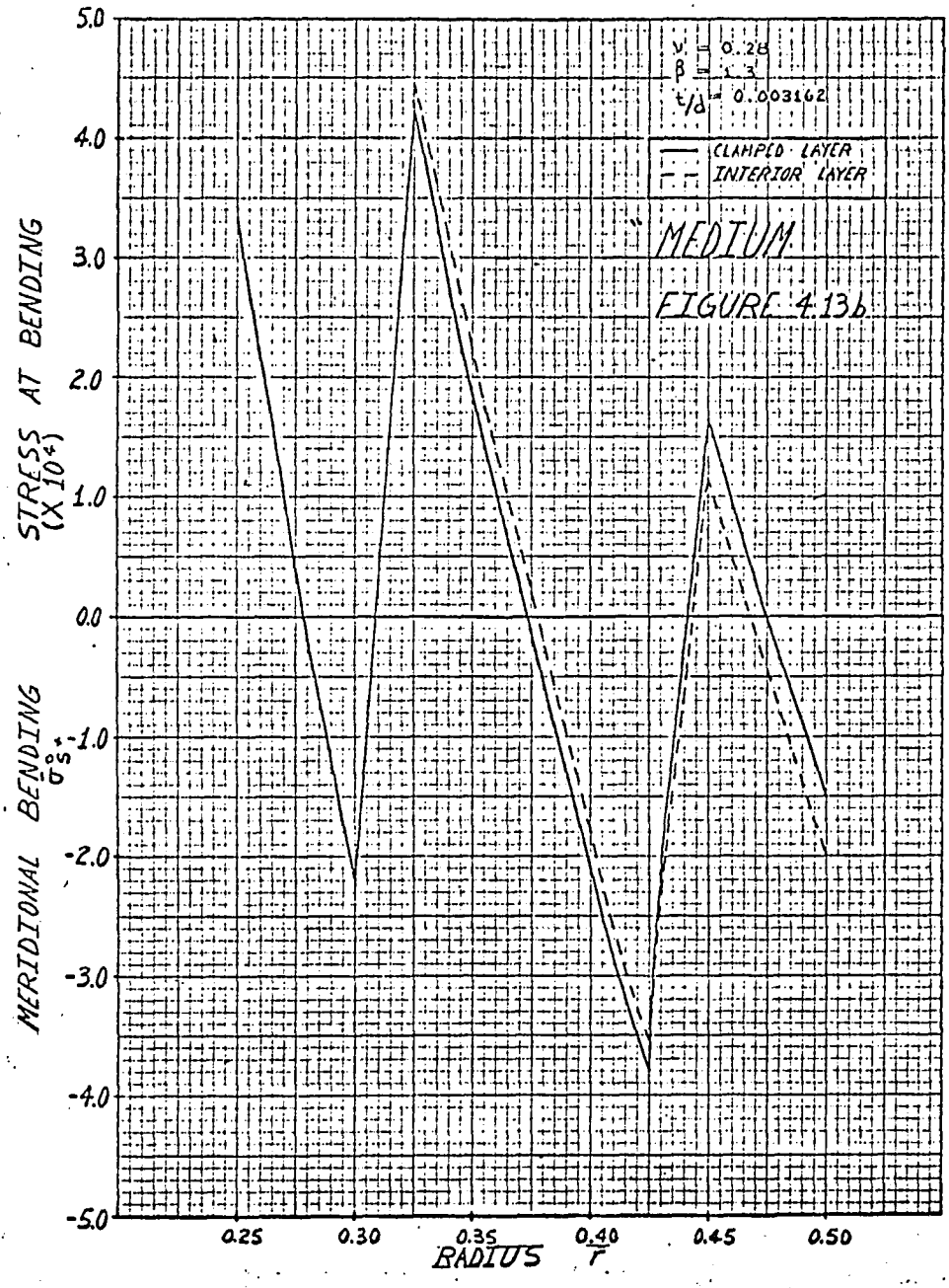
ν = 0.28
β = 1.3
t/a = 0.003162
CLAMPED LAYER
INTERIOR LAYER
MEDIUM
MERIDIONAL BENDING STRESS AT BENDING
σ_{ss} (X 10^4)
5.0
4.0
3.0
2.0
1.0
0.0
-1.0
-2.0
-3.0
-4.0
-5.0
0.25
0.30
0.35
0.40
0.45
0.50
RADIUS r

FIGURE 4.13b

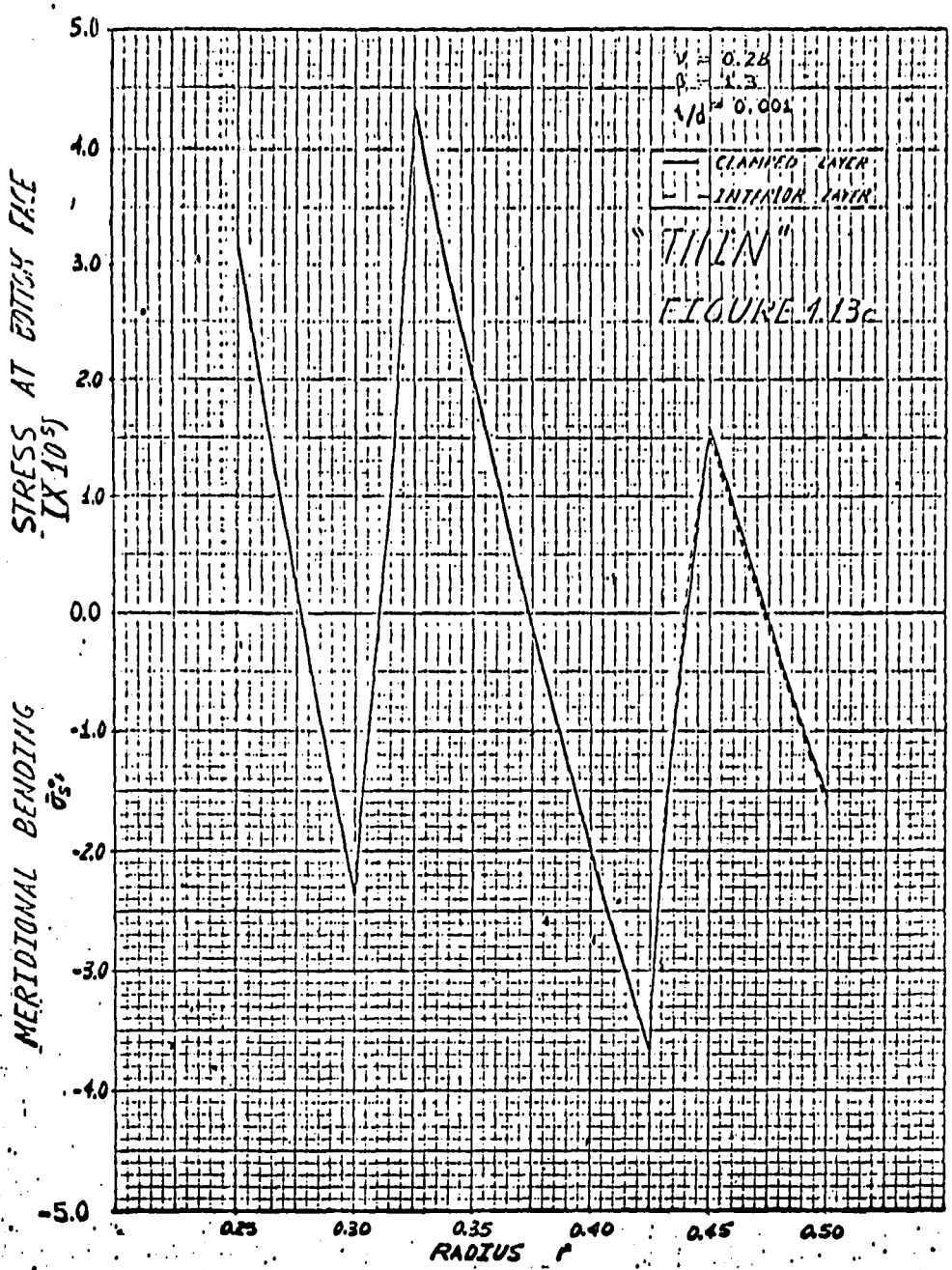
ν = 0.28
β = 1.3
t/a = 0.001
CLAMPED LAYER
INTERIOR LAYER
"TIN"
FIGURE 1.13c
MERIDIONAL BENDING STRESS AT EDGE FACE
$\bar{\sigma}_s^s$ (X 10^5)
5.0
4.0
3.0
2.0
1.0
0.0
-1.0
-2.0
-3.0
-4.0
-5.0
0.25
0.30
0.35
0.40
0.45
0.50
RADIUS r

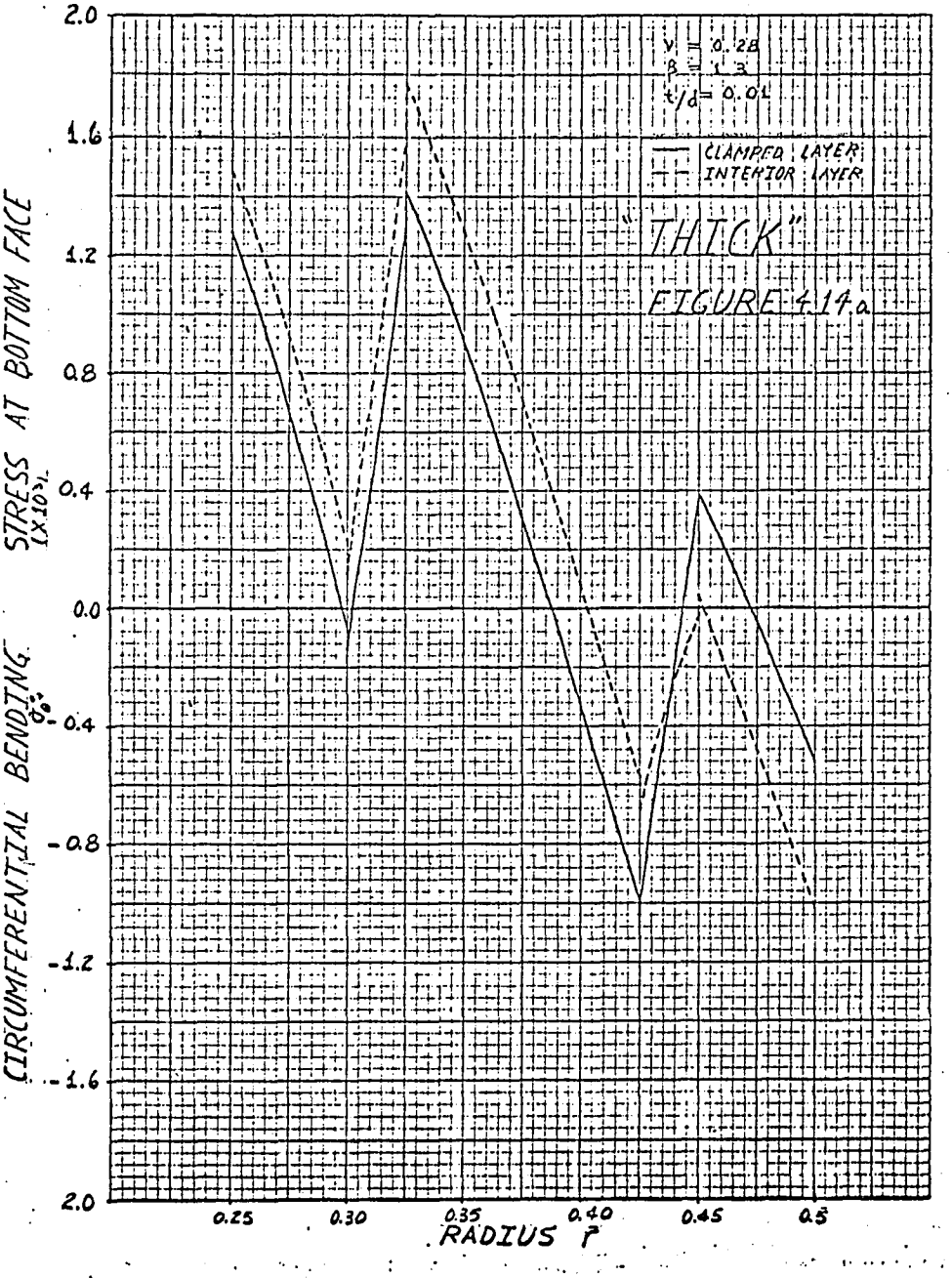
2.0
1.6
1.2
0.8
0.4
0.0
-0.4
-0.8
-1.2
-1.6
-2.0
0.25
0.30
0.35
0.40
0.45
0.5
RADIUS r
CIRCUMFERENTIAL BENDING STRESS AT BOTTOM FACE
(1x10³)
ν = 0.28
β = 1.3
t/d = 0.01
CLAMPED LAYER
INTERIOR LAYER
THICK"
FIGURE 4.14a

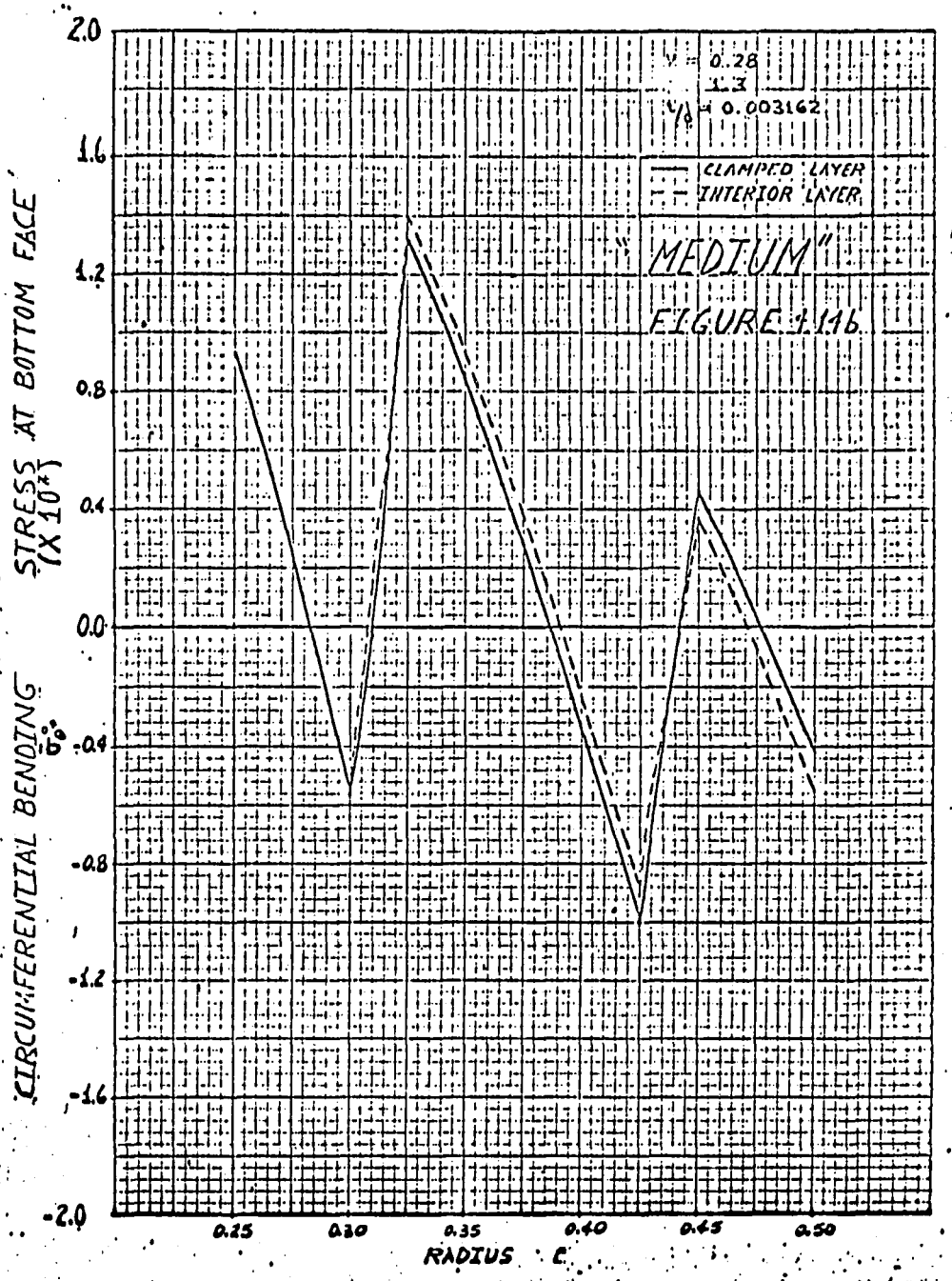
ν = 0.28
1.3
V/b = 0.003162
CLAMPED LAYER
INTERIOR LAYER
"MEDIUM"
FIGURE 1.16b
CIRCUMFERENTIAL BENDING STRESS AT BOTTOM FACE (X 10⁴)
2.0
1.6
1.2
0.8
0.4
0.0
-0.4
-0.8
-1.2
-1.6
-2.0
0.25
0.30
0.35
0.40
0.45
0.50
RADIUS

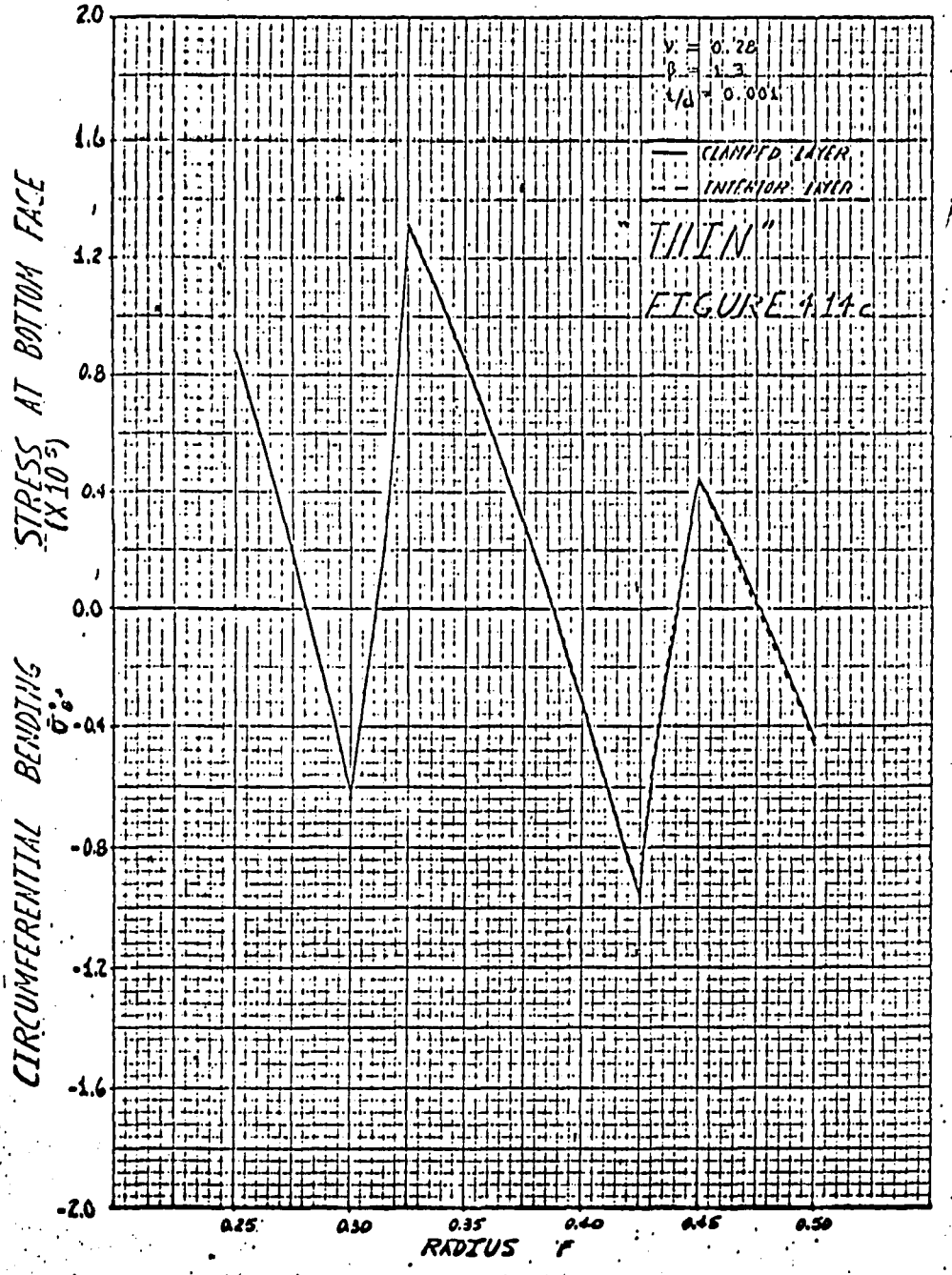
CIRCUMFERENTIAL BENDING STRESS AT BOTTOM FACE
$\sigma_{\theta\theta}$ (X 10^{-5})
2.0
1.6
1.2
0.8
0.4
0.0
-0.4
-0.8
-1.2
-1.6
-2.0
0.25
0.30
0.35
0.40
0.45
0.50
RADIUS r
ν = 0.28
β = 1.3
t/a = 0.001
CLAMPED LAYER
INTERIOR LAYER
T/IN"
FIGURE 4.14c

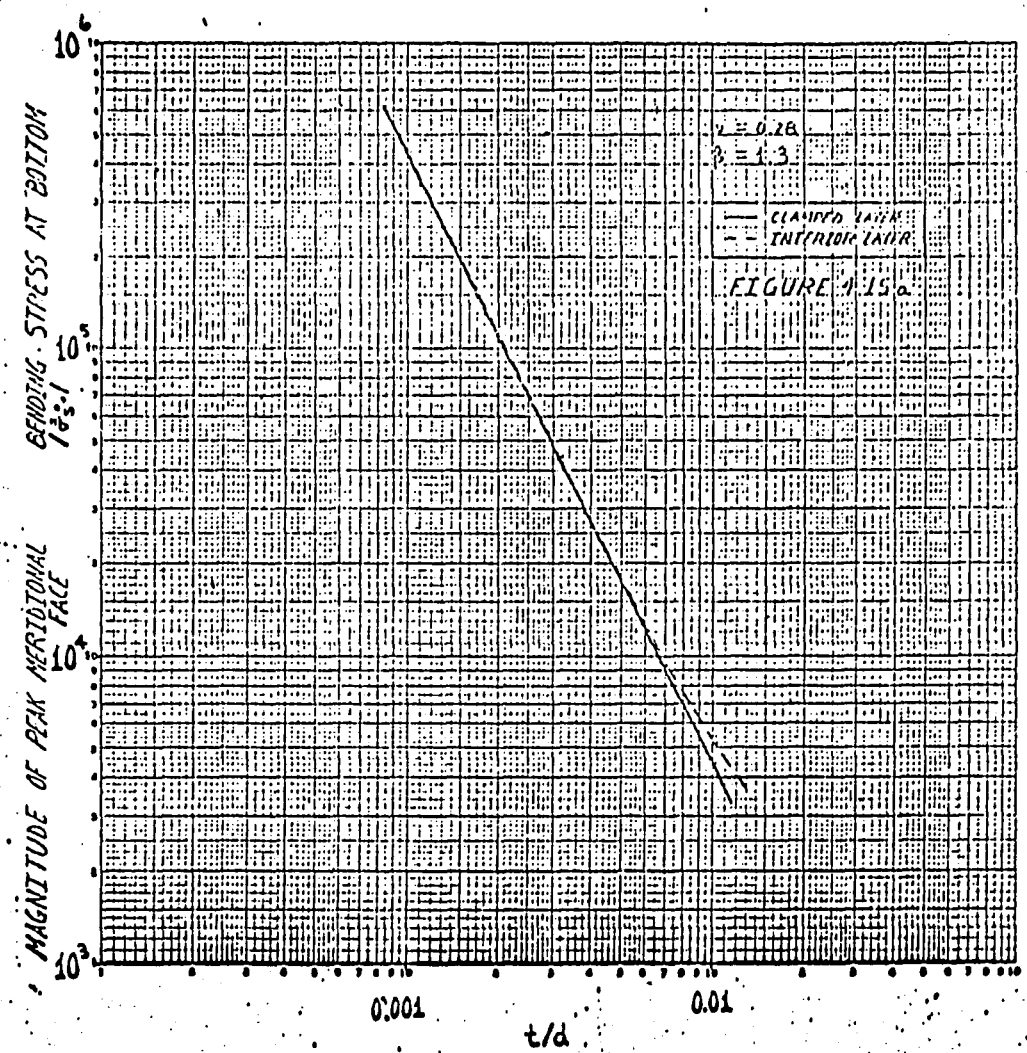
MAGNITUDE OF PEAK MERIDIONAL BENDING STRESS AT EDITOR FACE
10^6
10^5
10^4
10^3
0.001
0.01
t/d
ν = 0.28
β = 1.3
CLAMPED EDGE
INTERIOR EDGE

FIGURE 4.15a

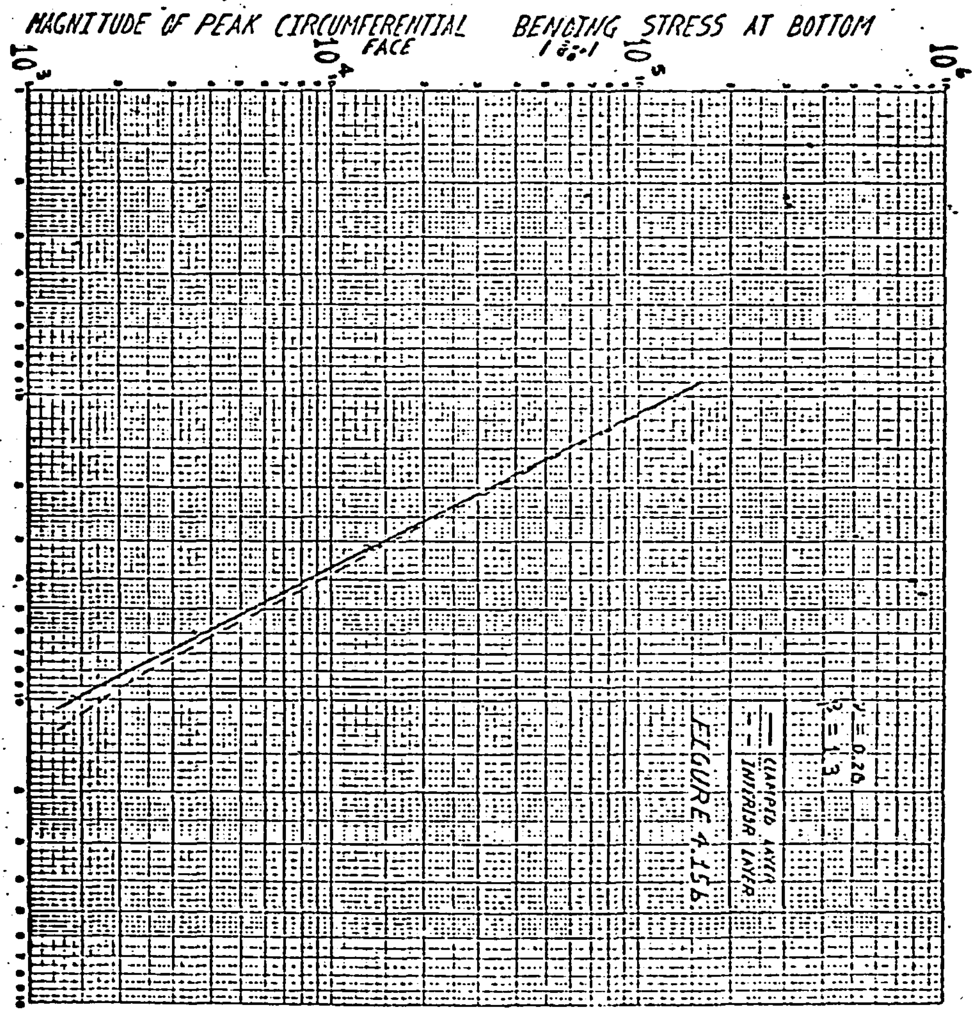
MAGNITUDE OF PEAK CIRCUMFERENTIAL BENDING STRESS AT BOTTOM FACE
10^3
10^4
10^5
10^6
t/d
0.001
0.01
= 0.20
= 1.3
CLAMPED LAYER
INTERIOR LAYER

FIGURE 4.15b.

force decreases because of the factors $\bar{t}^3$ and $\bar{t}$, respectively. However, the ratio of peak bending stress (regardless of direction) to peak membrane stress (regardless of direction) does not decrease, as one might expect, but increases. These results indicate the inapplicability over the entire practical range of thickness-diameter-ratios of the assertion frequently[30] made that for shells which are sufficiently thin, bending effects can be neglected in comparison with membrane effects. This assertion may be true for the resultant bending moments, but certainly not for the local bending stresses which are among the quantities actually determining failure.

4.2.5 SOME OTHER IMPORTANT PHYSICAL QUANTITIES

Another group of quantities which are of considerable importance for determining failure in welded bellows are the total stress components. At the top and bottom face of any layer, these total stress components are defined respectively as:

$$\bar{\sigma}_s^- = \bar{\sigma}_s^e + \bar{\sigma}_s^{o-} \qquad (4.2.5\text{-}1a)$$

$$\bar{\sigma}_\theta^- = \bar{\sigma}_\theta^e + \bar{\sigma}_\theta^{o-} \qquad (4.2.5\text{-}1b)$$

$$\bar{\sigma}_s^+ = \bar{\sigma}_s^e + \bar{\sigma}_s^{o+} \qquad (4.2.5\text{-}1c)$$

$$\bar{\sigma}_\theta^+ = \bar{\sigma}_\theta^e + \bar{\sigma}_\theta^{o+} \qquad (4.2.5\text{-}1d)$$

The values of total stress for any point between the top and bottom face of any layer are obtained by linear interpolation.

For each of the three $\frac{t}{d}$ ratios studied, all of the total stress components exhibit the same type of variation (except for magnitude), namely a double-frequency variation. This is due to the fact that the bending stresses, which also exhibit a double-frequency variation, are larger than the corresponding membrane stresses which exhibit single-frequency behavior. Except for the thick case corresponding to the meridional direction at the top and bottom face and the circumferential direction at the bottom face for the thick and medium case, the peak values of total stress in both the meridional and circumferential directions occur in the plate at point "D" in Fig. 4.12a. In every case except the circumferential direction at the top face, the peak total stresses for the meridional and circumferential directions in a "thick" welded bellows occur at the innermost point ($\bar{r} = 0.25$).

The variation of the total stresses as a function of $\bar{r}$ is presented in Figs. 4.16a-c through 4.19a-c. For each value of $\frac{t}{d}$, the peak values of total stress in the meridional and circumferential directions are somewhat higher in the interior layer than the clamped layer. This is probably due to the fact that the interior layer always has a larger $\bar{W}$ deflection. The variation of peak total stress (in absolute value) as a function of thickness-diameter-ratio is presented in Figs. 4.20a-b. For each value of $\frac{t}{d}$, the <u>peak</u> value of <u>total</u>

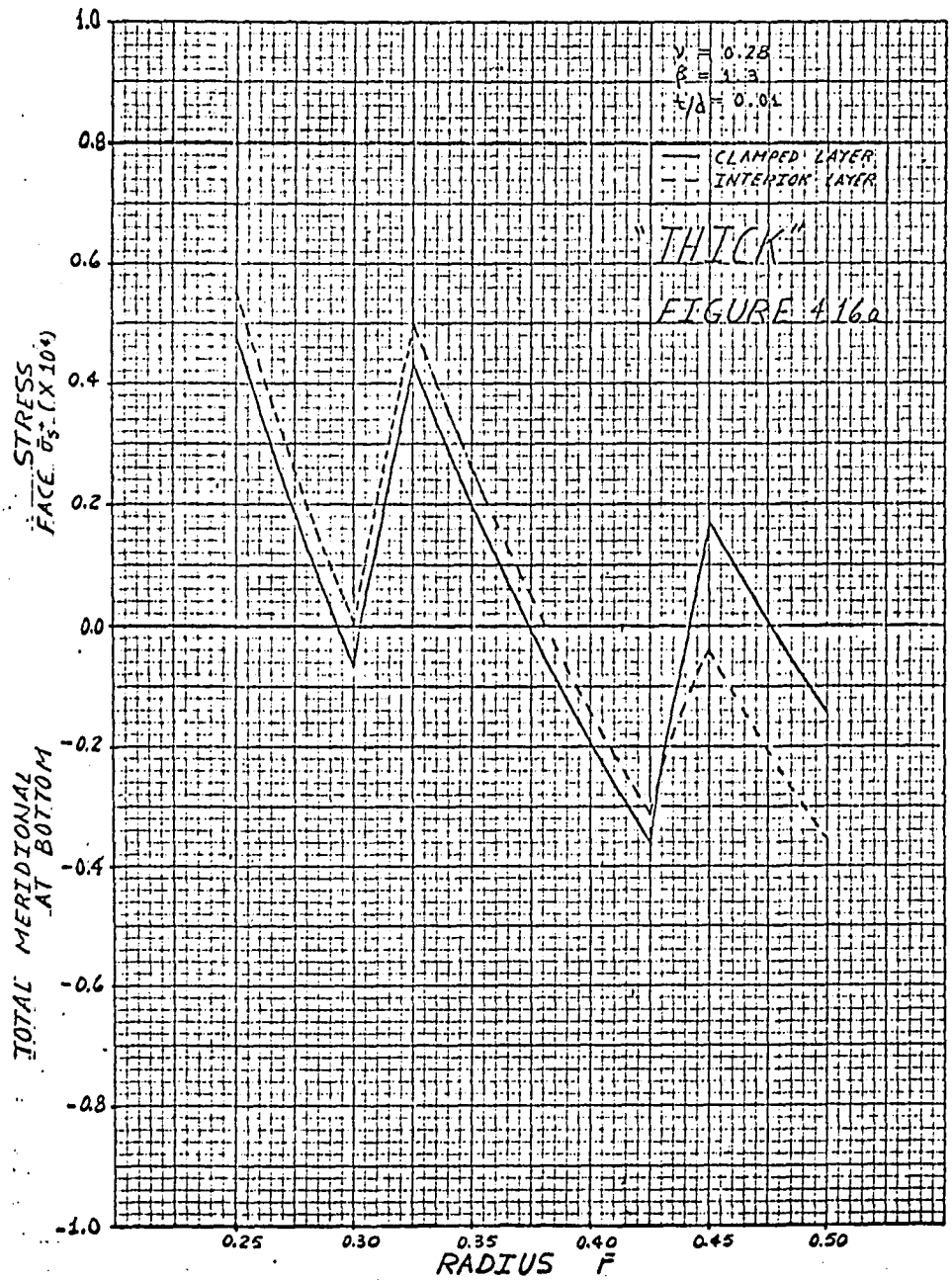
1.0
0.8
0.6
0.4
0.2
0.0
-0.2
-0.4
-0.6
-0.8
-1.0
0.25
0.30
0.35
0.40
0.45
0.50
RADIUS r
TOTAL MERIDIONAL STRESS AT BOTTOM FACE $\bar{\sigma}_{s^-}$ (X 10⁴)
ν = 0.28
β = 1.3
t/a = 0.01
CLAMPED LAYER
INTERIOR LAYER
"THICK"
FIGURE 4.16a

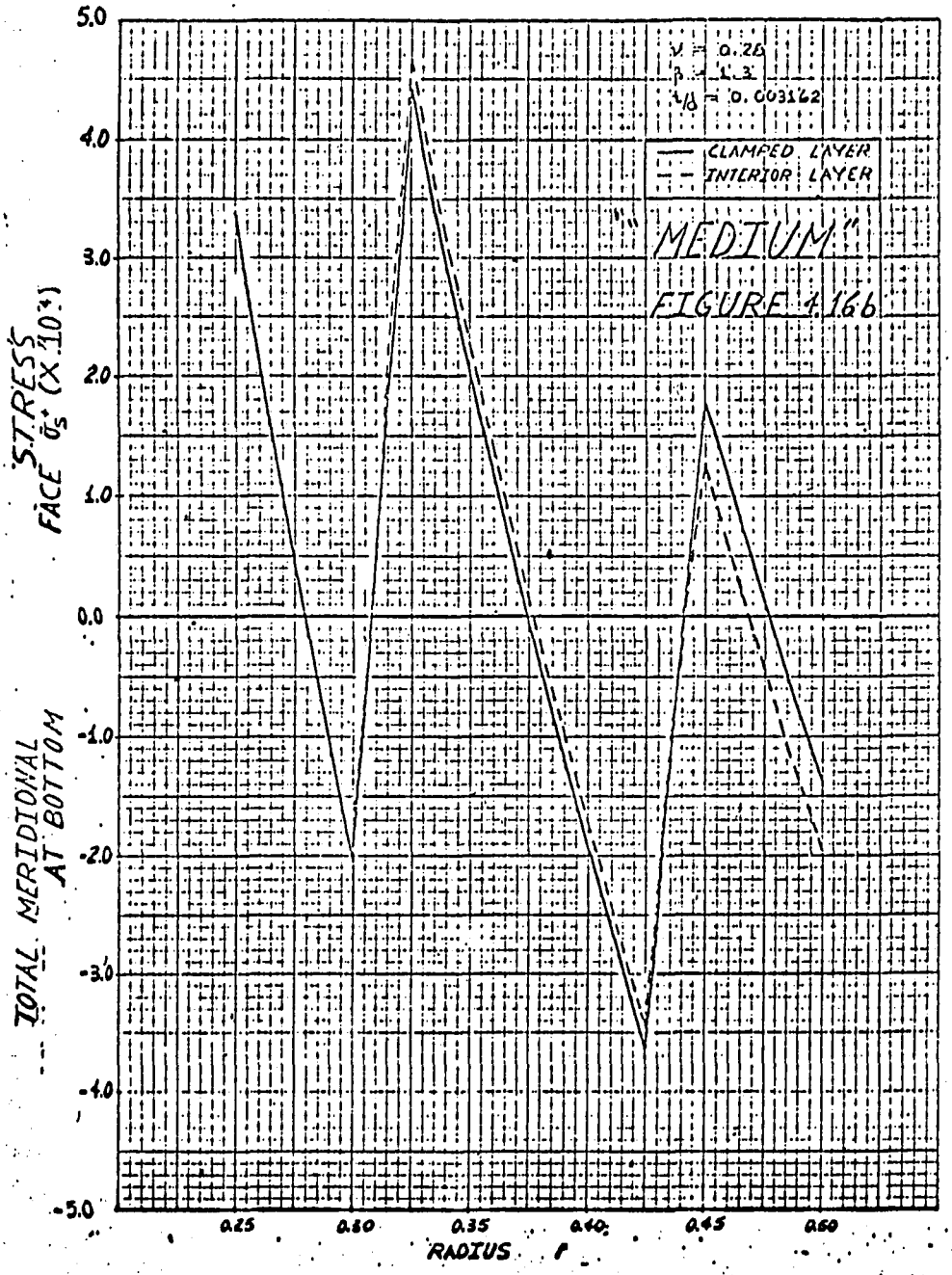
ν = 0.26
β = 1.3
t/a = 0.003162
CLAMPED LAYER
INTERIOR LAYER
"MEDIUM"
FIGURE 4.166
TOTAL MERIDIONAL STRESS AT BOTTOM FACE $\bar{\sigma}_s$ (X 10³)
5.0
4.0
3.0
2.0
1.0
0.0
-1.0
-2.0
-3.0
-4.0
-5.0
0.25
0.30
0.35
0.40
0.45
0.50
RADIUS r

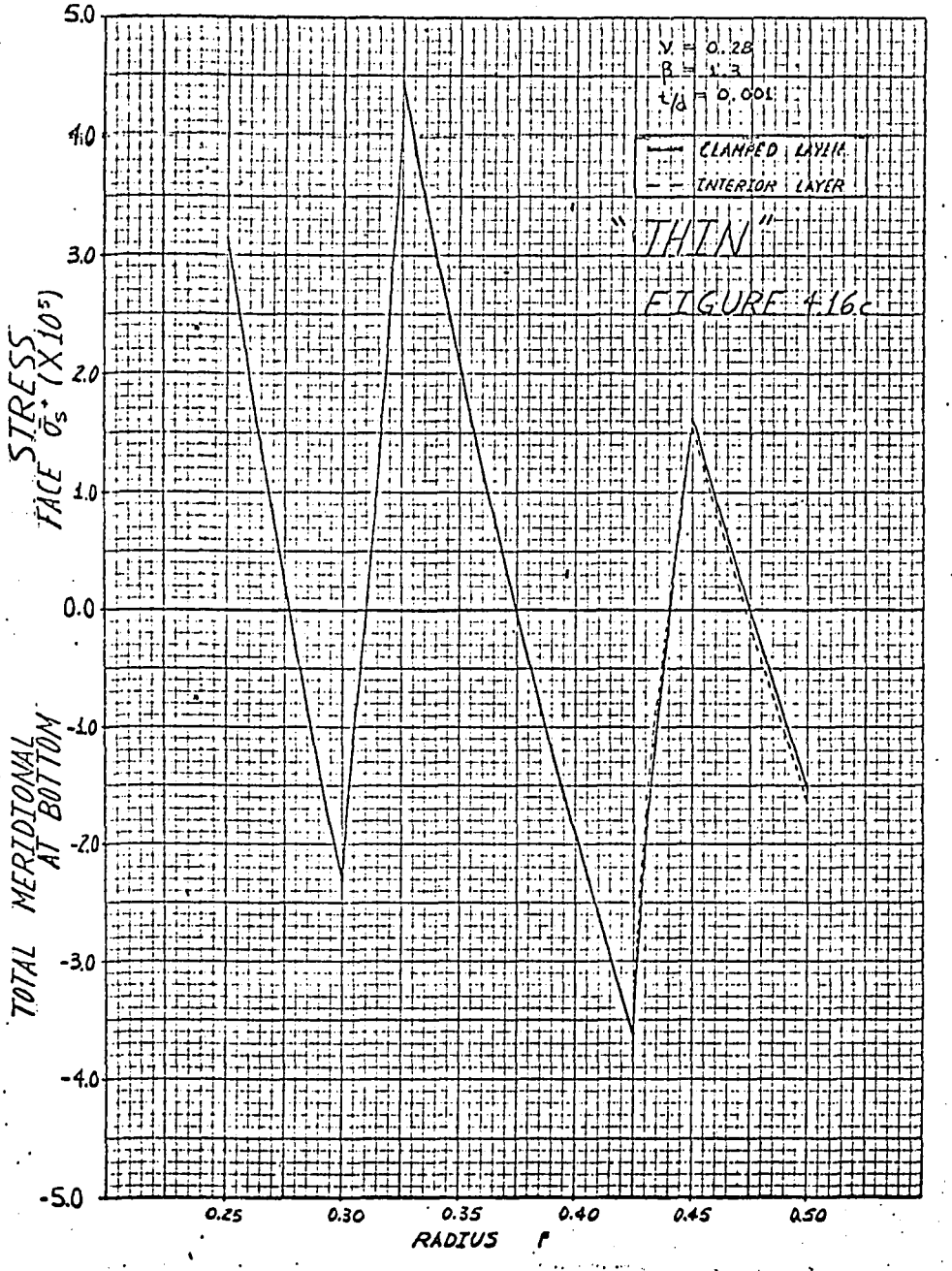
5.0
4.0
3.0
2.0
1.0
0.0
-1.0
-2.0
-3.0
-4.0
-5.0
0.25
0.30
0.35
0.40
0.45
0.50
RADIUS r
TOTAL MERIDIONAL STRESS FACE AT BOTTOM $\bar{\sigma}_s$ (X 10^5)
ν = 0.28
β = 1.3
t/a = 0.001
CLAMPED LAYER
INTERIOR LAYER
"THIN"

FIGURE 4.16c

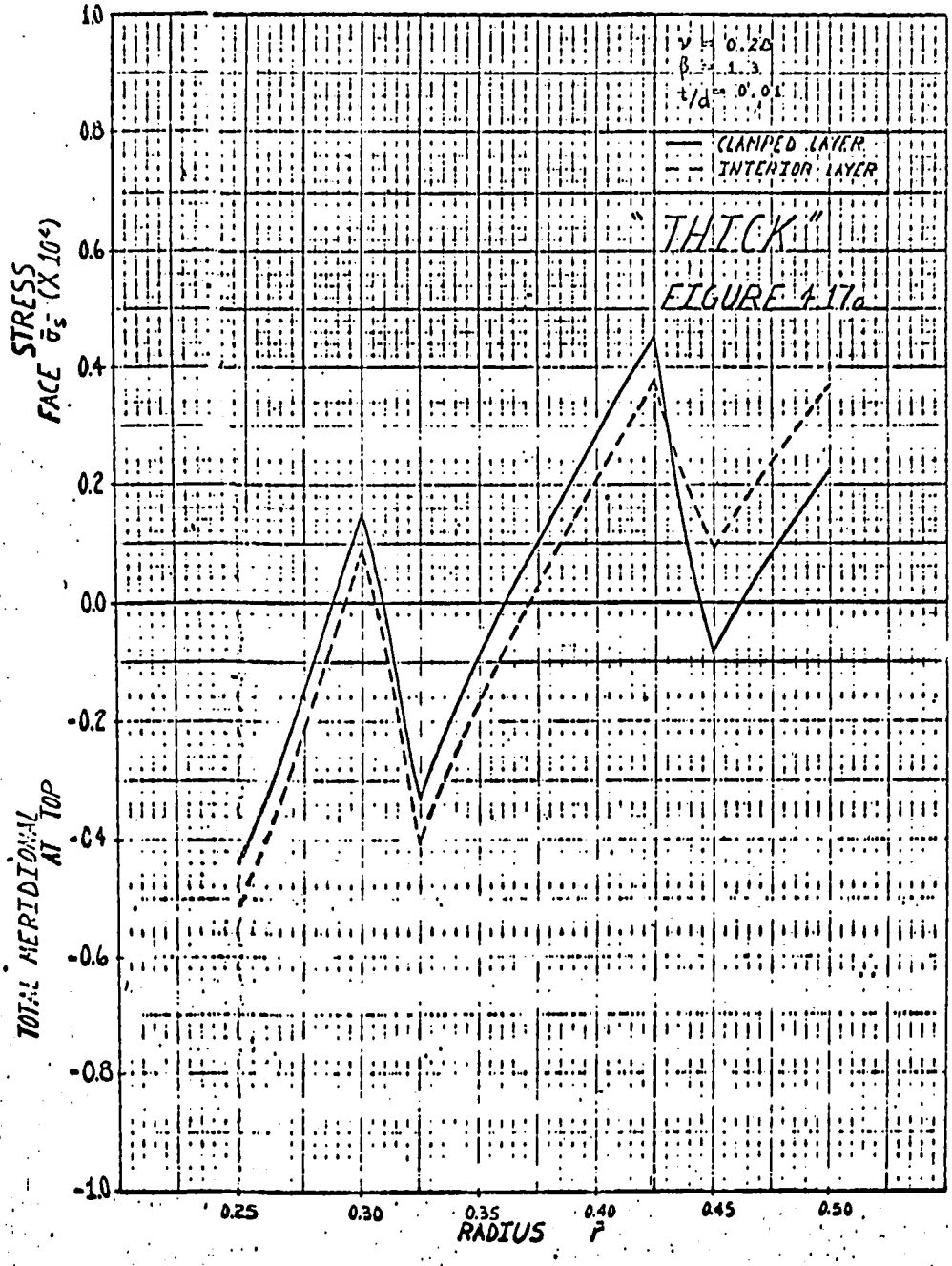
ν = 0.20
β = 1.3
t/d = 0.01
CLAMPED LAYER
INTERIOR LAYER
"THICK"
FIGURE 4.17a
FACE STRESS $\bar{\sigma}_s$ (X 10⁴)
TOTAL MERIDIONAL AT TOP
1.0
0.8
0.6
0.4
0.2
0.0
-0.2
-0.4
-0.6
-0.8
-1.0
0.25
0.30
0.35
0.40
0.45
0.50
RADIUS $\bar{r}$

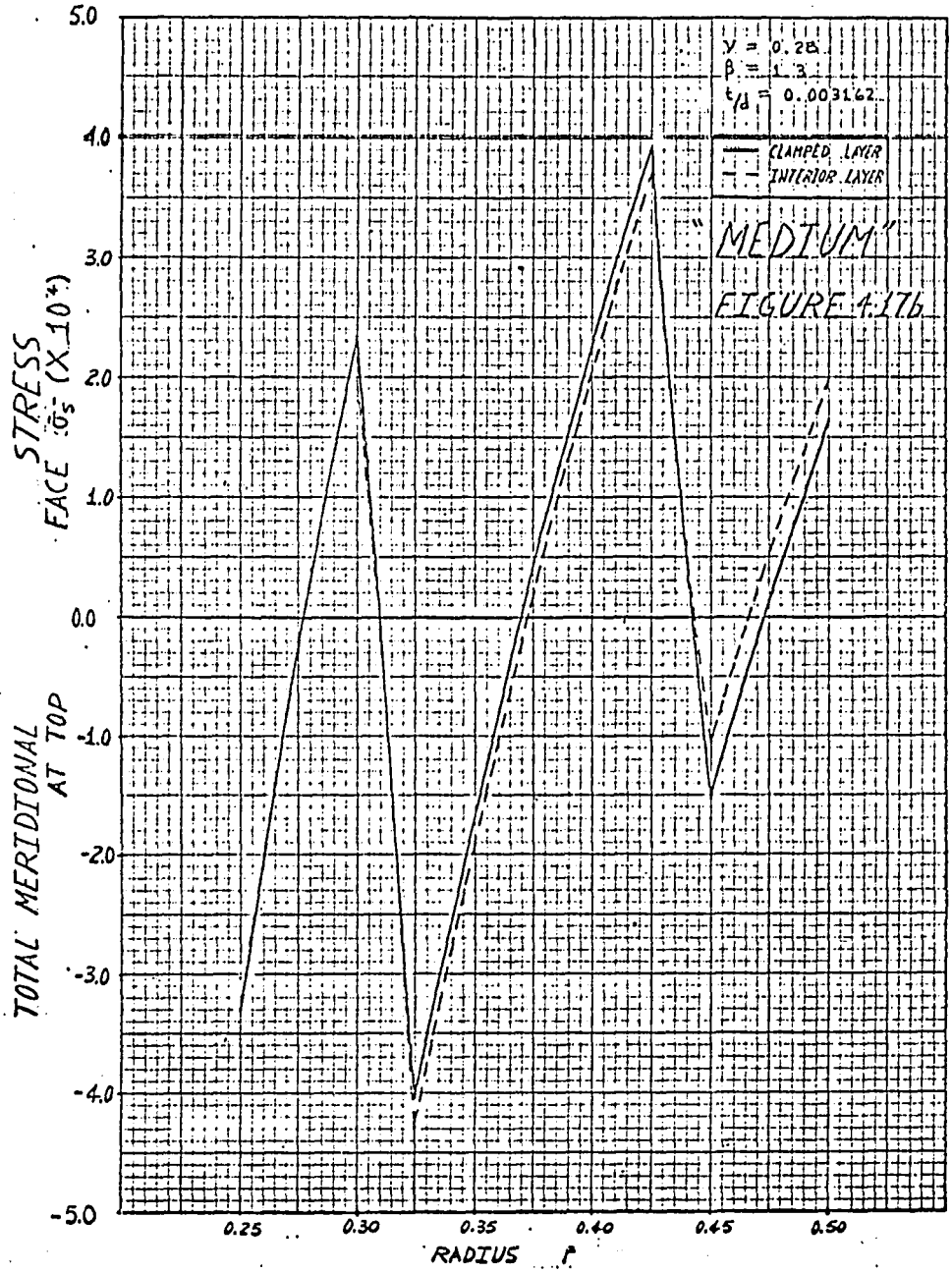
ν = 0.28
β = 1.3
t/d = 0.003162
CLAMPED LAYER
INTERIOR LAYER
"MEDIUM"
FIGURE 4.17b
TOTAL MERIDIONAL STRESS AT TOP FACE σs (X 10⁴)
5.0
4.0
3.0
2.0
1.0
0.0
-1.0
-2.0
-3.0
-4.0
-5.0
0.25
0.30
0.35
0.40
0.45
0.50
RADIUS r

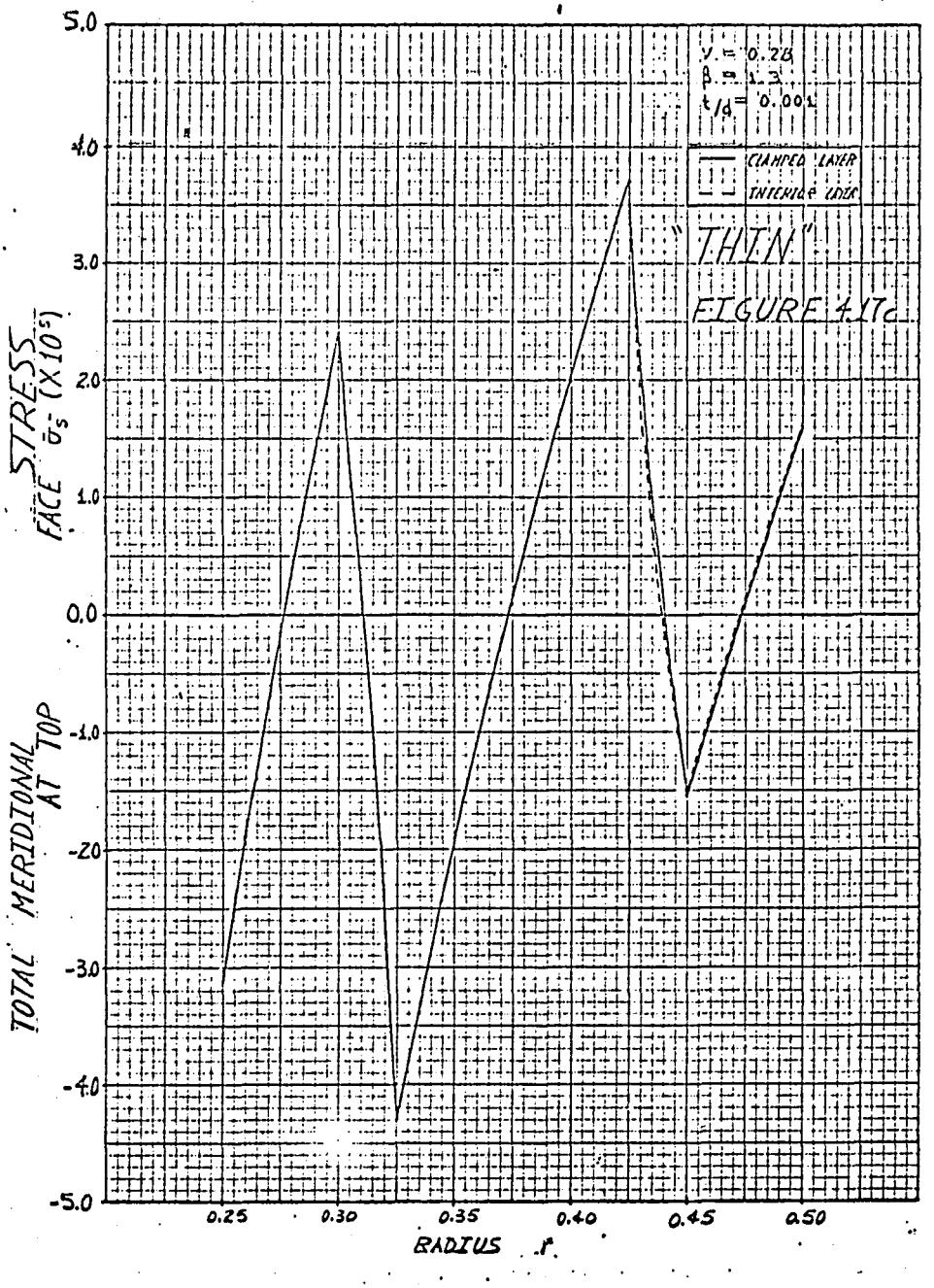
5.0
4.0
3.0
2.0
1.0
0.0
-1.0
-2.0
-3.0
-4.0
-5.0
0.25
0.30
0.35
0.40
0.45
0.50
RADIUS r
TOTAL MERIDIONAL STRESS AT TOP FACE $\bar{\sigma}_s$ ($\times 10^5$)
$\nu = 0.28$
$\beta = 1.3$
$t/a = 0.001$
CLAMPED LAYER
INTERIOR LAYER
"THIN"
FIGURE 4.11c

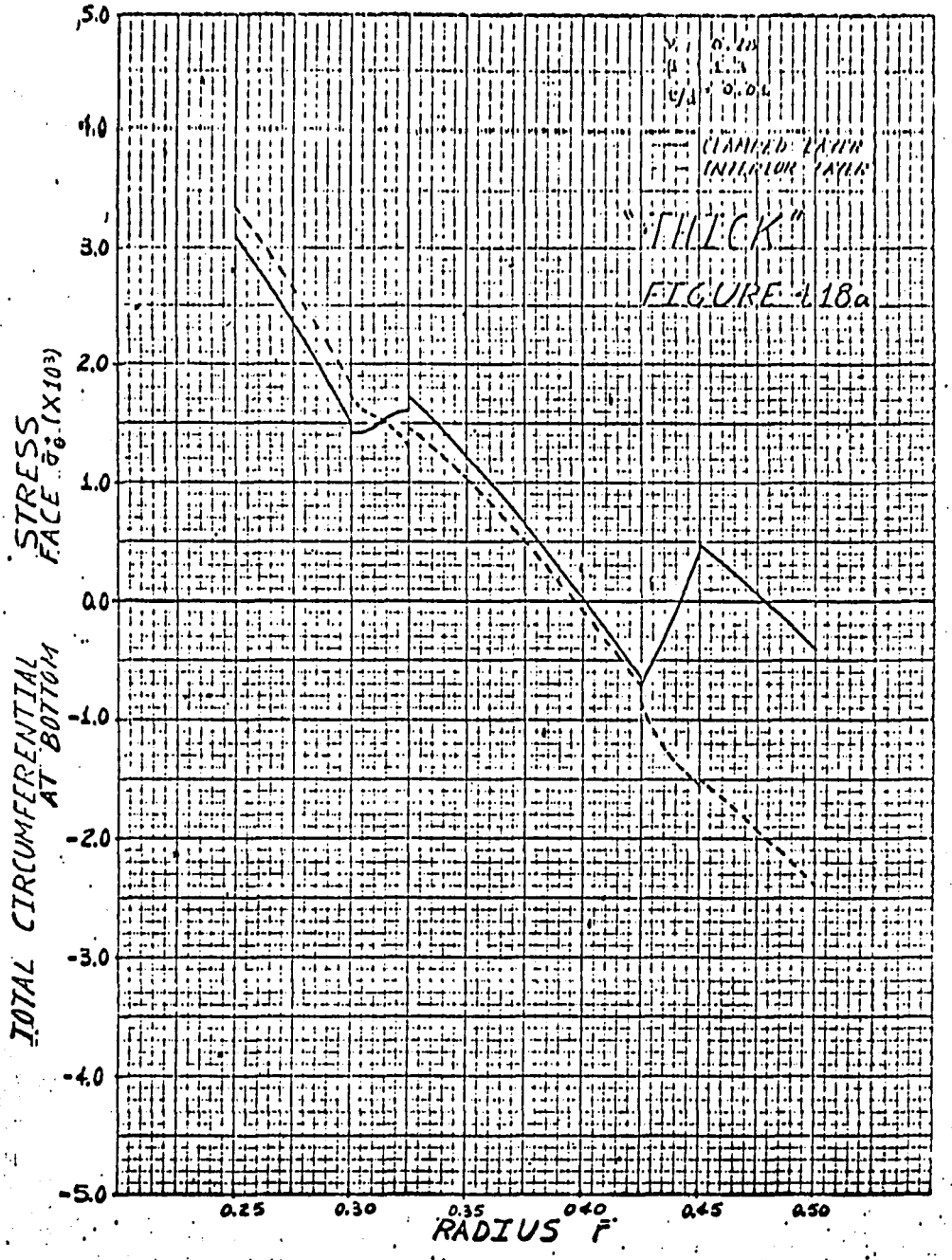
5.0
4.0
3.0
2.0
1.0
0.0
-1.0
-2.0
-3.0
-4.0
-5.0
0.25
0.30
0.35
0.40
0.45
0.50
RADIUS r
TOTAL CIRCUMFERENTIAL STRESS AT BOTTOM FACE σ_θ (X 10³)
CLAMPED EDGE
INTERIOR FACE
"THICK"
FIGURE 4.18a

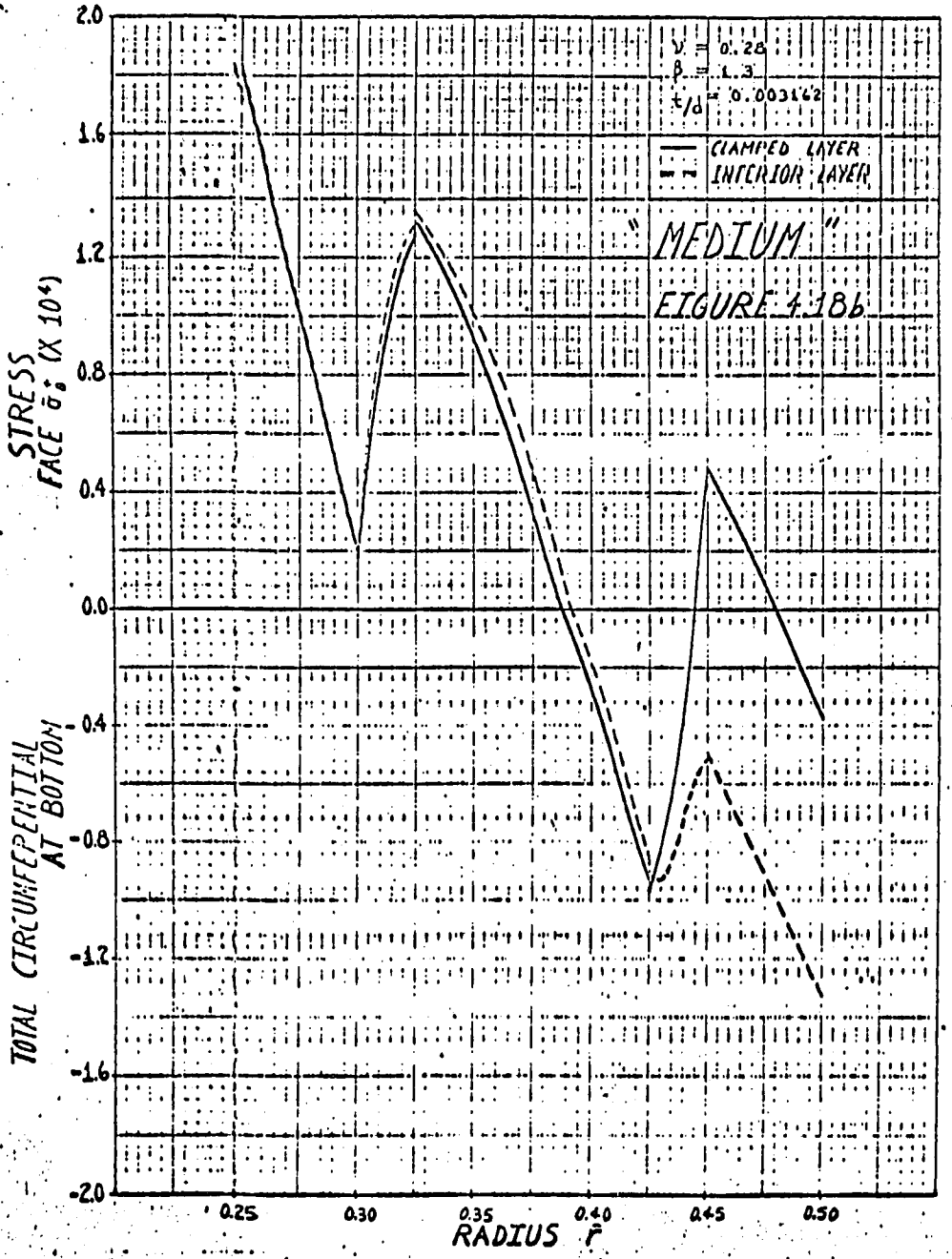
ν = 0.28
β = 1.3
t/d = 0.003162
CLAMPED LAYER
INTERIOR LAYER
"MEDIUM"
FIGURE 4.18b
STRESS FACE σ̄θ (X 10⁴)
TOTAL CIRCUMFERENTIAL AT BOTTOM
RADIUS r̄
2.0
1.6
1.2
0.8
0.4
0.0
-0.4
-0.8
-1.2
-1.6
-2.0
0.25
0.30
0.35
0.40
0.45
0.50

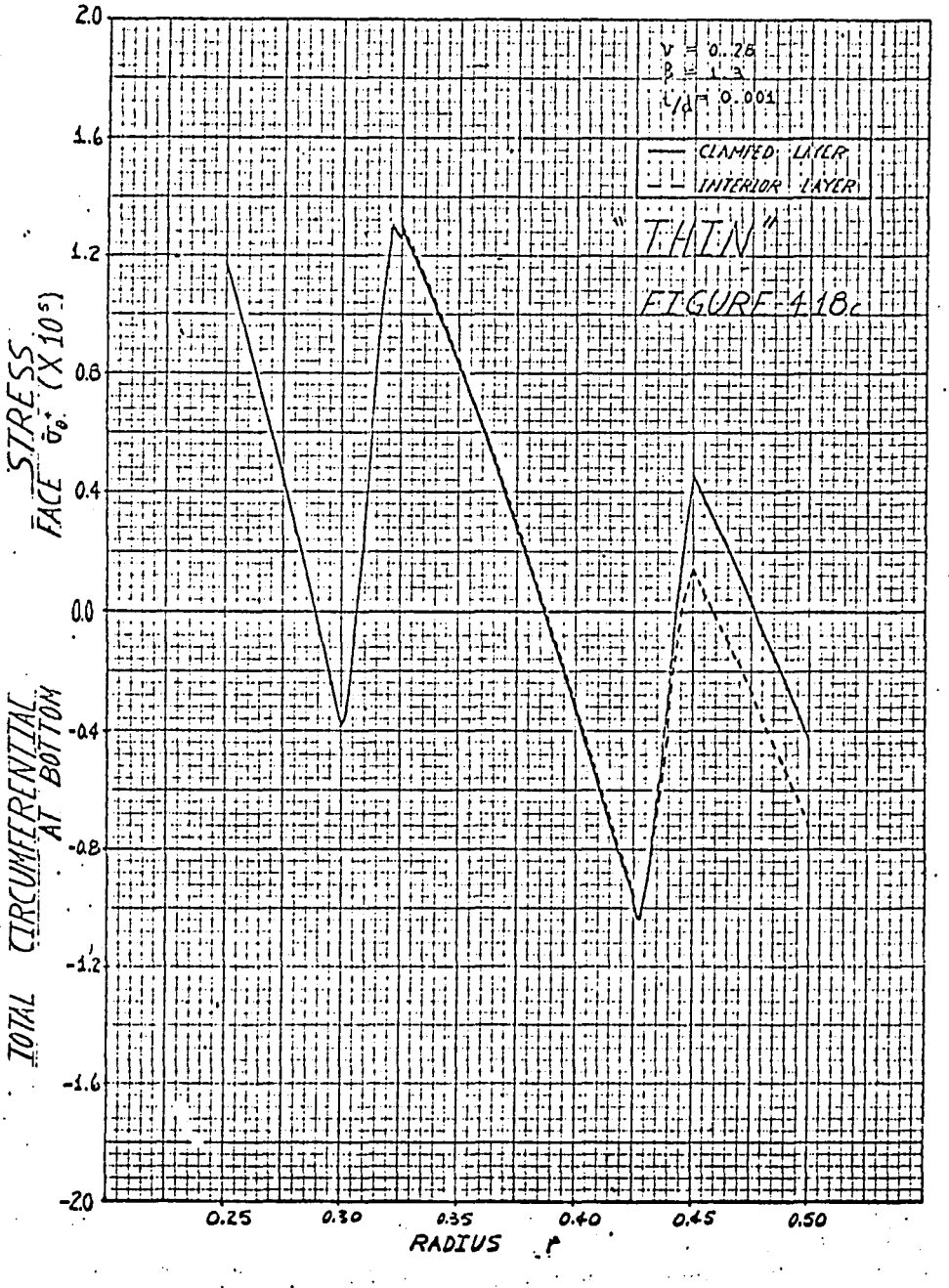
ν = 0.28
β = 1
t/d = 0.001
CLAMPED LAYER
INTERIOR LAYER
"THIN"
FIGURE 4.18c
TOTAL CIRCUMFERENTIAL STRESS AT BOTTOM FACE $\bar{\sigma}_\theta$ (X 10⁵)
2.0
1.6
1.2
0.8
0.4
0.0
-0.4
-0.8
-1.2
-1.6
-2.0
0.25
0.30
0.35
0.40
0.45
0.50
RADIUS r

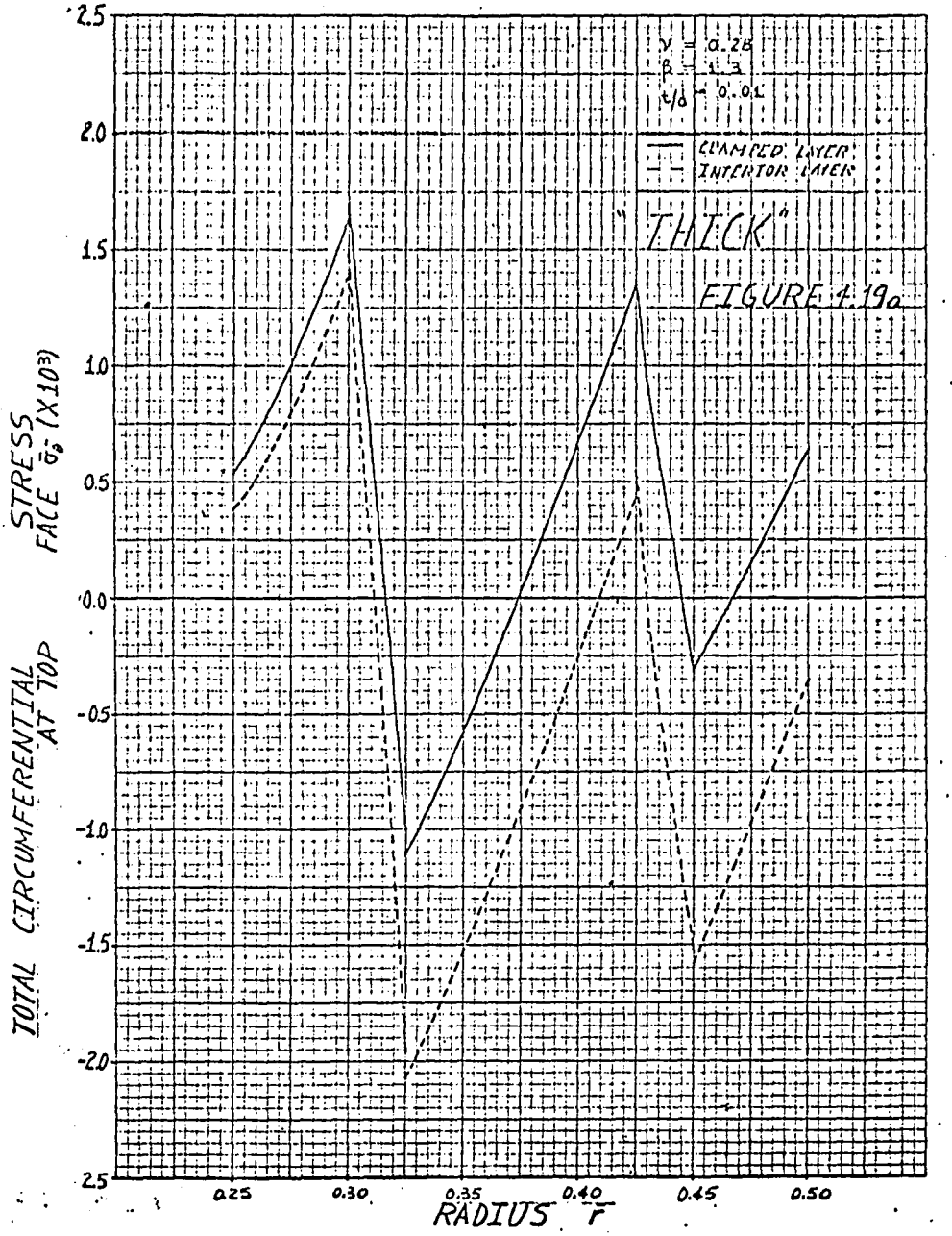
ν = 0.28
β = 1.3
t/a = 0.01
CLAMPED LAYER
INTERIOR LAYER
"THICK"
FIGURE 4.19a
TOTAL CIRCUMFERENTIAL STRESS AT TOP FACE $\bar{\sigma}_\theta$ (X10³)
RADIUS $\bar{r}$
2.5
2.0
1.5
1.0
0.5
0.0
-0.5
-1.0
-1.5
-2.0
-2.5
0.25
0.30
0.35
0.40
0.45
0.50

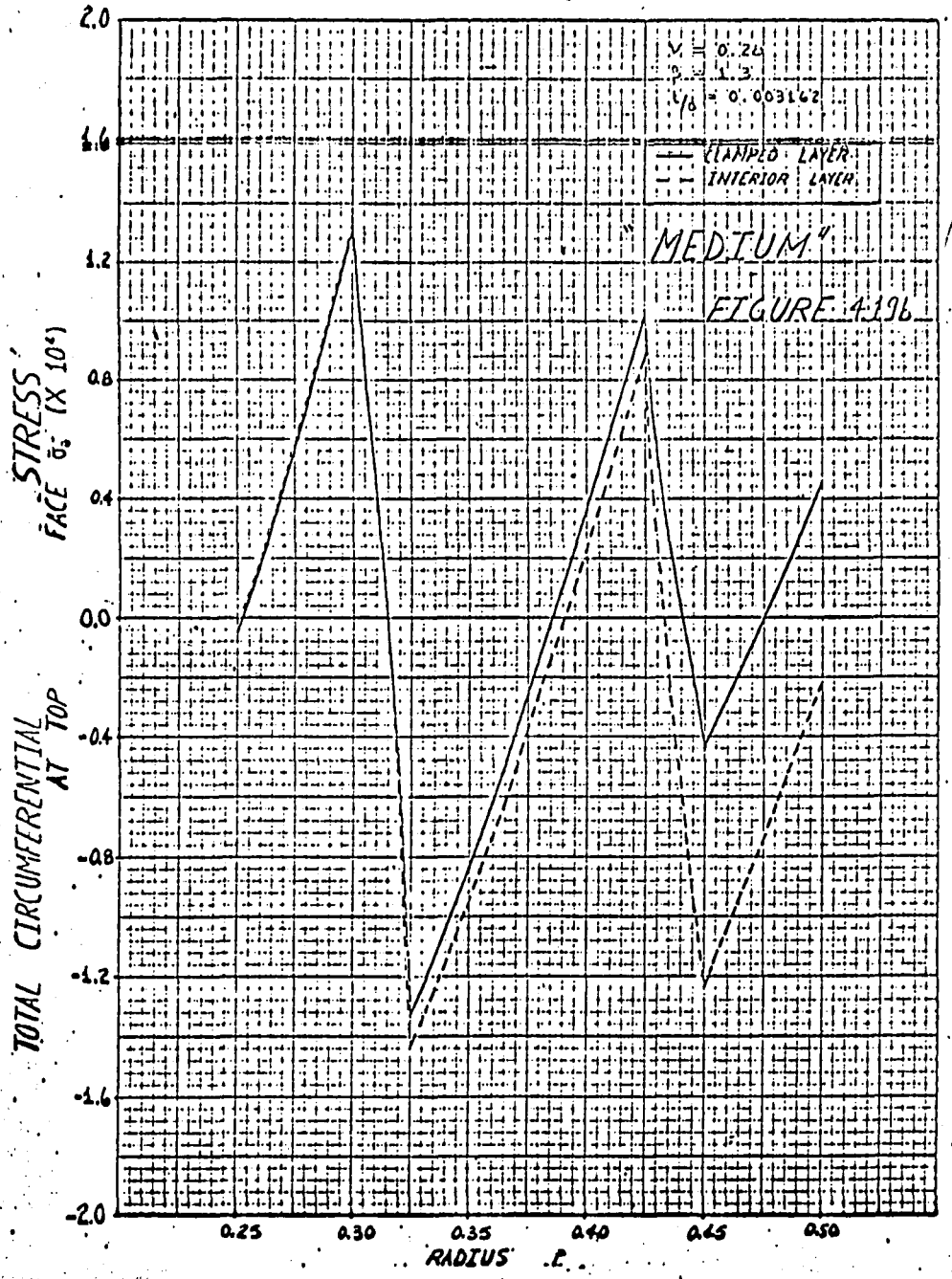
2.0
1.6
1.2
0.8
0.4
0.0
-0.4
-0.8
-1.2
-1.6
-2.0
0.25
0.30
0.35
0.40
0.45
0.50
RADIUS r
TOTAL CIRCUMFERENTIAL STRESS AT TOP FACE $\bar{\sigma}_\theta$ (X 10⁴)
ν = 0.24
ρ = 1.3
t/a = 0.003162
CLAMPED LAYER
INTERIOR LAYER
"MEDIUM"
FIGURE 4-19b

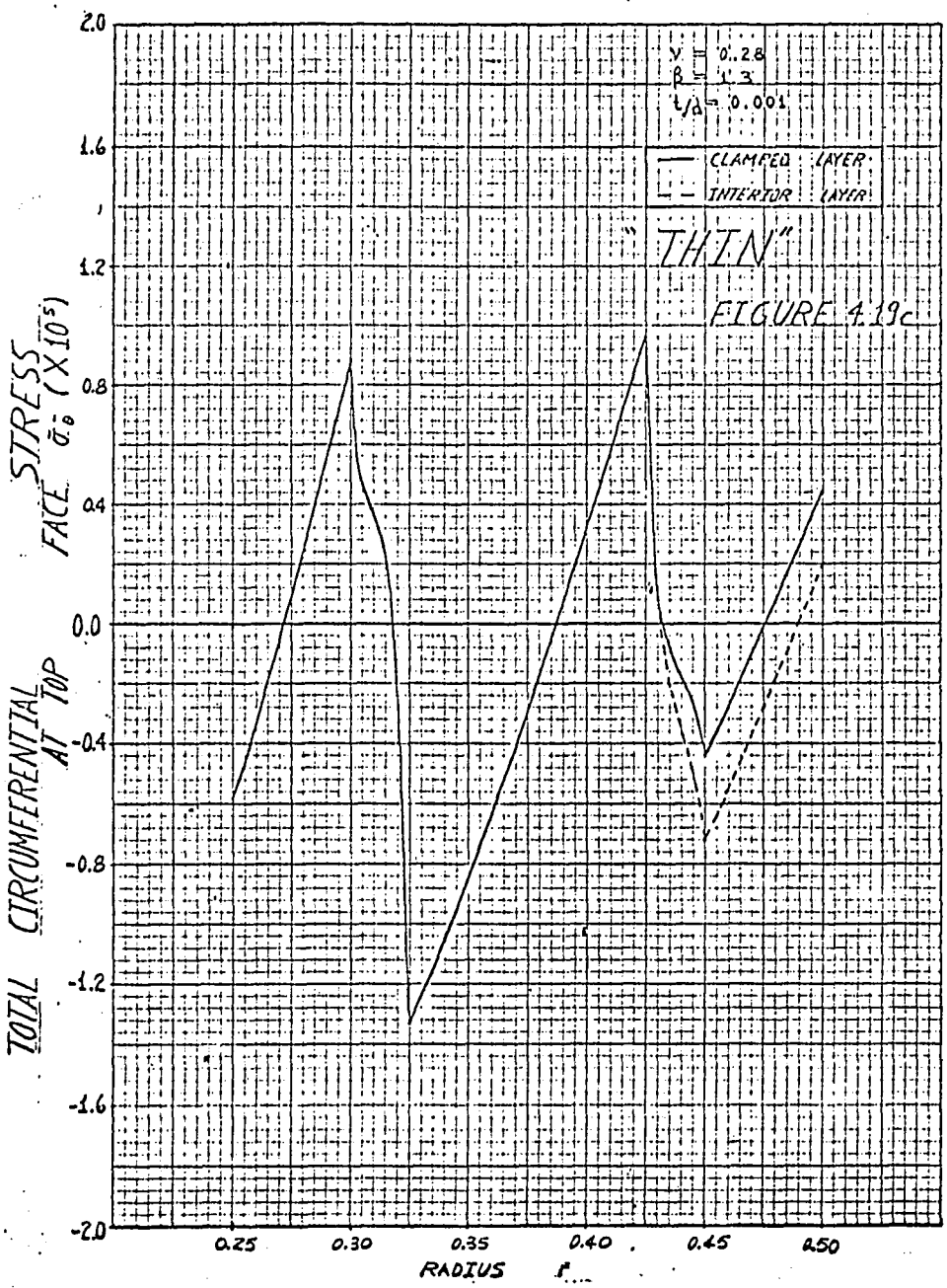
ν = 0.28
β = 1.3
t/a = 0.001
CLAMPED LAYER
INTERIOR LAYER
"THIN"
FIGURE 4.19c
TOTAL CIRCUMFERENTIAL STRESS AT TOP FACE $\bar{\sigma}_\theta$ ($\times 10^5$)
2.0
1.6
1.2
0.8
0.4
0.0
-0.4
-0.8
-1.2
-1.6
-2.0
0.25
0.30
0.35
0.40
0.45
0.50
RADIUS

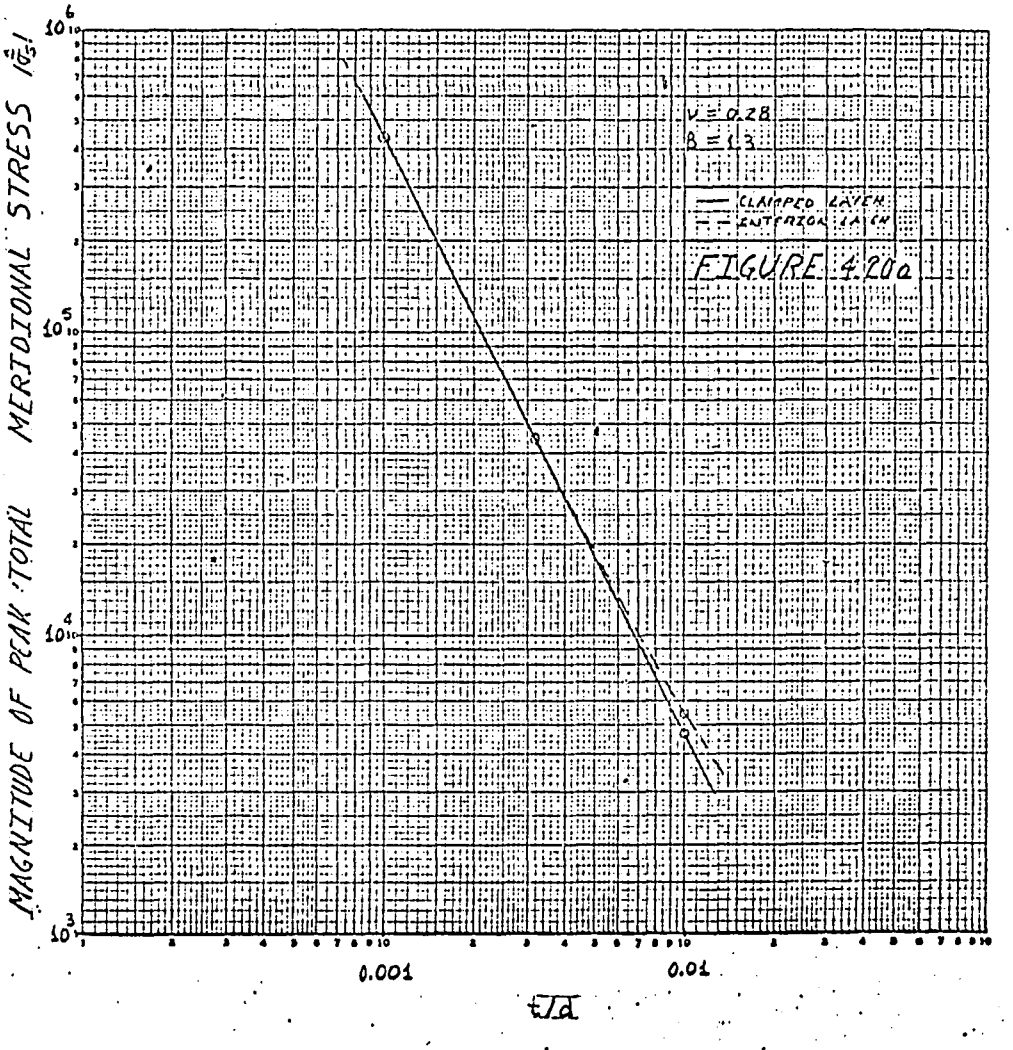
MAGNITUDE OF PEAK TOTAL MERIDIONAL STRESS 10^{-5}
10^6
10^5
10^4
10^3
0.001
0.01
t/d
ν = 0.28
β = 1.3
CLAMPED LAYER
INTERFACE LAYER

FIGURE 4.20a

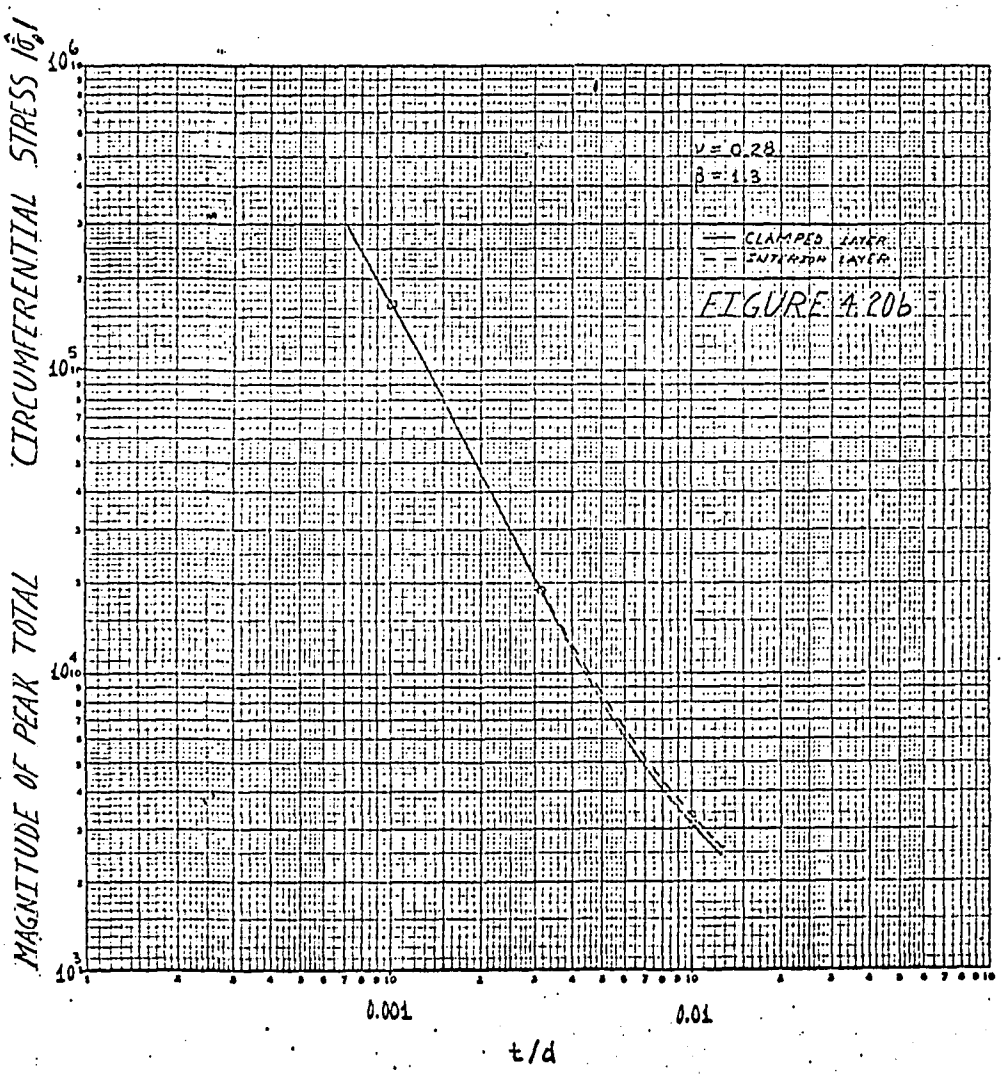
MAGNITUDE OF PEAK TOTAL CIRCUMFERENTIAL STRESS $|\tilde{\sigma}_\theta|$
10^6
10^5
10^4
10^3
$\nu = 0.28$
$\beta = 1.3$
CLAMPED LAYER
ENTRATION LAYER
0.001
0.01
t/d

FIGURE 4.206

meridional stress exceeds the peak value of total circumferential stress by more than 200%. This is true for the clamped and interior layer. Nevertheless, the total stresses in both the meridional and circumferential directions will be important.

Since the shearing strength is usually lower than the tensile strength, the largest possible shearing stress might conceivably be the most important quantity relating to welded bellows failure. Therefore, we will now compute the maximum shearing stress. At the top and bottom face for each point within the bellows, a local (s, θ, z) coordinate system yields $\overline{\tau}_{sz} = \overline{\tau}_{\theta s} = \overline{\tau}_{z\theta} = 0$, provided that $Y = 0$ in equation (2.4-1a). Hence, at each point, the principal stresses at the top and bottom faces are $\overline{\sigma}^{-}_{s}$, $\overline{\sigma}^{-}_{\theta}$, $\overline{\sigma}^{-}_{z} = 0$, and $\overline{\sigma}^{+}_{s}$, $\overline{\sigma}^{+}_{\theta}$, $\overline{\sigma}^{+}_{z} = 0$, respectively. The largest possible shearing stress at either face is then obtained by taking the appropriate set of principal stresses and forming one half the difference between the algebraically largest principal stress and the algebraically smallest principal stress. The results for the absolute value of the largest possible shearing stress at the bottom and top face are presented in Figs. 4.21a-c and 4.22a-c, respectively. Except for magnitude, the variation of $\hat{\overline{\tau}}_{+}$ and $\hat{\overline{\tau}}_{-}$ is the same. The variation of peak $\hat{\overline{\tau}}_{+}$ and $\hat{\overline{\tau}}_{-}$ as a function of $\frac{t}{d}$ for both the clamped and interior layer is presented in Figs. 4.23a-b, respectively. Here, we notice that throughout the $\frac{t}{d}$ range, the peak values of $\hat{\overline{\tau}}_{+}$ and $\hat{\overline{\tau}}_{-}$ in the interior layer exceed their respective peak values in the clamped layer.

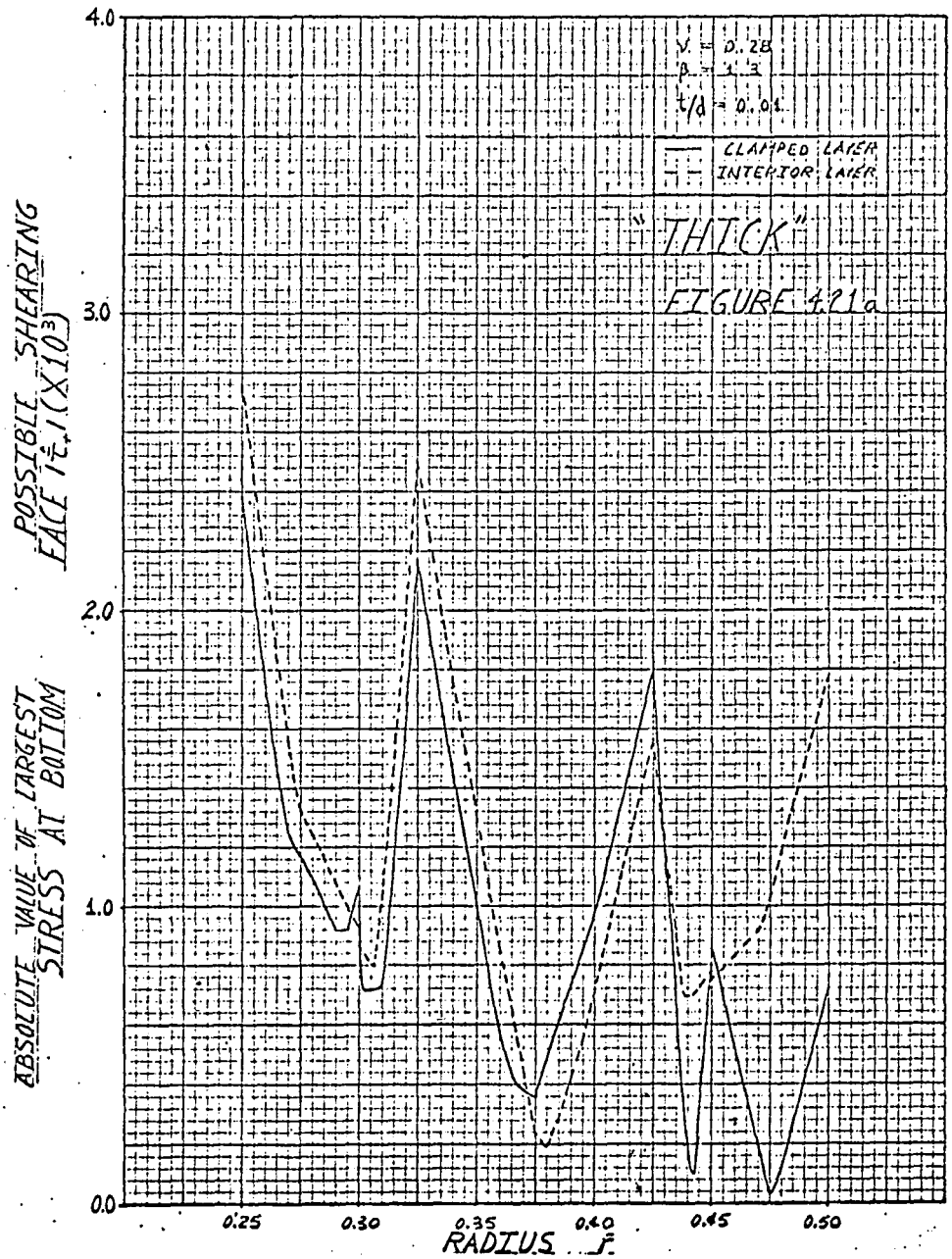
4.0
3.0
2.0
1.0
0.0
0.25
0.30
0.35
0.40
0.45
0.50
RADIUS r
ABSOLUTE VALUE OF LARGEST STRESS AT BOTTOM FACE $\tau_{r\theta}$ (X 10³)
ν = 0.28
β = 1.3
t/a = 0.01
CLAMPED LAYER
INTERIOR LAYER
"THICK"
FIGURE 4.21a

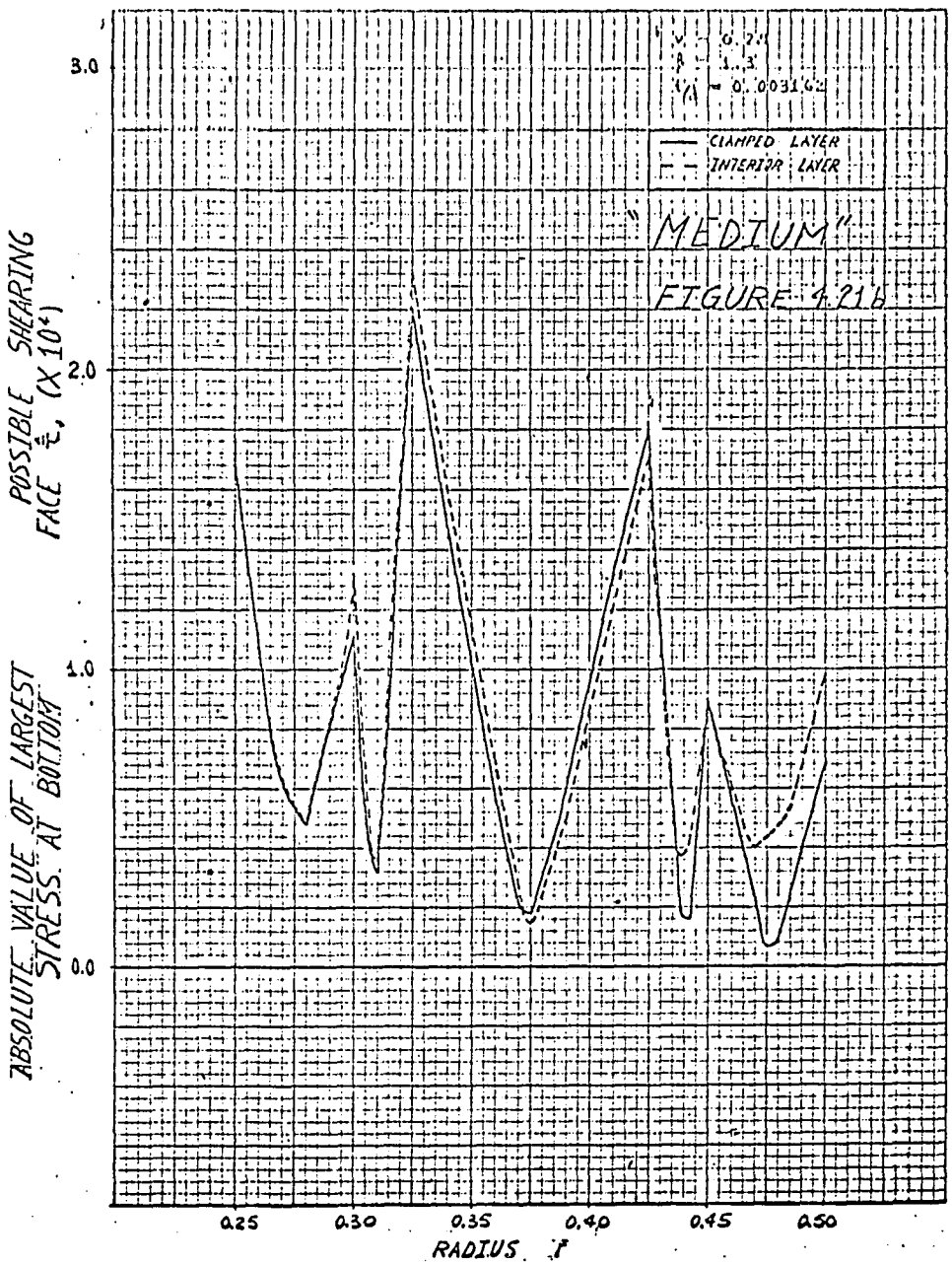
ν = 0.2
β = 1.3
γ/λ = 0.0031.62
CLAMPED LAYER
INTERIOR LAYER
"MEDIUM"
FIGURE 4.21b
POSSIBLE SHEARING FACE τ̂, (X 10⁴)
ABSOLUTE VALUE OF LARGEST STRESS AT BOTTOM
3.0
2.0
1.0
0.0
0.25
0.30
0.35
0.40
0.45
0.50
RADIUS r

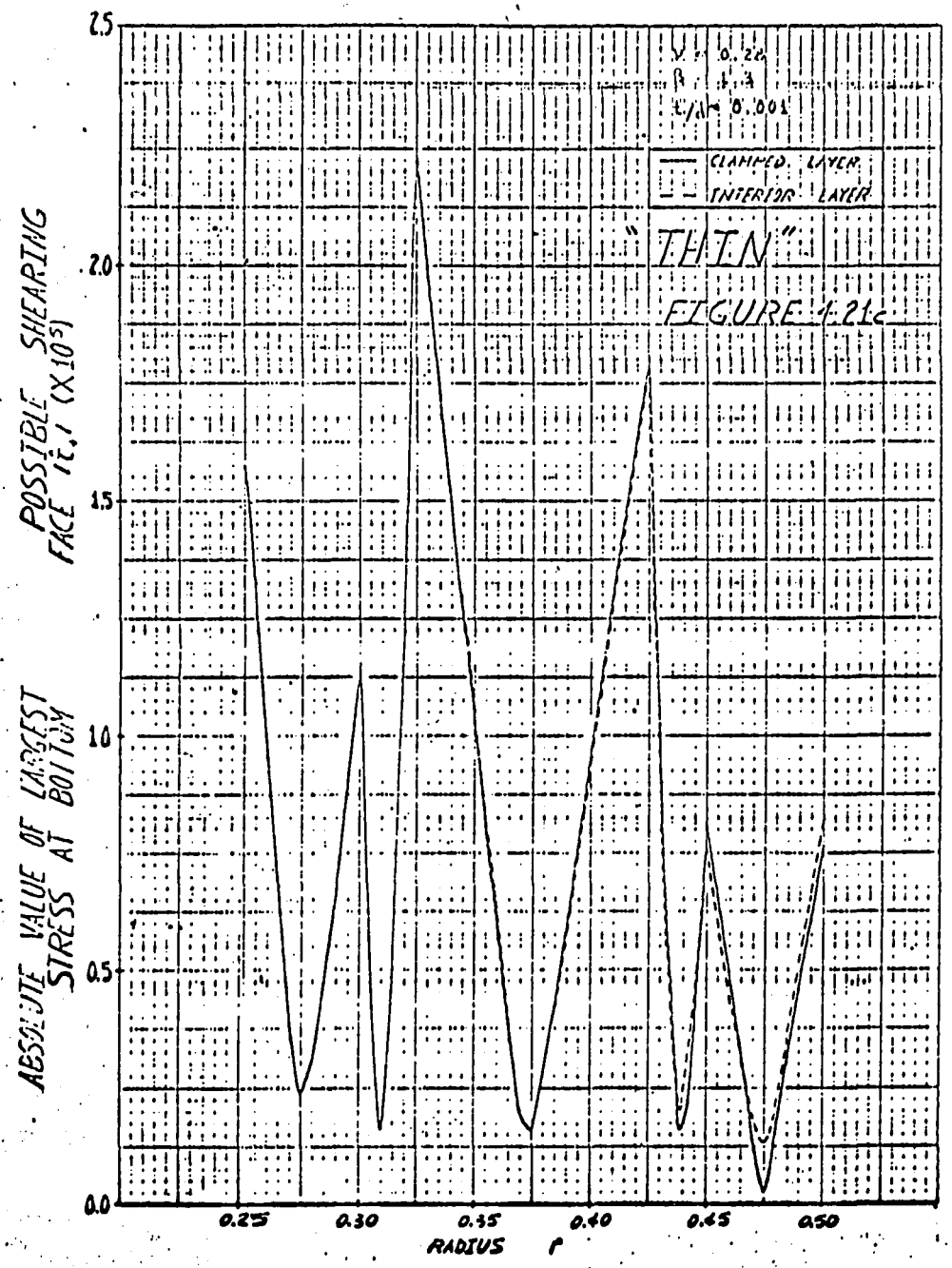
ABSOLUTE VALUE OF LARGEST STRESS AT BOTTOM
POSSIBLE SHEARING FACE $\tau_{r,r}$ ($\times 10^5$)
2.5
2.0
1.5
1.0
0.5
0.0
0.25
0.30
0.35
0.40
0.45
0.50
RADIUS r
ν = 0.22
β = 1.3
t/a = 0.001
CLAMPED LAYER
INTERIOR LAYER
"THIN"
FIGURE 4.21c

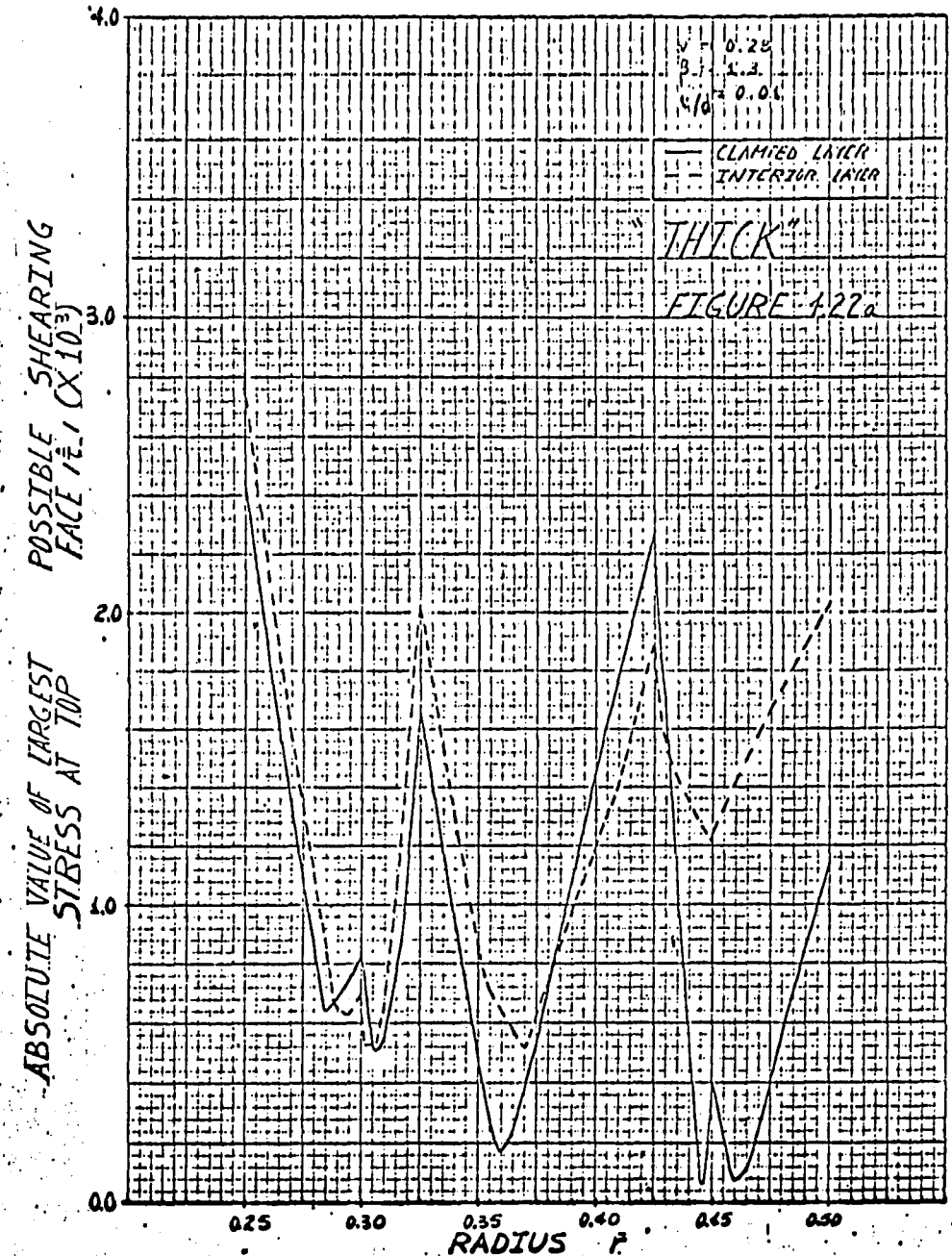
ABSOLUTE VALUE OF LARGEST POSSIBLE SHEARING STRESS AT TOP FACE $\tau_{z,1}$ ($\times 10^3$)
4.0
3.0
2.0
1.0
0.0
0.25
0.30
0.35
0.40
0.45
0.50
RADIUS r
ν = 0.25
β = 1.3
c/a = 0.01
CLAMPED LATER
INTERIOR LAYER
"THICK"

FIGURE 4.22a

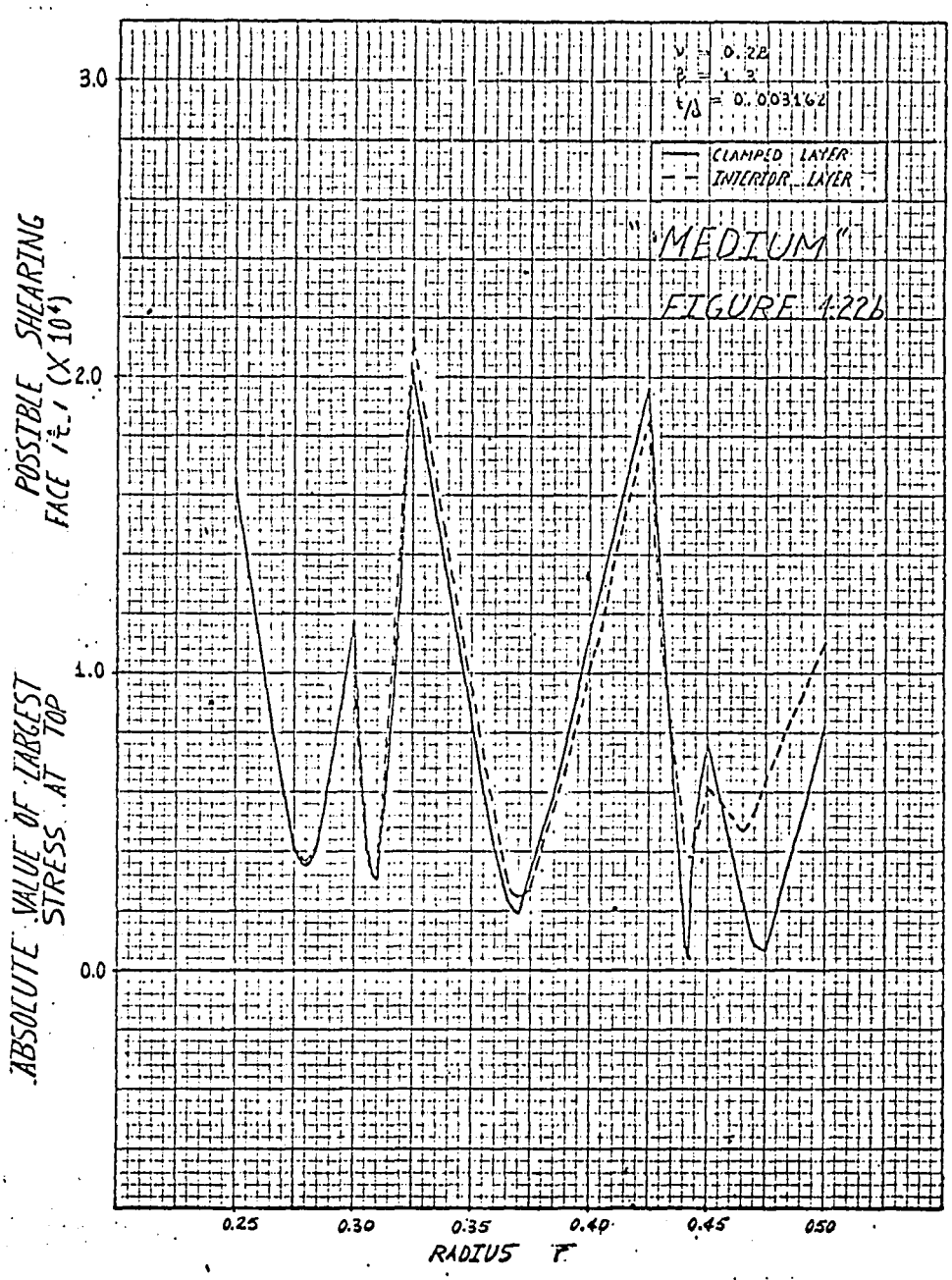
ν = 0.22
P = 1.3
t/a = 0.0.03162
CLAMPED LAYER
INTERIOR LAYER
"MEDIUM"
FIGURE 4.22b
ABSOLUTE VALUE OF LARGEST POSSIBLE SHEARING STRESS AT TOP FACE (X 10⁴)
3.0
2.0
1.0
0.0
0.25
0.30
0.35
0.40
0.45
0.50
RADIUS r

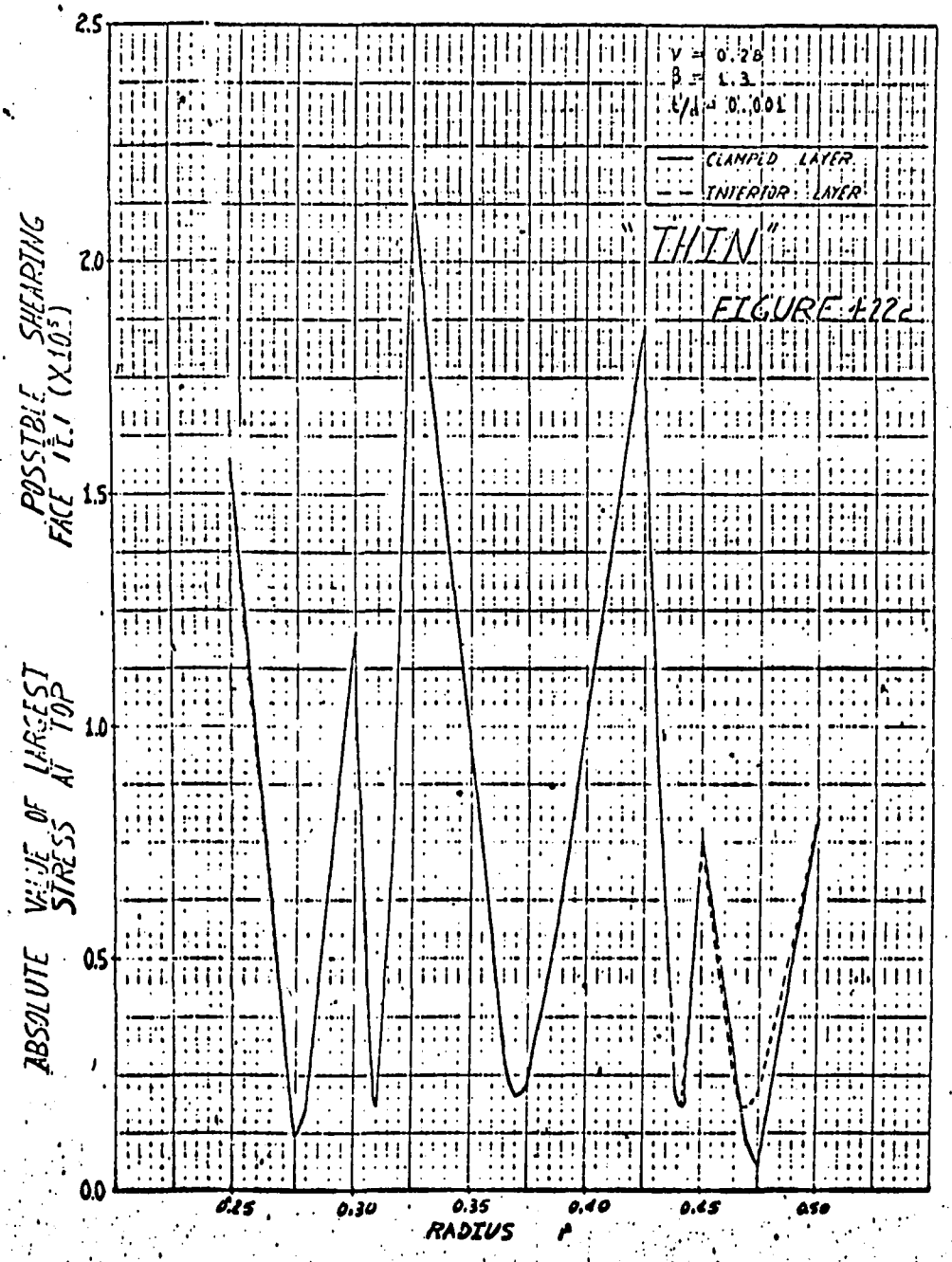
ABSOLUTE VALUE OF LARGEST POSSIBLE SHEARING STRESS AT TOP FACE IE.1 (X.10⁵)
2.5
2.0
1.5
1.0
0.5
0.0
0.25
0.30
0.35
0.40
0.45
0.50
RADIUS r
ν = 0.28
β = 1.3
t/a = 0.001
CLAMPED LAYER
INTERIOR LAYER
"THIN"
FIGURE 4.22c

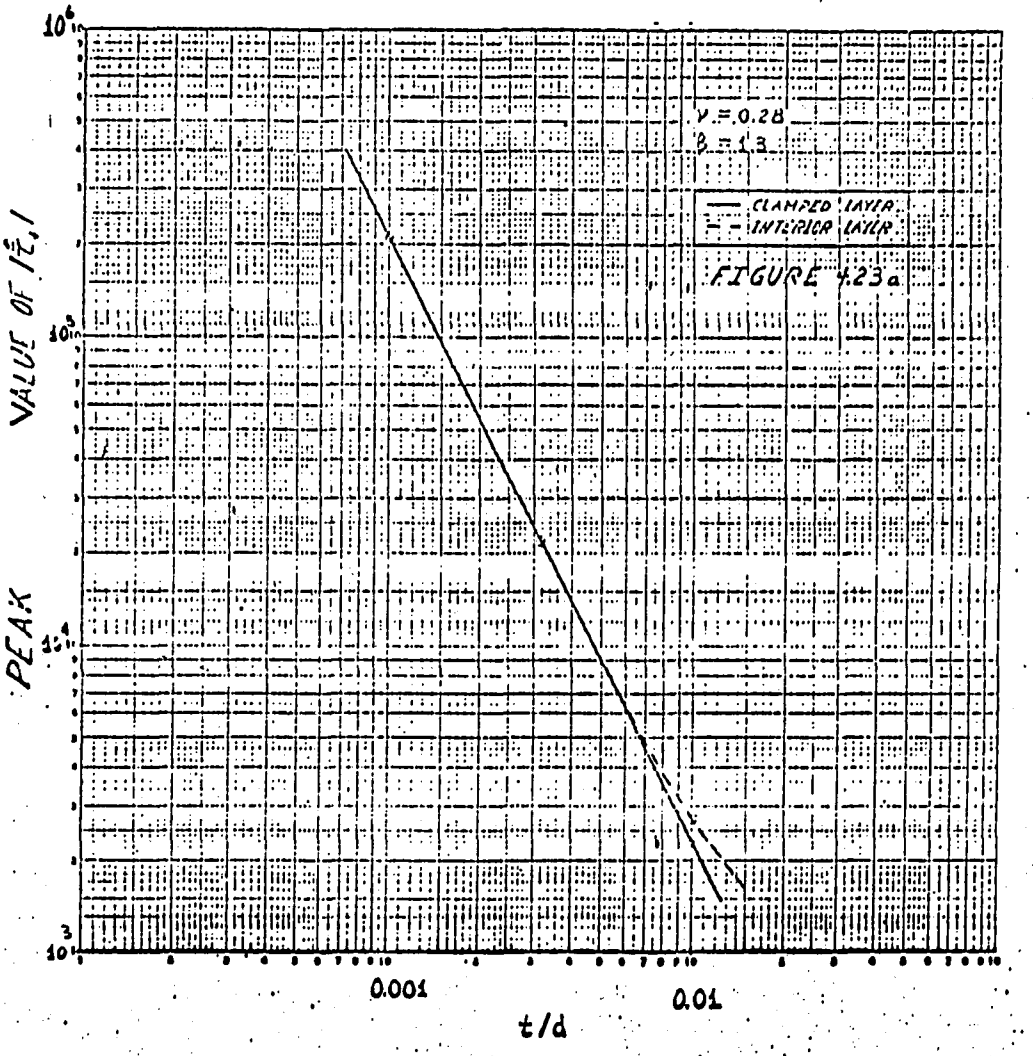
PEAK VALUE OF |ε|
ν = 0.28
β = 1.3
CLAMPED LAYER
INTERIOR LAYER
0.001
0.01
t/d

FIGURE 4.23a

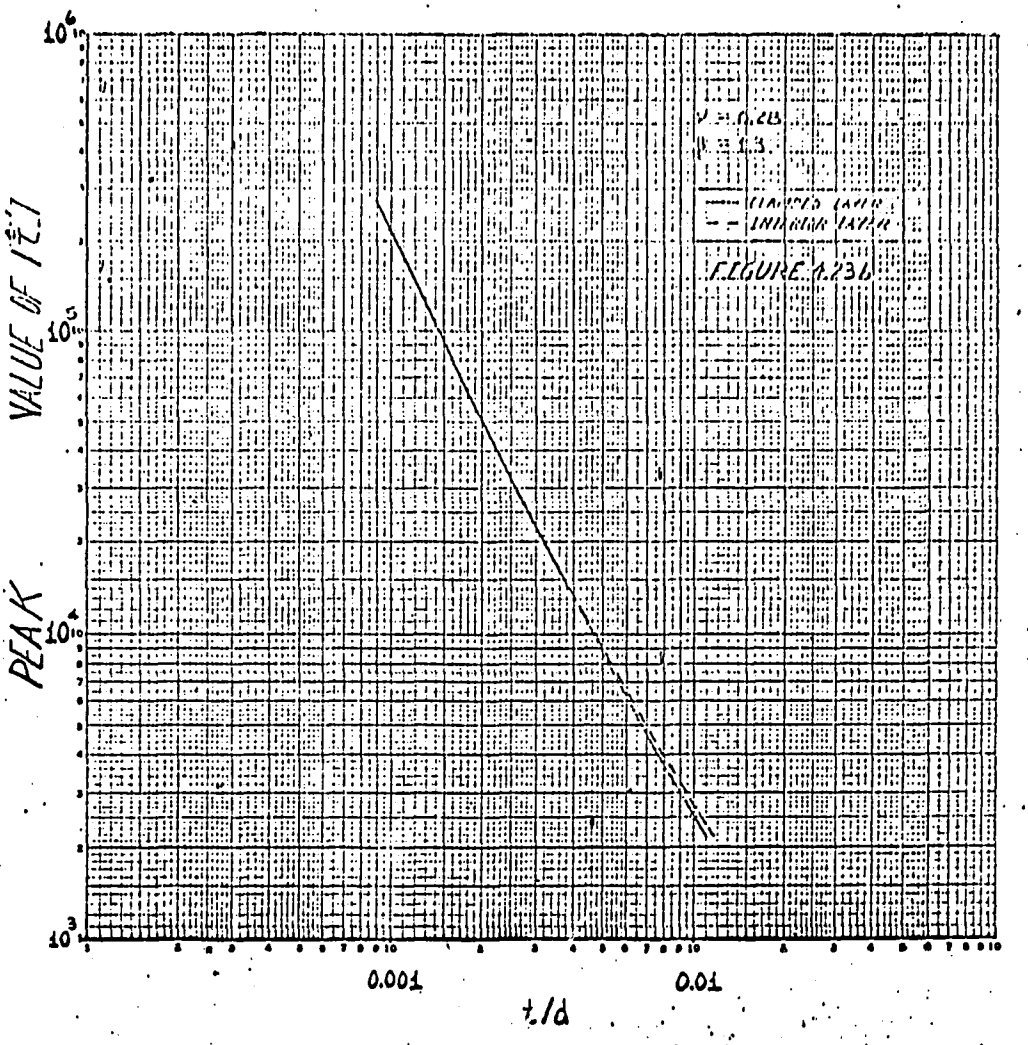
PEAK VALUE OF I'E'J
10^6
10^5
10^4
10^3
0.001
0.01
t/d
FIGURE A.23b

Another quantity of considerable interest for design purposes is the ratio of peak stress to the maximum vertical deflection which produces it. The magnitude of this ratio as a function of $\frac{t}{d}$ is presented in Fig. 4.24. One observes that for both the clamped and interior layer, "thin" welded bellows give a somewhat lower peak stress for a prescribed vertical deflection, as would be expected. For comparison, the dotted line represents the corresponding ratio for a clamped circular plate in pure bending.

The effect of the welds on the vertical deflection of the bellows is illustrated in Figs. 4.25a-c. Clearly welds decrease the flexibility of bellows, with their stiffening effect becoming more pronounced as $\frac{t}{d}$ increases.

4.3 A BOUNDARY LAYER EFFECT

A study of any component of displacement or stress presented in the preceeding sections shows that the displacement-stress behavior of any layer approaches the displacement-stress behavior associated with an interior layer as we move farther away from the rigid clamp at $\bar{r} = 0.5$. In effect, precision welded bellows exhibit a boundary layer effect, as Figs. 4.26a-c indicate.

4.3.1 DEFINITION OF AN INTERIOR LAYER

In any welded bellows, the displacement-stress behavior of the outermost layers approaches the displacement-stress behavior of an interior layer. Consequently the

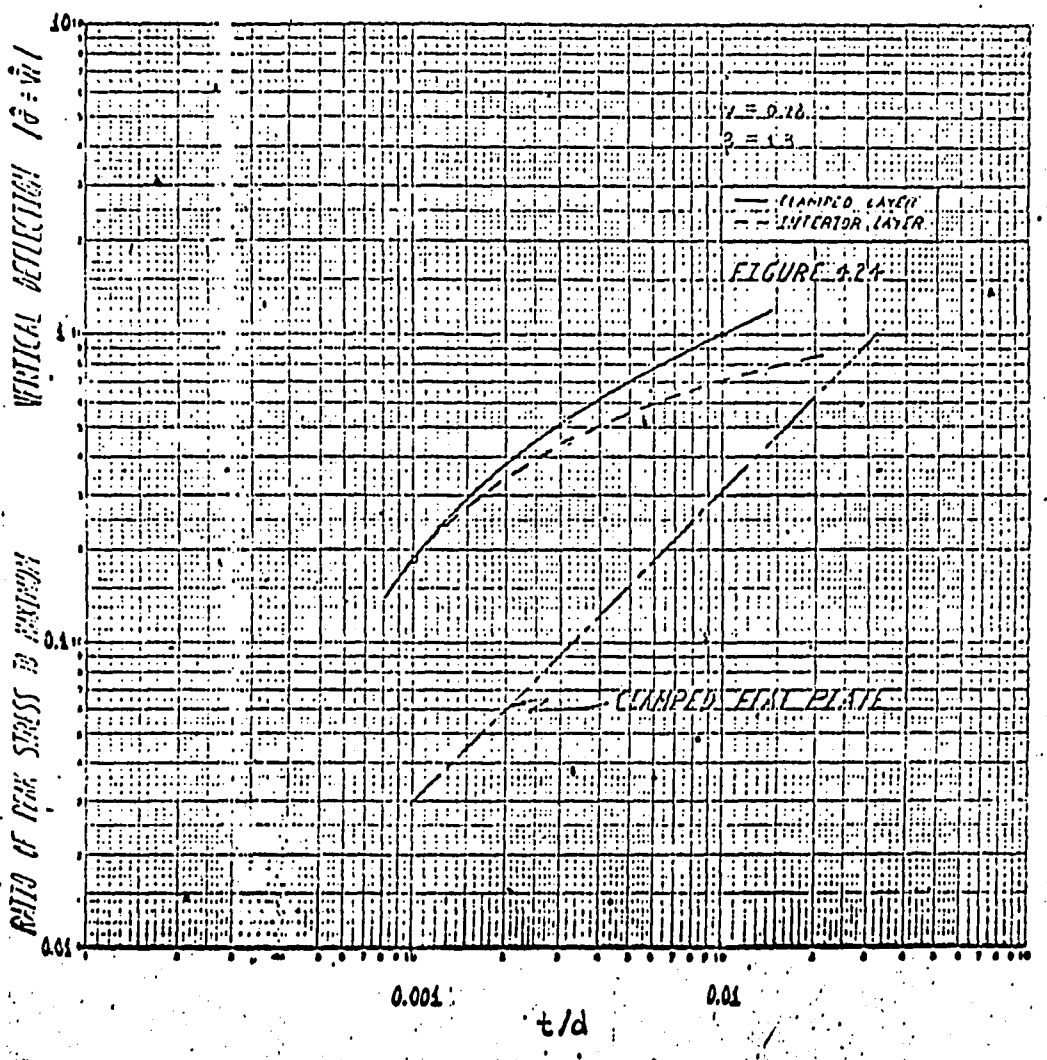
RATIO OF PEAK STRESS TO INCIDENT VERTICAL DEFLECTION (σ̂ = Ŵ)
10
1
0.1
0.01
0.001
0.01
t/d
ν = 0.18
β = 1.8
CLAMPED EDGE
LIMITATOR LAYER
CLAMPED FLAT PLATE

FIGURE 4.24

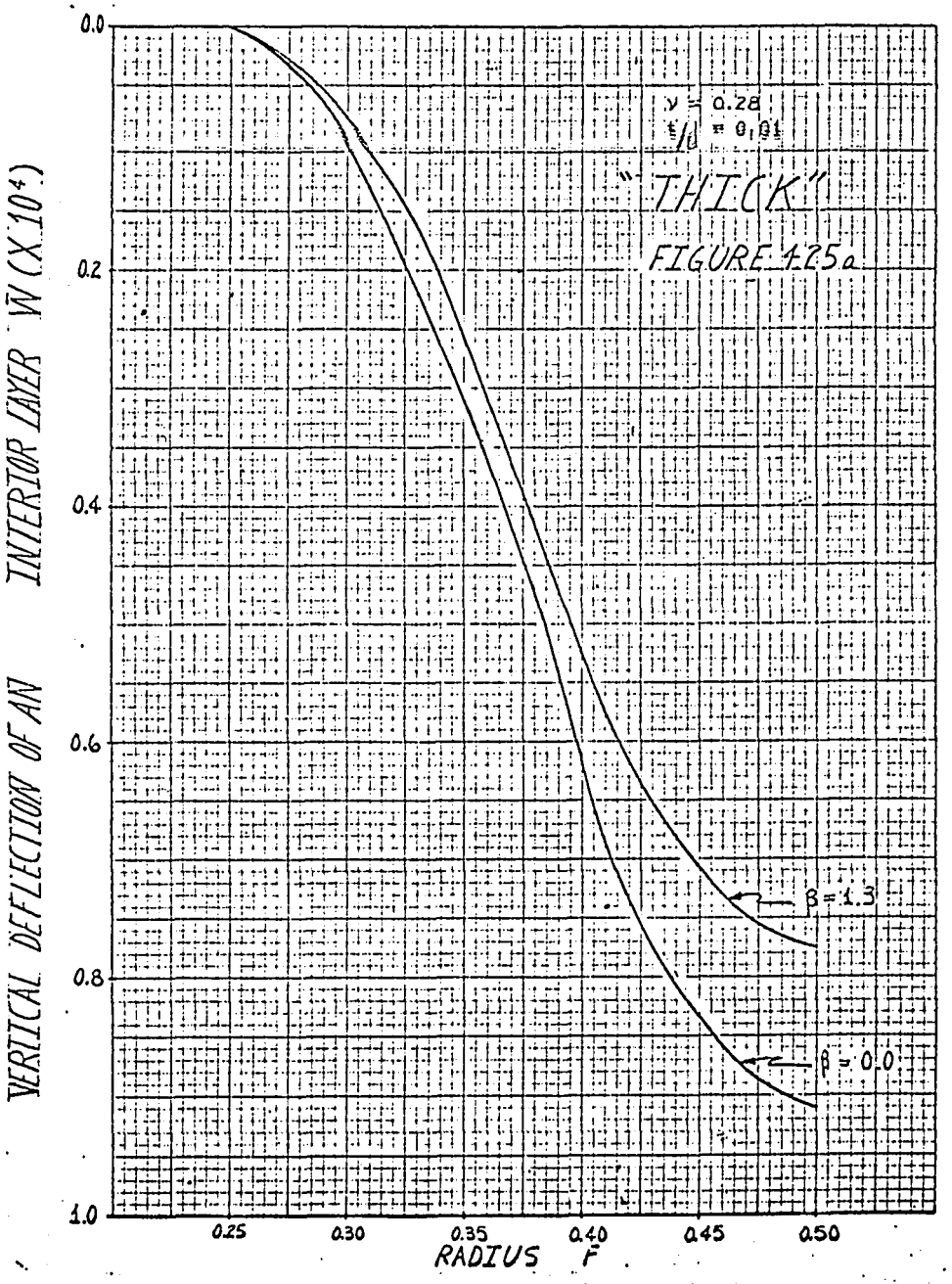
VERTICAL DEFLECTION OF AN INTERIOR LAYER W (X 10⁴)
0.0
0.2
0.4
0.6
0.8
1.0
0.25
0.30
0.35
0.40
0.45
0.50
RADIUS r
ν = 0.28
t/a = 0.01
"THICK"
β = 1.3
β = 0.0

FIGURE 12.5a

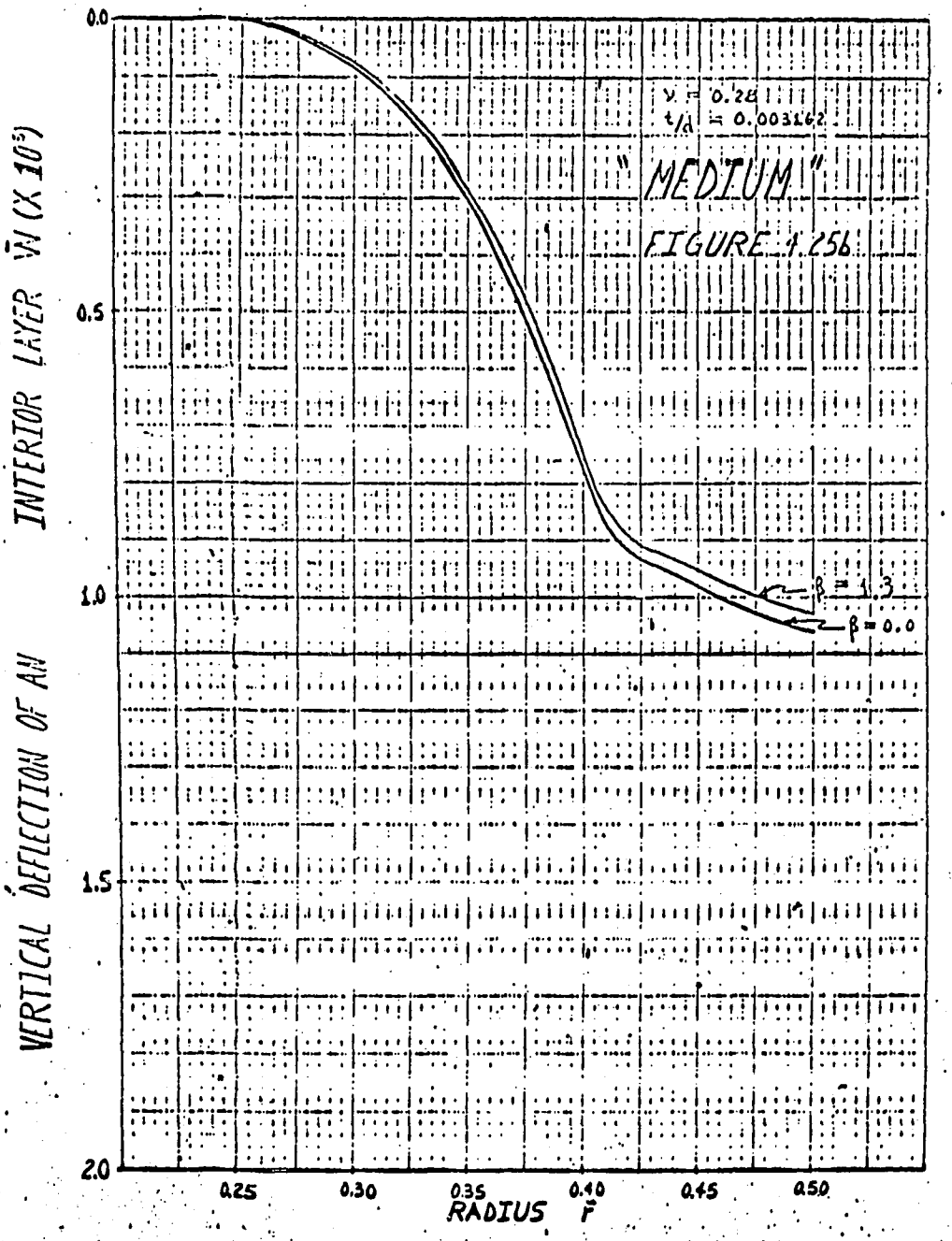
VERTICAL DEFLECTION OF AN INTERIOR LAYER Wi (X 10³)
0.0
0.5
1.0
1.5
2.0
0.25
0.30
0.35
0.40
0.45
0.50
RADIUS r
ν = 0.28
t/a = 0.003162
"MEDIUM"
FIGURE 4.256
β = 1.3
β = 0.0

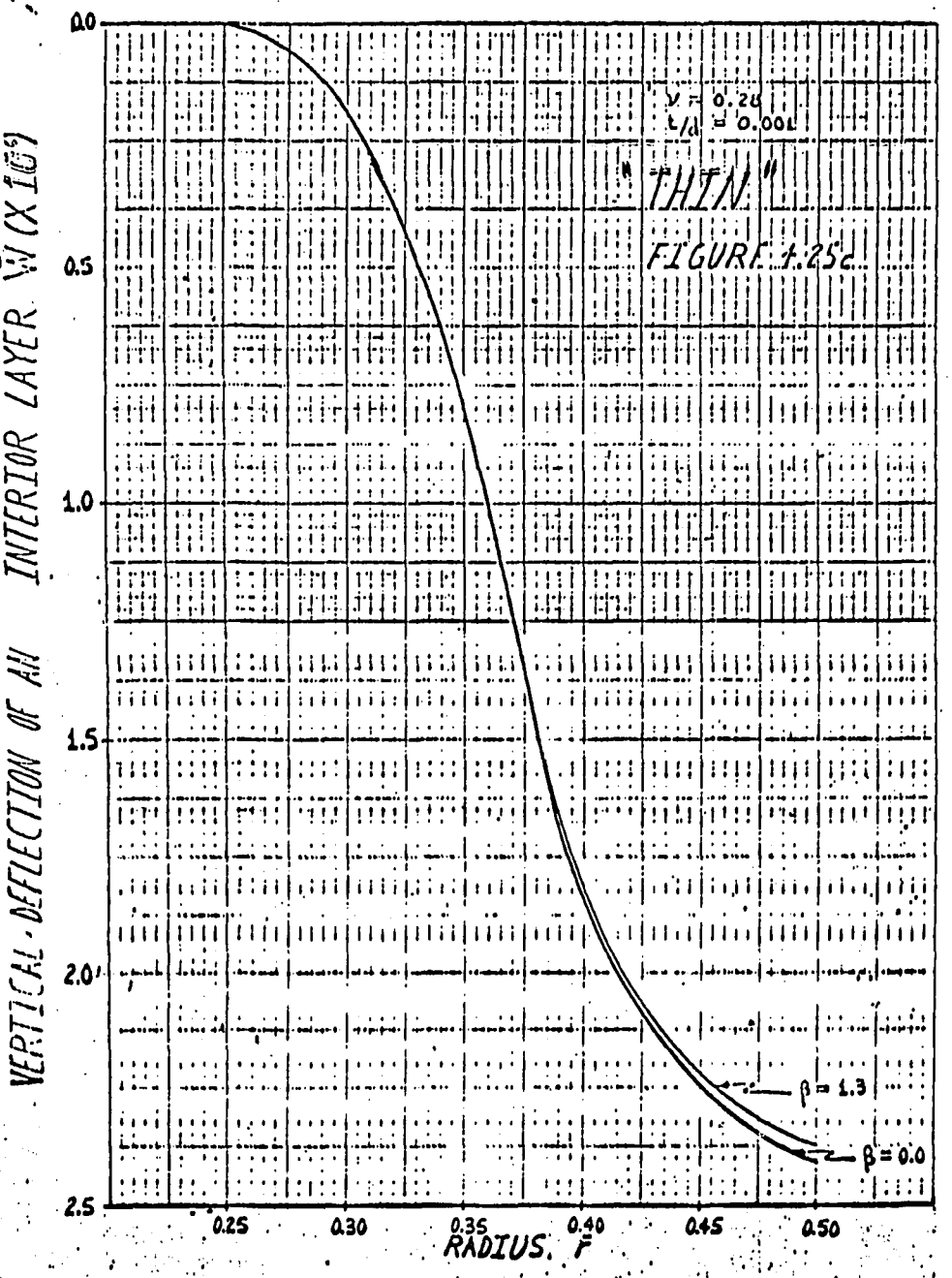
VERTICAL DEFLECTION OF MID INTERIOR LAYER W (X 10⁵)
0.0
0.5
1.0
1.5
2.0
2.5
0.25
0.30
0.35
0.40
0.45
0.50
RADIUS, r
ν = 0.28
t/d = 0.001
"THIN"
β = 1.3
β = 0.0

FIGURE 4.25c

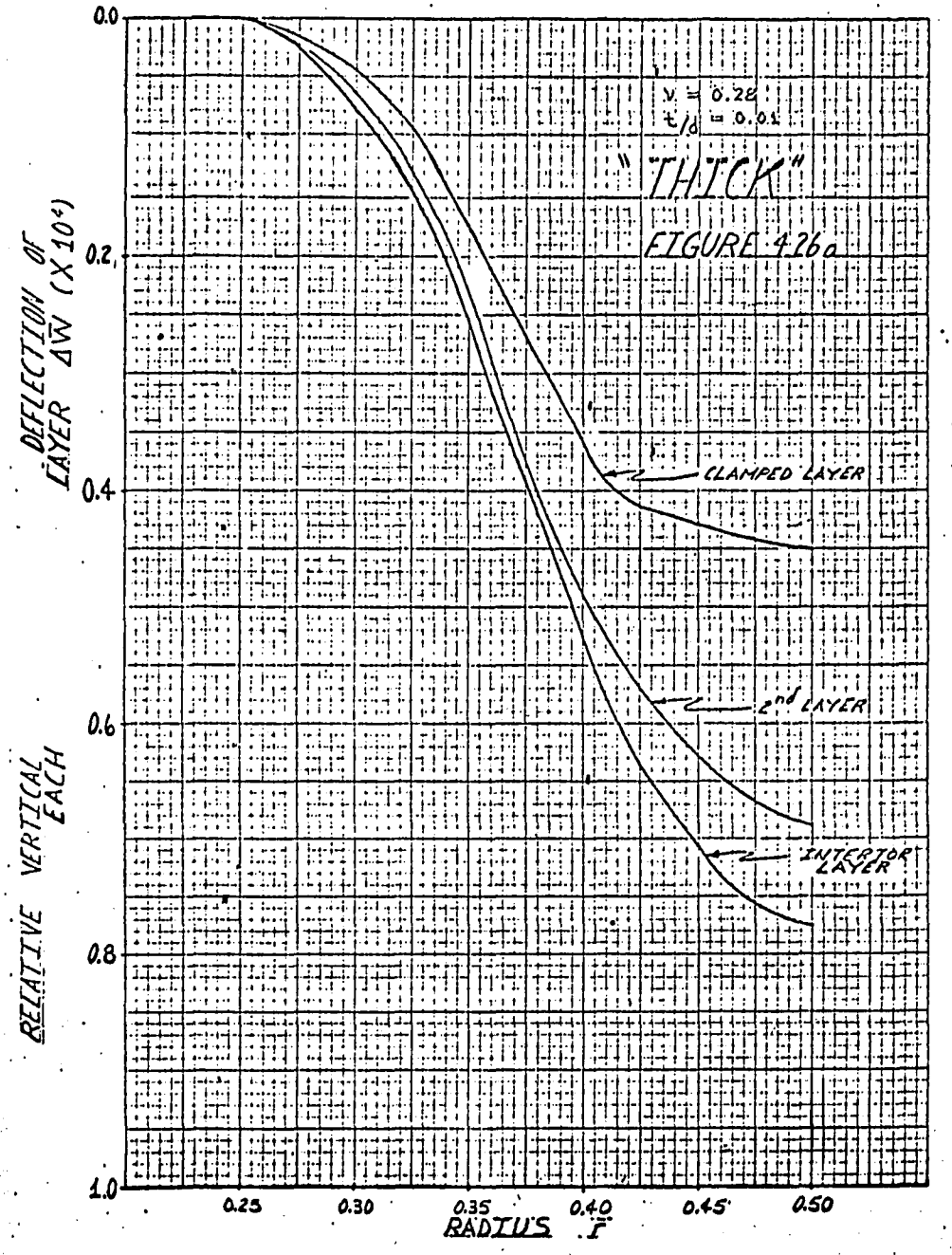
0.0
0.2
0.4
0.6
0.8
1.0
RELATIVE VERTICAL DEFLECTION OF EACH LAYER $\Delta\bar{w}$ ($\times 10^{-2}$)
0.25
0.30
0.35
0.40
0.45
0.50
RADIUS $\bar{r}$
$\nu = 0.28$
$t/a = 0.01$
"THICK"
CLAMPED LAYER
2nd LAYER
INTERIOR LAYER

FIGURE 4.26a

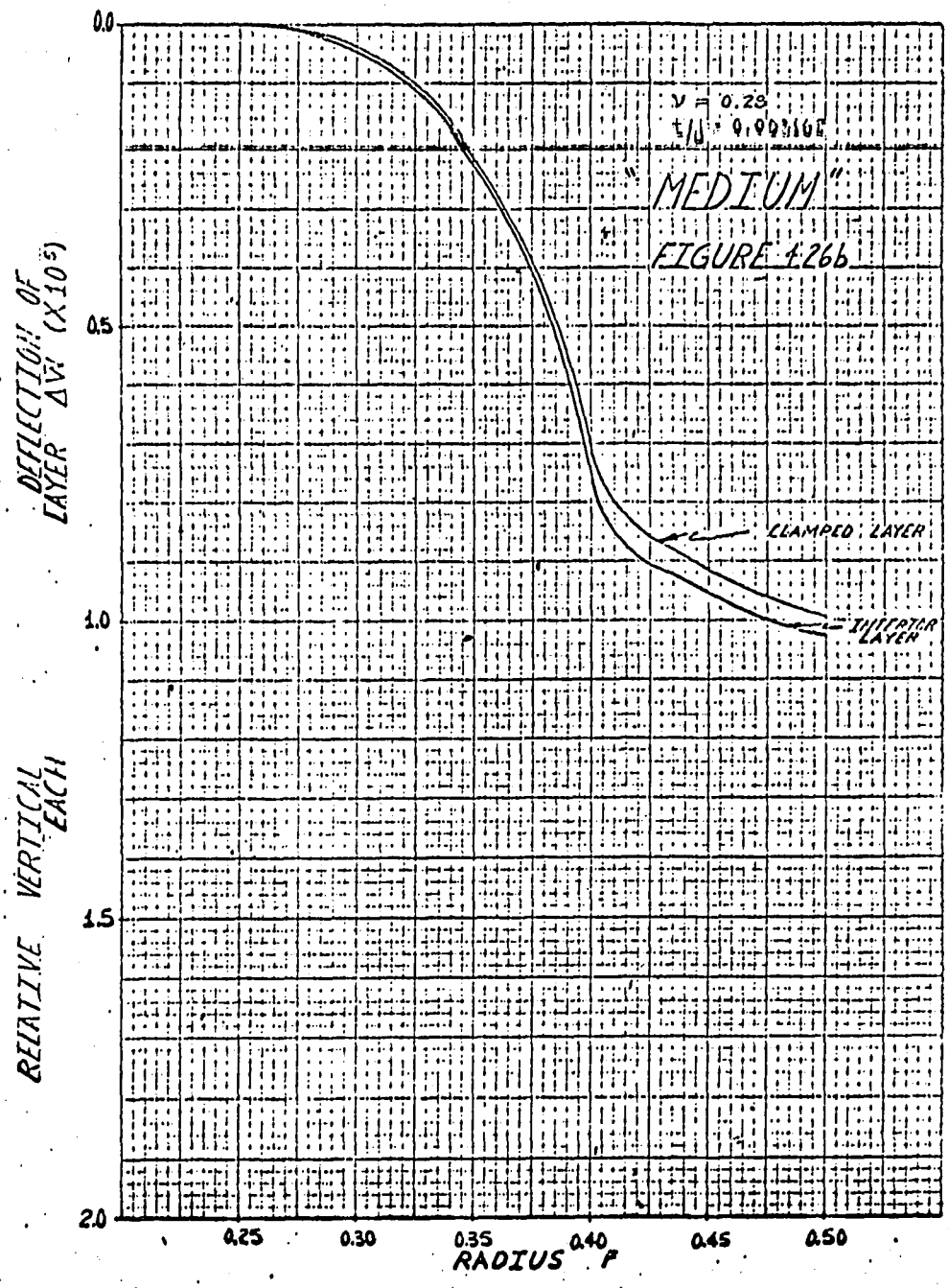
"MEDIUM"
FIGURE 4.26b
ν = 0.28
t/a = 0.00160
CLAMPED LAYER
INJECTOR LAYER
RELATIVE VERTICAL DEFLECTION OF EACH LAYER Δw (X10⁵)
RADIUS r
0.0
0.5
1.0
1.5
2.0
0.25
0.30
0.35
0.40
0.45
0.50

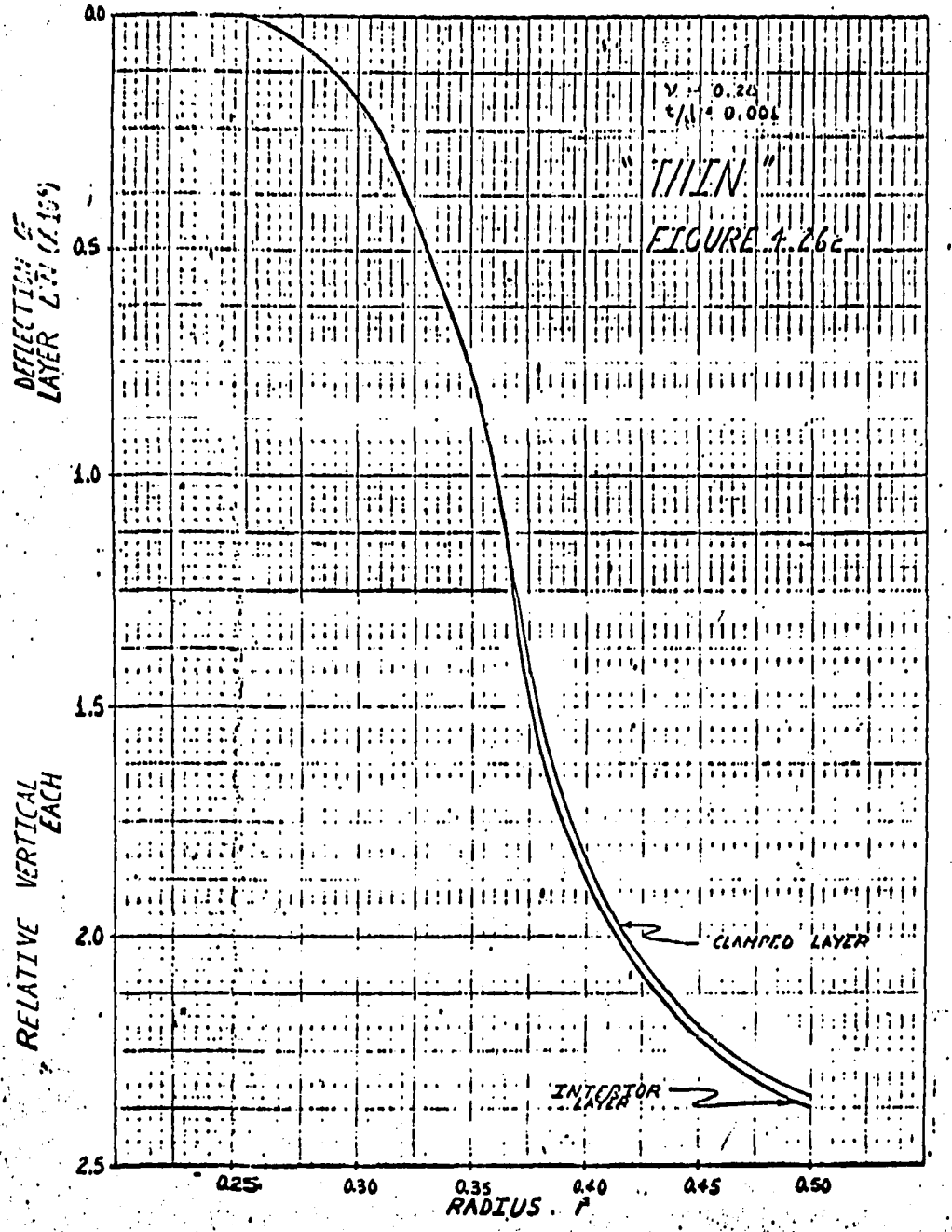
0.0
0.5
1.0
1.5
2.0
2.5
RELATIVE VERTICAL DEFLECTION OF EACH LAYER
0.25
0.30
0.35
0.40
0.45
0.50
RADIUS, r
ν = 0.20
t/l = 0.001
"THIN"
FIGURE 4.26c
CLAMPED LAYER
INTERIOR LAYER

analysis of an interior layer is of primary value for the solution of welded bellows having many layers. Since any interior layer is so far removed from the rigid clamp (or any other type of outer support), the associated boundary conditions, i.e., the boundary conditions given by equations (2.6-1a-c) have been "lost". As a result, this layer cannot determine its position with respect to the bellows' mid-plane of symmetry. Hence an interior layer will be subject to the final three boundary conditions which apply to a layer which terminates at the mid-plane of symmetry. The other three boundary conditions are given by equations (2.6-1a-c) and (2.11-1).

4.3.2 DEFINITION OF THE BOUNDARY LAYER

There are two basic ways in which a boundary layer effect can exist mathematically: (1) by reduction of order of the governing differential equations when some parameter is set equal to zero, and (2) by loss of a singularity in some term of the governing differential equations when a parameter is set equal to zero; this type of boundary layer effect is not well known, but an example in hydrodynamics was first analyzed by Dressler[31].

It is clear that we have no singularities in our bellows problem, so we will investigate our boundary layer effect from the standpoint of (1), a possible reduction of order. The classical example here is, of course, the one in

viscous flow, where the boundary layer thickness decreases as viscosity $\mu \to 0$. Setting $\mu = 0$ reduces the order of the Navier Stokes equations, hence a boundary condition (the "no slip" condition) must be lost. In our bellows, we shall show how the boundary layer thickness decreases as shell thickness $\bar{t} \to 0$.

In elasticity the two best known boundary layer effects are both due to reduction of order:

(1a) The edge effect in pure bending of plates. This was first considered heuristically by Kelvin and Tait[32], and finally explained mathematically by Friedrichs and Dressler[33]. The approximate plate equation, the biharmonic, is only of order four, whereas it should be of order six, and hence the bending twist cannot be imposed separately as a boundary condition. Our bellows equations contain both bending and stretching effects, and their order six is sufficiently high (for rotationally symmetric shells) to permit satisfaction of all boundary conditions, hence our boundary layer effect is not related to (1a).

(1b) The edge effect associated with the membrane theory of shells[34]. Since bending moments contain the factor t^3 and membrane forces the factor t, the bending moments are sometimes neglected in the equilibrium equations if the shell thickness t is very small. This results in the "membrane theory" of shells, which for our rotationally symmetric case would only be of order four; this implies an edge effect at

the boundary, which is explained by stating that the bending moments in the full shell equations (order six) may be large at the edge, but must decay towards zero in the interior. Our exact solutions, however, for $\overline{\sigma}^{\,o}$ versus $\overline{\sigma}^{\,e}$ (see Figs. 4.27a-d) in the bellows do <u>not</u> exhibit this decay of $\overline{\sigma}^{\,o}$, hence our boundary layer is not directly explicable by the membrane theory when applied to the entire problem. In our solutions, the bending stresses always remain larger than the membrane stresses throughout the interior.

A more detailed study of our edge effect reveals that just one portion of our total solution contains this boundary layer, and that its decay is related to the decrease in both the bending stresses and membrane stresses from the boundary to the interior domain. An outline of this analysis proceeds as follows:

4.3.3 THE FULL PROBLEM DECOMPOSED INTO A PURE INTERIOR PROBLEM ("A") AND A PURE EDGE PROBLEM ("B")

For simplicity we restrict ourselves to the bellows without welds as the welds can in no way produce the edge effect near the rigid clamp, and merely complicate the investigation in the interior. Inspection shows that our outer boundary conditions for a single "interior" layer contain both $\frac{d\bar{w}}{d\bar{s}} = 0$ and $\bar{Q} = 1$, the two causes of bending, which are identical with two of the boundary conditions at the bottom rigid clamp. Therefore, bending effects cannot be expected

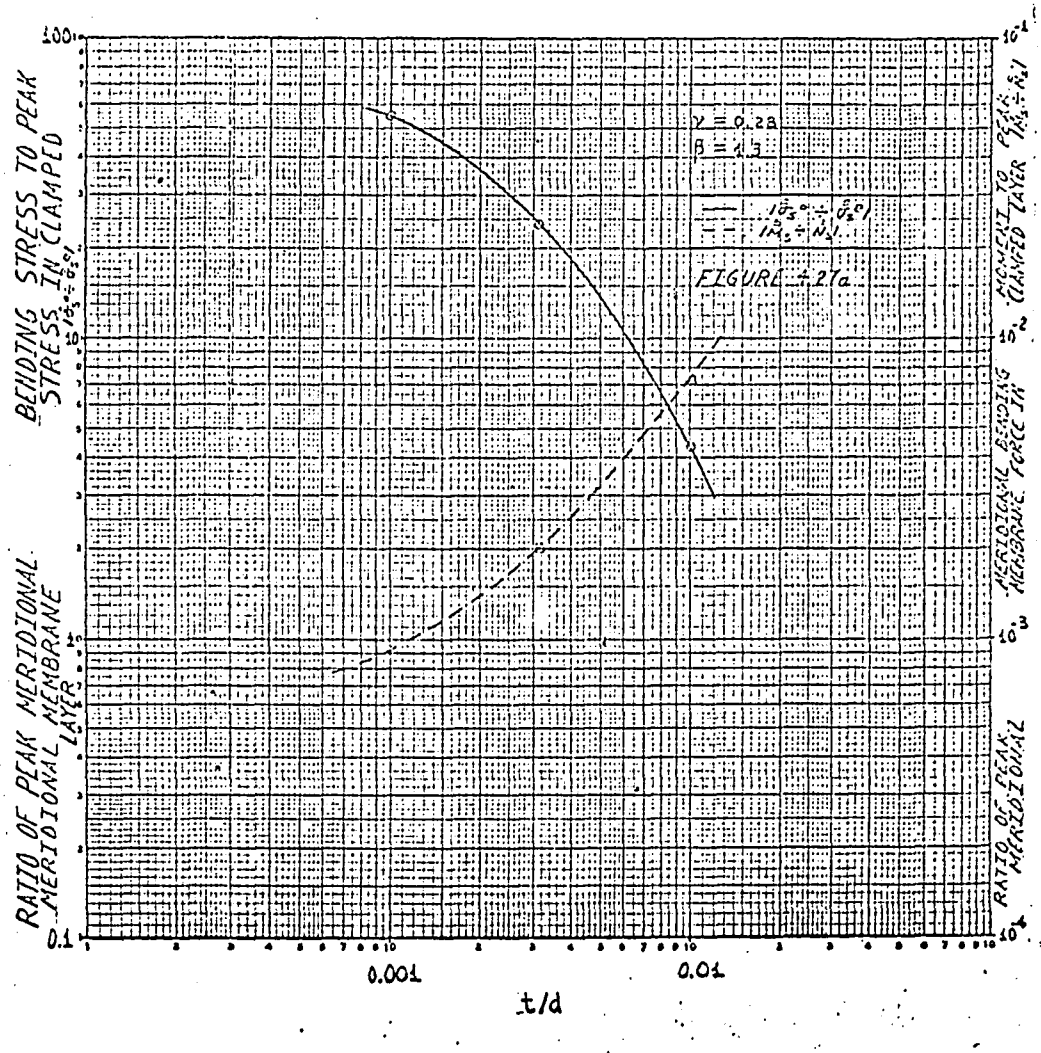
RATIO OF PEAK MERIDIONAL MEMBRANE LAYER
BENDING STRESS TO PEAK STRESS IN CLAMPED
MERIDIONAL BENDING MEMBRANE FORCE IN
RATIO OF PEAK MERIDIONAL MOMENT TO CLAMPED LAYER PEAK
γ = 0.28
β = 1.3
FIGURE 4.27a
0.001
0.01
t/d

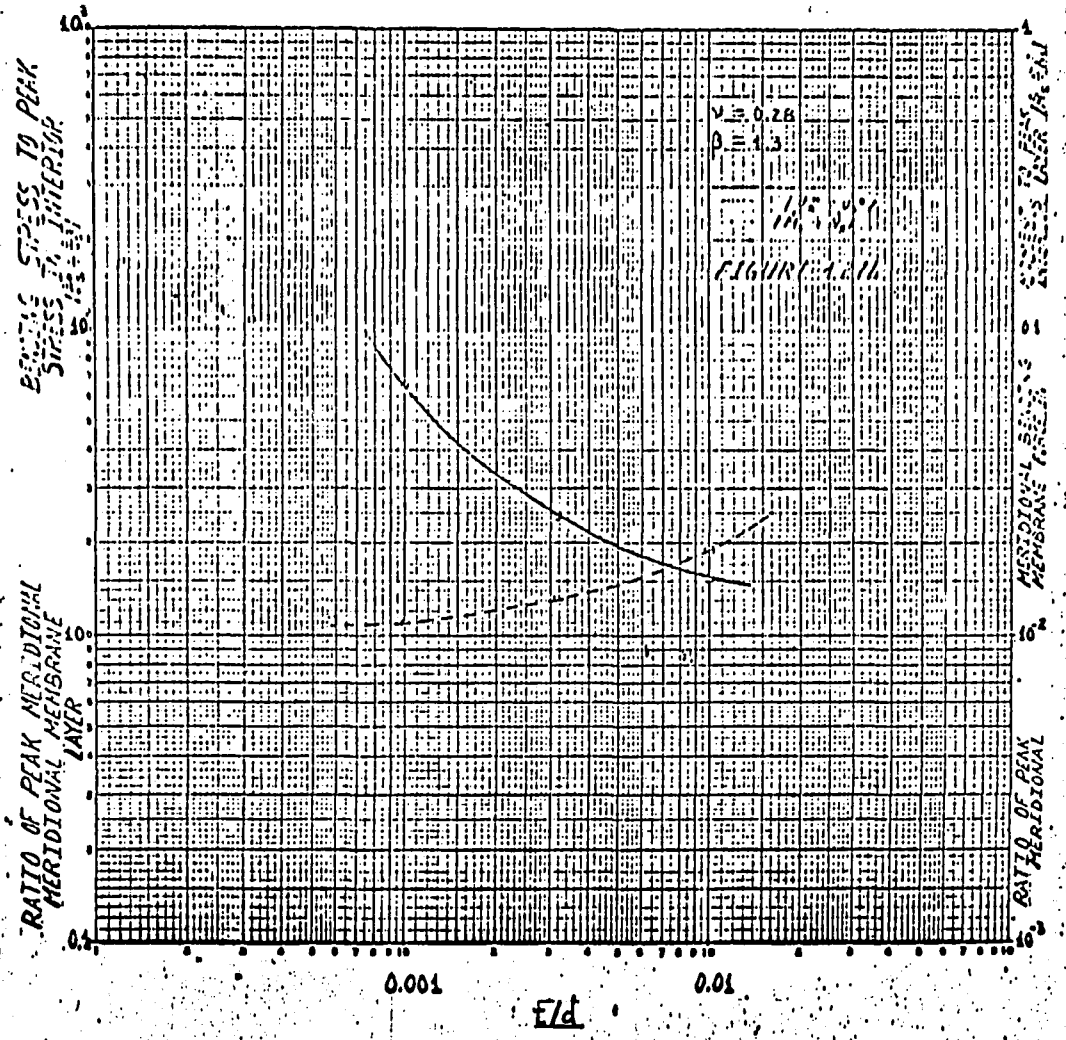
RATIO OF PEAK MERIDIONAL MEMBRANE LAYER
MERIDIONAL MEMBRANE STRESS
RATIO OF PEAK MERIDIONAL
ν = 0.28
ρ = 1.3
0.001
0.01
f/d

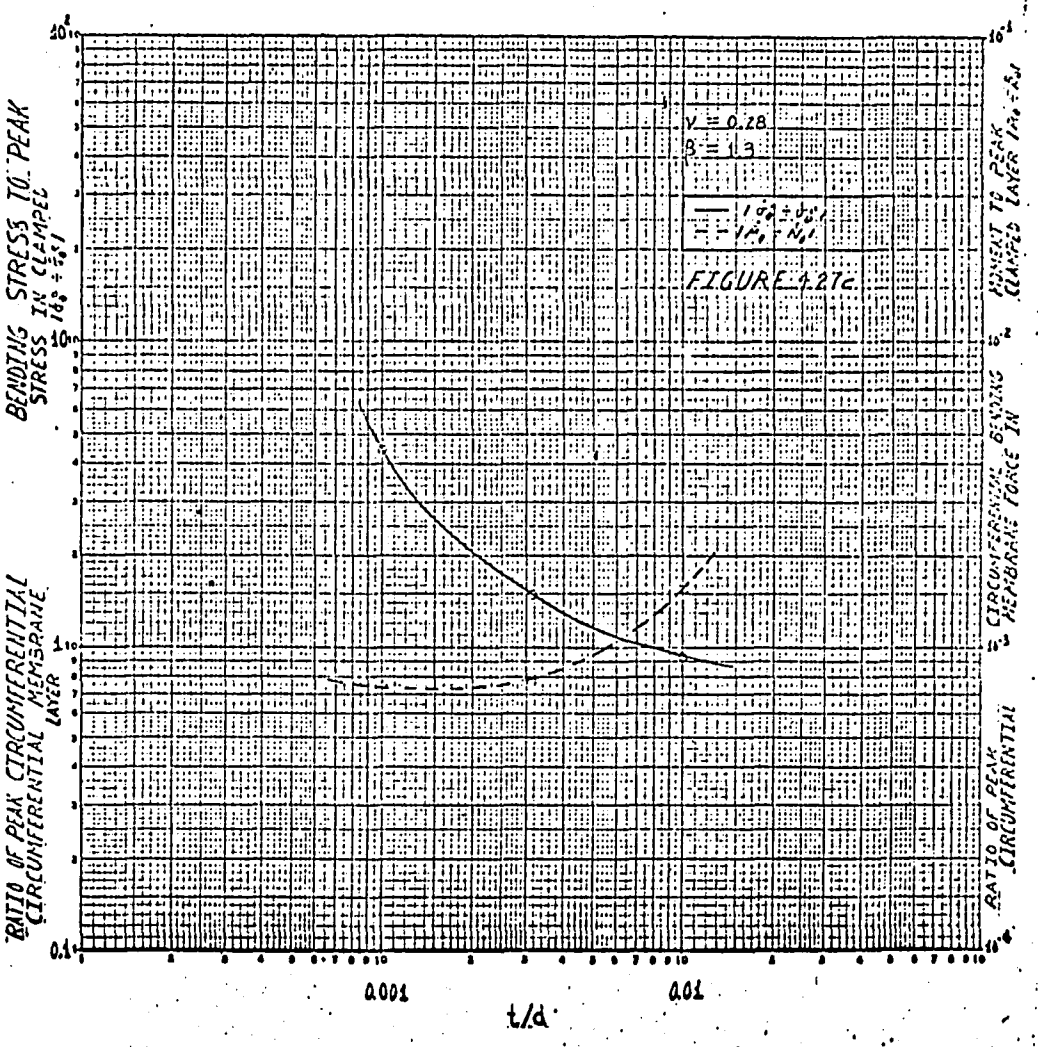
BENDING STRESS TO PEAK STRESS IN CLAMPED
RATIO OF PEAK CIRCUMFERENTIAL MEMBRANE LAYER
CIRCUMFERENTIAL BENDING MOMENT TO PEAK CLAMPED LAYER
CIRCUMFERENTIAL MEMBRANE FORCE IN
RATIO OF PEAK CIRCUMFERENTIAL
ν = 0.28
β = 1.3
0.001
0.01
t/d

FIGURE 4.27c.

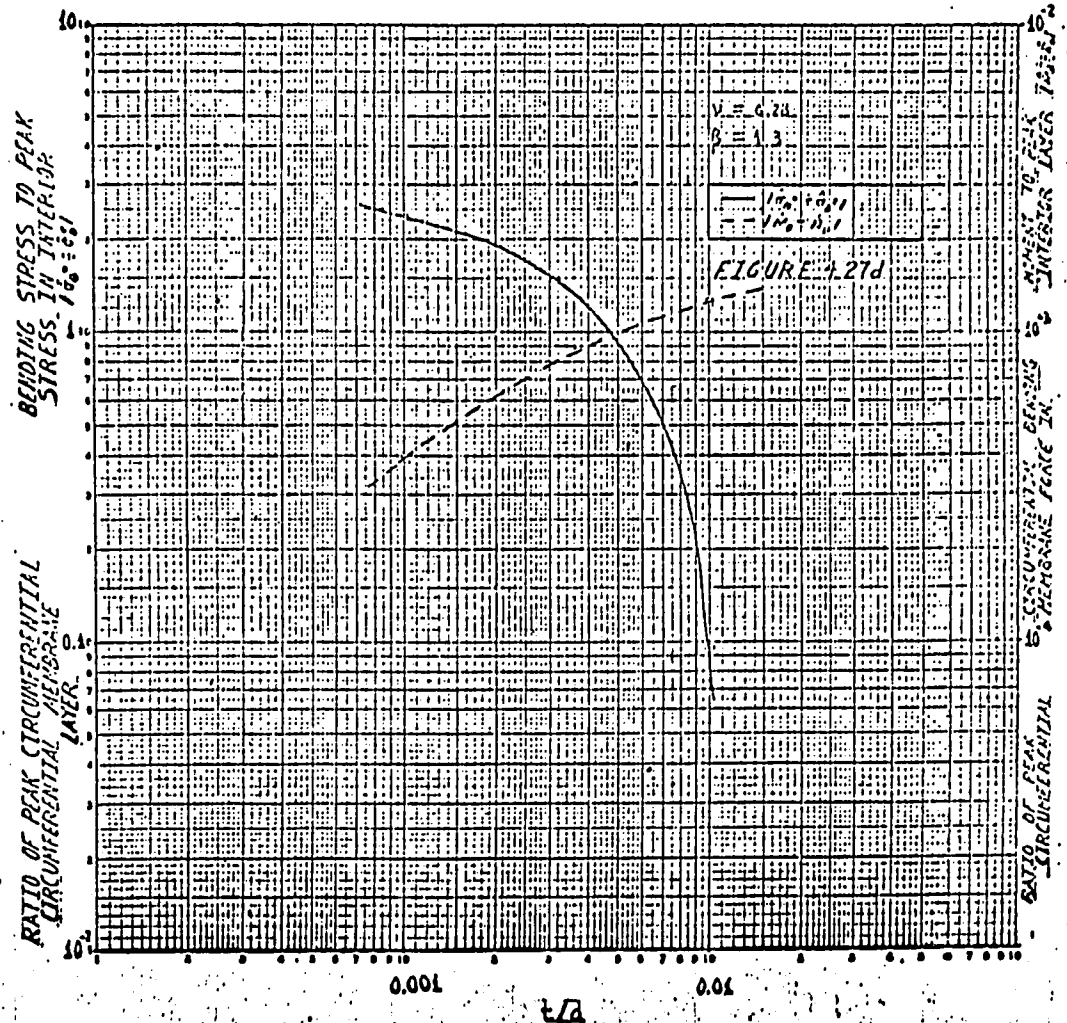
BENDING STRESS TO PEAK STRESS IN INTERIOR LAYER
RATIO OF PEAK CIRCUMFERENTIAL MEMBRANE STRESS IN INTERIOR LAYER
RATIO OF PEAK CIRCUMFERENTIAL MEMBRANE FORCE IN INTERIOR LAYER
RATIO OF PEAK CIRCUMFERENTIAL BENDING MOMENT TO PEAK MEMBRANE FORCE IN INTERIOR LAYER
ν = 0.28
β = 1.3
FIGURE 4.27d
0.001
0.01
t/a

to die out relatively in our "interior" domain regardless of the shell thickness.

The "full" problem for several layers with our rigid clamp has outer boundary conditions $\bar{v} = 0$, $\frac{d\bar{w}}{d\bar{s}} = 0$, $\bar{Q} = 1$. Let us replace this solution by the sum of the solutions of two problems, "A" and "B", defined as follows: "A" and "B" have identical homogeneous boundary conditions at the end (i.e., the bellows' mid-plane of symmetry). At the beginning, namely $\bar{s} = 0$, "A" has the boundary conditions $\bar{N}_s = 0$, $\frac{d\bar{w}}{d\bar{s}} = 0$, $\bar{Q} = 1$, identical with those for an interior layer. It is easy to prove that the solution to problem "A" is precisely a periodic solution (with period equal to twice the arc length of one layer) consisting of a chain of single interior layer solutions attached to each other. Therefore problem "A" is totally independent of any boundary layer effect since its bending stresses predominate over the membrane stresses throughout the whole range of $\frac{t}{d}$. From the solution of problem "A", we can obtain the tangential displacement at $\bar{s} = 0$ which is denoted as $\bar{v}_{clamp}$. Problem "B" is then defined at the rigid clamp ($\bar{s} = 0$) by the boundary conditions $\bar{v} = -\bar{v}_{clamp}$, $\frac{d\bar{w}}{d\bar{s}} = 0$, $\bar{Q} = 0$. The solution to "B" contains the edge effect relevant to our problem. The boundary condition $\bar{v} = -\bar{v}_{clamp}$ will cause a deflection $\bar{W}_B$ of sign opposite to $\bar{W}_A$, and the function $\bar{W}_B$ should die out at a distance $\bar{\delta} \propto \sqrt{\bar{t}}$, as we will show in Fig. 4.29. Details of this boundary layer analysis will be the subject of a subsequent paper.

In order to establish the relation which describes how this boundary layer decays, we plotted the relative vertical deflection of each layer as a function of arc length. This was done for each of the three $\frac{t}{d}$ values. The corresponding results are shown in Figs. 4.28a-c. It is noteworthy, that for each value of $\frac{t}{d}$, the relative vertical deflection of each layer approaches that of an interior layer asymptotically. The rate at which any relative vertical deflection approaches the corresponding interior layer's value is seen to be highly dependent upon the value of $\frac{t}{d}$. In order to determine the dependence of the boundary layer "thickness" on $\frac{t}{d}$, we chose a deflection equal to 95% of the interior layer's deflection and then recorded the corresponding value of $\bar{s}$. This procedure yielded three values of $\bar{s}$ which we plotted on doubly logarithmic paper. The resulting graph is shown in Fig. 4.29. From Fig. 4.29 we can readily determine that the relation between the boundary layer "thickness" and $\frac{t}{d}$ is:

$$\bar{\delta} = 6.5 \sqrt{\frac{t}{d}} \qquad (4.3.3\text{-}1)$$

The thickness of the boundary layer for <u>our particular shape</u> and geometry of welded bellows as described by equation (4.3.3-1) is analogous to the result for the classical fluid mechanics problem investigated by Blasius[35]. It must be emphasized that equation (4.3.3-1) applies <u>only to our specific shape</u> which is defined in Fig. 4.1. For other meridional profiles, the factor 6.5 will change, however, we expect the dependence upon the square root of $\frac{t}{d}$ to remain. It is expected

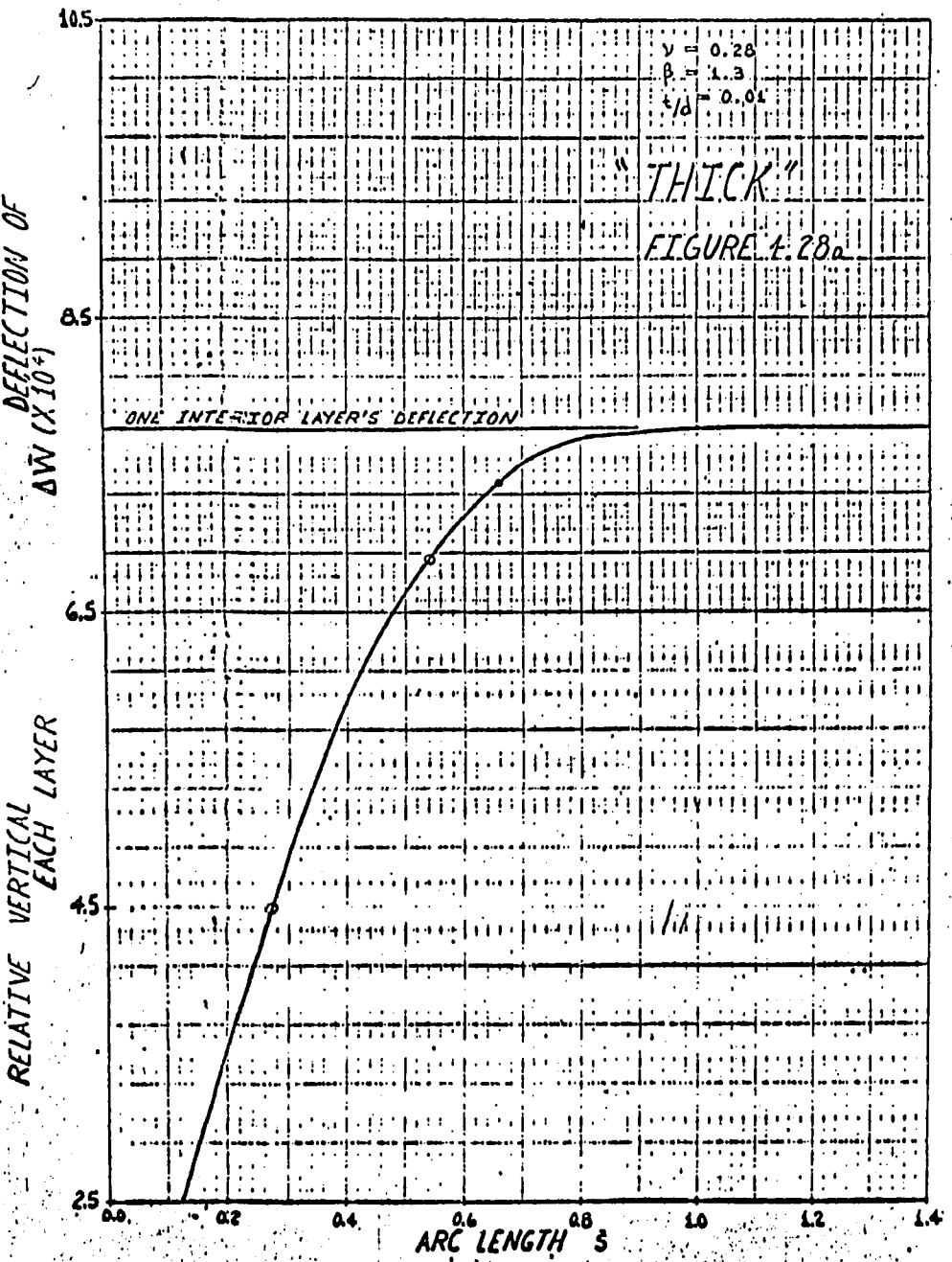
10.5
8.5
6.5
4.5
2.5
0.0
0.2
0.4
0.6
0.8
1.0
1.2
1.4
ν = 0.28
β = 1.3
t/a = 0.01
"THICK"
FIGURE 4.28a
ONE INTERIOR LAYER'S DEFLECTION
RELATIVE VERTICAL DEFLECTION OF EACH LAYER
ΔW (X 10⁻⁴)
ARC LENGTH S

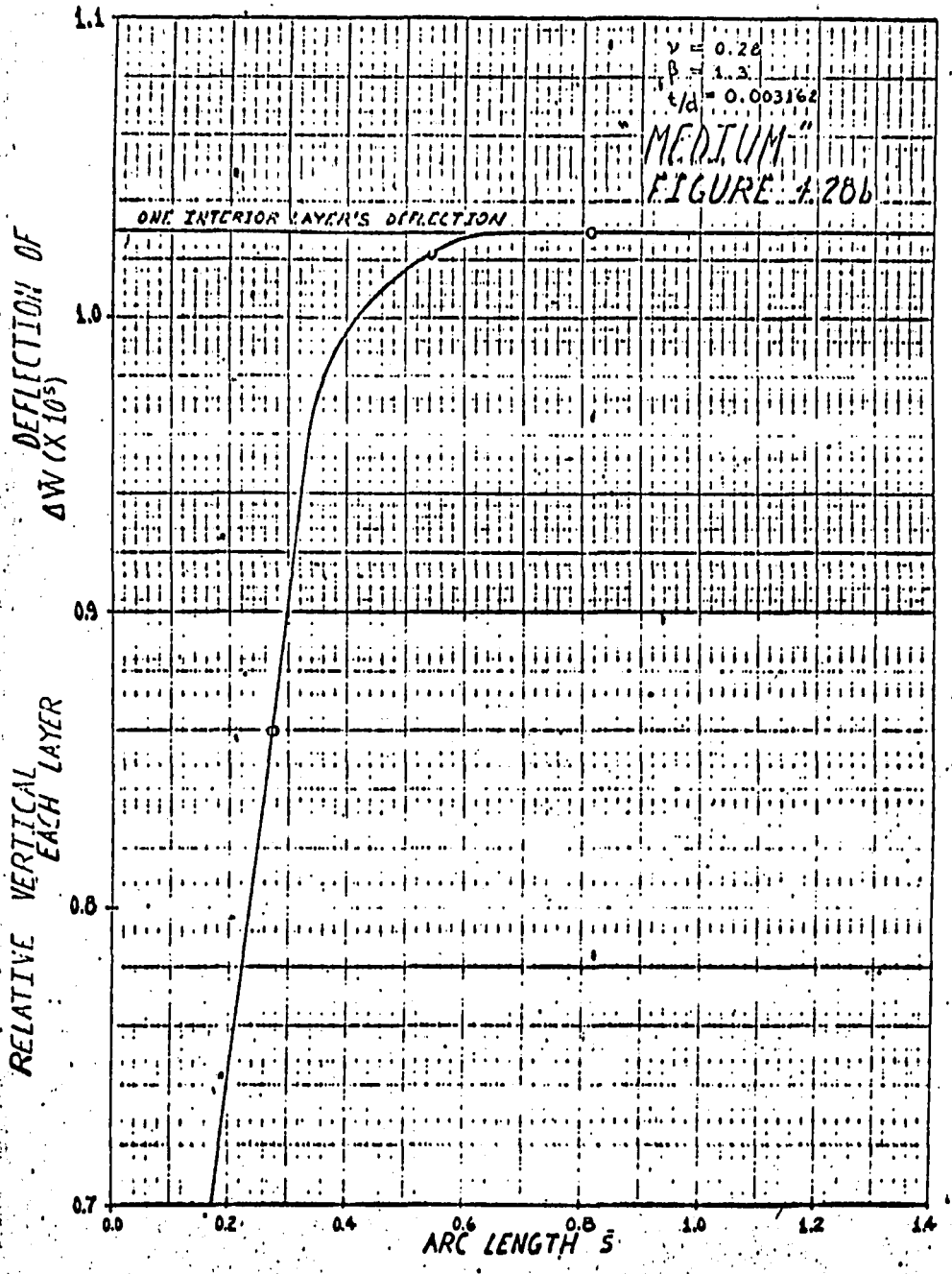
ν = 0.28
β = 1.3
t/d = 0.003162
"MEDIUM"
FIGURE 4.28b
ONE INTERIOR LAYER'S DEFLECTION
RELATIVE VERTICAL DEFLECTION OF EACH LAYER
ΔW (X 10⁵)
1.1
1.0
0.9
0.8
0.7
0.0
0.2
0.4
0.6
0.8
1.0
1.2
1.4
ARC LENGTH S

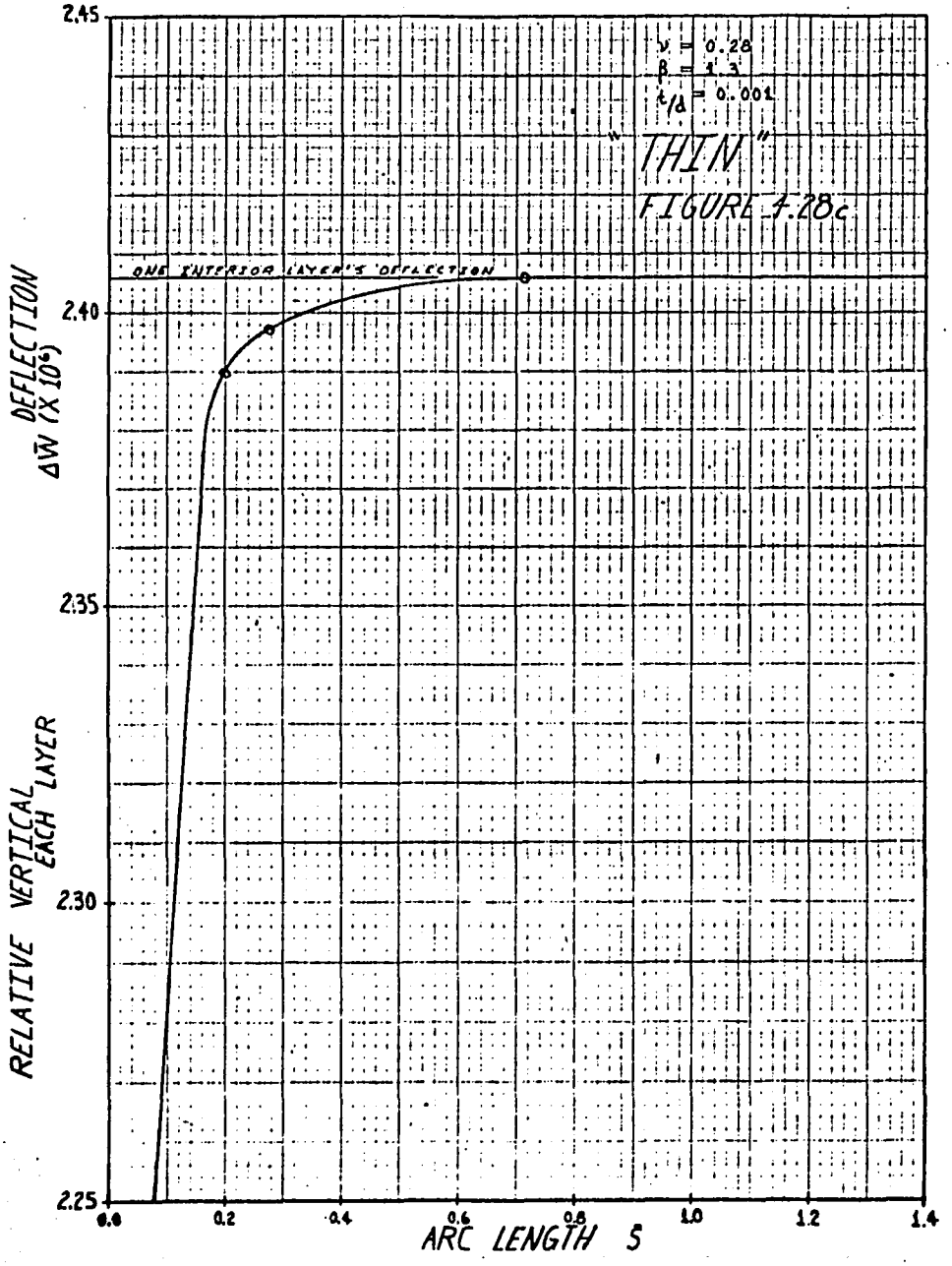
2.45
2.40
2.35
2.30
2.25
0.0
0.2
0.4
0.6
0.8
1.0
1.2
1.4
ν = 0.28
β = 1.3
t/d = 0.001
"THIN"
ONE INTERIOR LAYER'S DEFLECTION
RELATIVE VERTICAL DEFLECTION EACH LAYER ΔW (X 10⁶)
ARC LENGTH S

FIGURE 4.28c

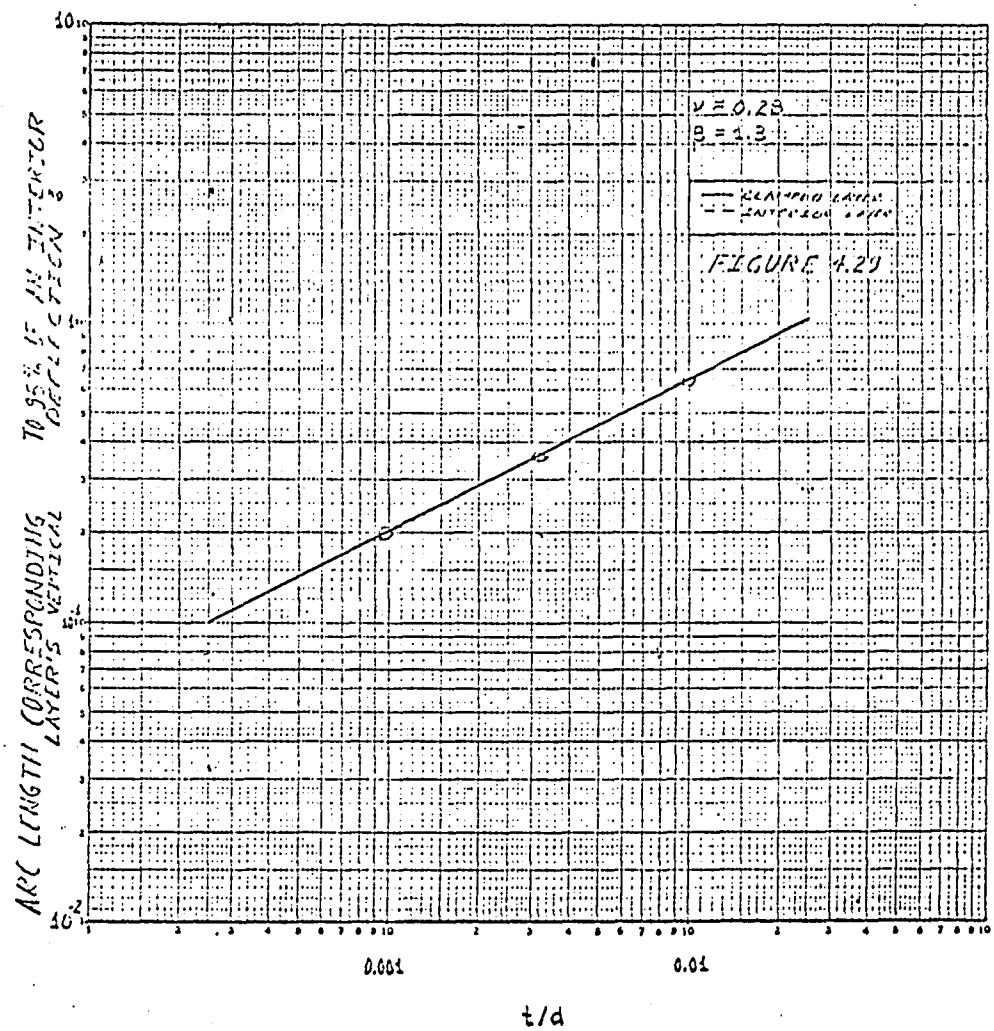
ν = 0.28
β = 1.3
FIGURE 4.29
ARC LENGTH CORRESPONDING TO 95% OF VERTICAL DISPLACEMENT
LAYER'S VERTICAL
0.001
0.01
t/d

that for other meridional profiles containing more curvatures and fewer plates the 6.5 factor will significantly decrease, i.e., the boundary layer thickness will decrease.

The direct application of equation (4.3.3-1) along with the analysis of an interior layer will lead to a general method of solution which can be applied to obtain the displacement-stress behavior of any welded bellows with any large number of layers. The development of this method will be presented in the following section.

4.4 APPLICATION OF THE INTERIOR LAYER CONCEPT TO THE ANALYSIS OF WELDED BELLOWS HAVING MANY LAYERS

Since most welded bellows have many layers, a general approach to the problem of accurately determining the displacement-stress behavior of any welded bellows is of special interest. To this end, we will use the following procedure:

i) Generate a solution for an interior layer.

ii) From the given value of $\frac{t}{d}$, obtain the corresponding value of $\bar{\delta}$ from equation (4.3.3-1).

iii) Using the value of $\bar{\delta}$ found in (ii), calculate the number (rounded to the next highest integer) of layers whose overall vertical deflection differs from an interior layer's vertical deflection by more than any prescribed percentage, e.g., 5%. Denote this number as n*.

iv) Using the method described in Chapter 3, analyze exactly n* layers.

4.4.1 DETERMINATION OF STRESSES

The method described in Section 4.4 can be used to determine any particular stress that is of interest. Specifically, any stress within the first n* layers is obtained from (iv) of Section 4.4. The stresses in the remaining layers (i.e., interior layers) are obtained from (i) of Section 4.4. Since our solutions indicate that peak stresses always occur in an interior layer, information concerning peak stresses can be obtained directly by only analyzing a single interior layer.

4.4.2 DETERMINATION OF DISPLACEMENTS

In order to determine the overall displacement of a welded bellows, we apply the following procedure:

i) Using the boundary layer curves shown in Figs. 4.28a-c, determine what percentage of an interior layer's deflection each of the first n* layers deflect. Denote these percentages as:

$$\alpha_i, \qquad i = 1,\ldots,n^* \qquad (4.4.2\text{-}1)$$

ii) Calculate the deflection of one interior layer.

Making use of the bellows' symmetry about its midplane and equation (4.4.2-1), we obtain the following relation for the overall displacement of the bellows:

$$\overline{\Delta}_T = 2\left[\sum_{i=1}^{n^*} \alpha_i + (n - n^*)\right]\overline{\Delta}^o \qquad (4.4.2\text{-}2)$$

where:

$\overline{\Delta}_T$ = Overall deflection of bellows

$\overline{\Delta}^o$ = Deflection of one interior layer

n = Number of layers counted from the rigid clamp to the bellows' mid-plane of symmetry

A study of Figs. 4.2a and 4.3 shows that n* never exceeds the maximum number of layers that can be analyzed accurately in single precision using our code, i.e., with an error tolerance for $\bar{Q}$ of less than 1%. Furthermore, because of the general nature of the curvature in our equations, our method can be applied to welded bellows having any rotationally symmetric shape whatsoever.

4.5 EXPERIMENTAL CORROBORATION OF THE THEORETICAL METHOD

In order to confirm the validity of the theoretical method developed, we used a precision welded bellows in our possession having 34 layers and made of a high strength nickel alloy known as "Inconel-X" ($E = 31 \times 10^6$ psi, $\nu = 0.409$). Although this experimental bellows consisted of cones, plates, and toroidal welds, its dimensions were considerably different from the shape which we analyzed, as there were slight (3^o)

cones adjacent to the outer welds. We then performed the following experiment: the bellows was loaded in tension with a set of weights. Various weights were successively removed, and the resulting deflections were recorded. The fact that the outside diameter of this particular welded bellows was less than one inch made the precise determination of the overall displacement rather difficult. Consequently, a very accurate vernier height gage with a high power eye piece was set up to record the amount that the bellows deflected. The resulting experimental deflection-load curve is shown in Fig. 4.30.

The fact that the deflection-load curve is linear, indicates that for the applied loads, the bellows has not departed from its linear range. The point (0.0143,100) on this experimental deflection-load curve gives a flexibility of 0.065 in./lb..

In order to calculate the flexibility mathematically, we first had to inspect a single wafer magnified 20 times under a "shadowgraph" machine. The resulting dimensions are shown in Fig. 4.31a.

When welded bellows are fabricated, the outer and inner plates may be welded parallel to each other with an air gap as shown in Fig. 4.31b. They may also be "pinched" together and welded to form an inclined air gap. Inspection of the experimental bellows magnified 20 times under the shadowgraph indicated that the latter welding procedure was

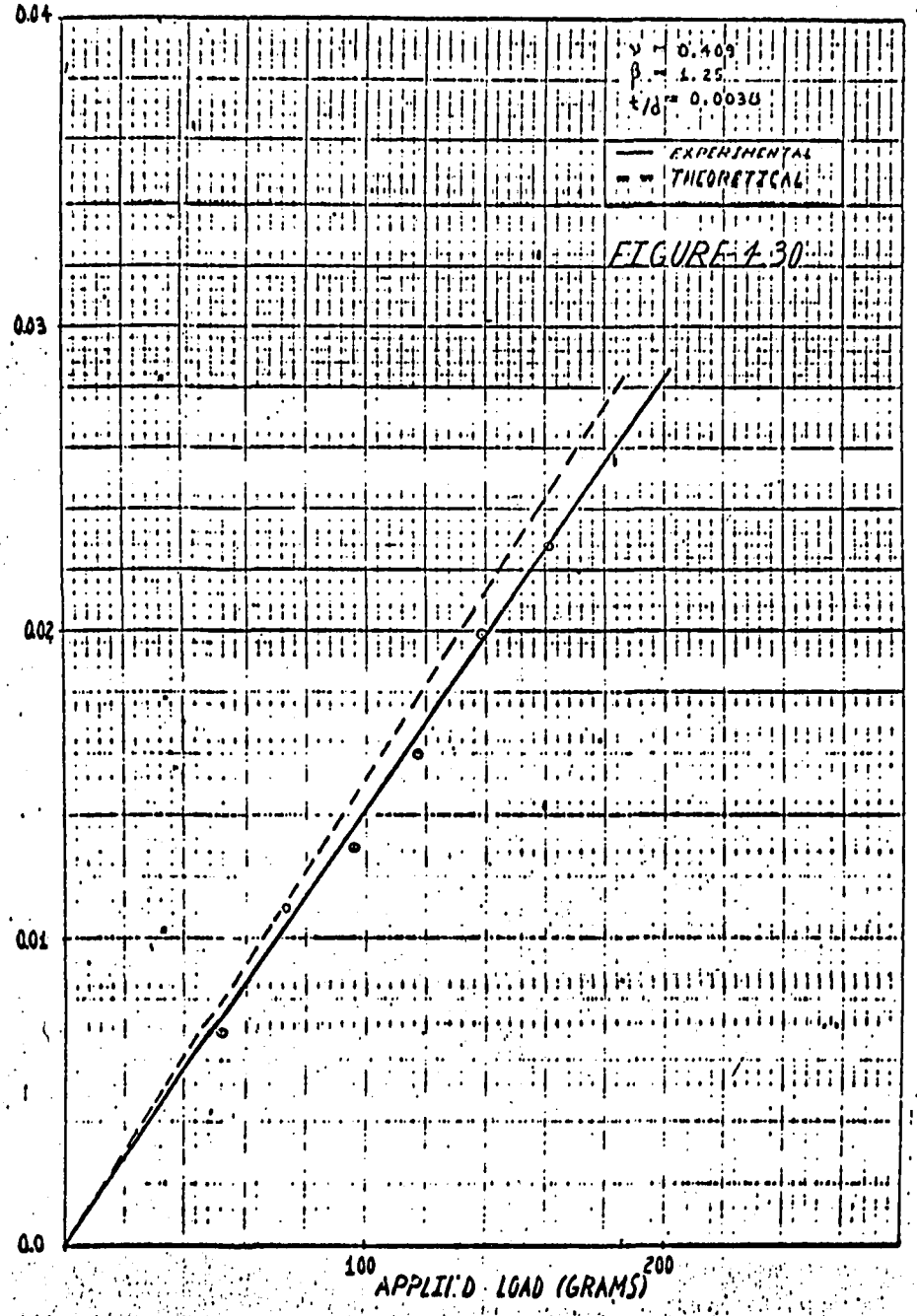
0.04
0.03
0.02
0.01
0.0
100
200
APPLIED LOAD (GRAMS)
OVERALL DEFLECTION OF EXPERIMENTAL BELLOWS (INCHES)
ν = 0.403
β = 1.25
t/d = 0.0038
EXPERIMENTAL
THEORETICAL

FIGURE 130

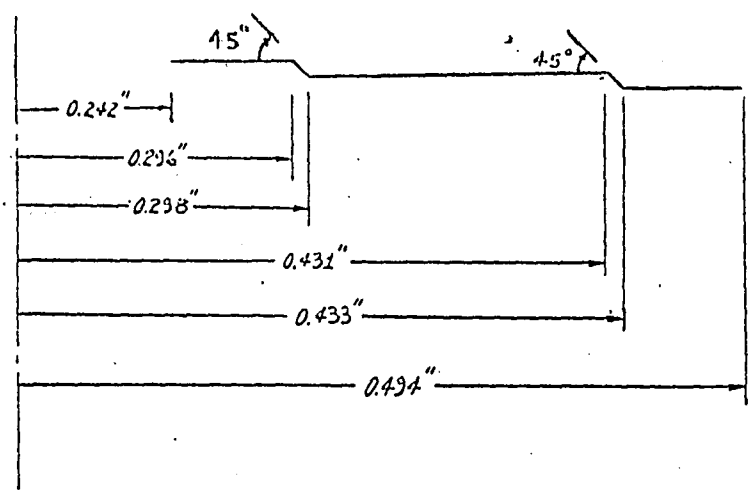

FIGURE 4.31a DIMENSIONS OF A SINGLE WAFER FROM THE EXPERIMENTAL BELLOWS

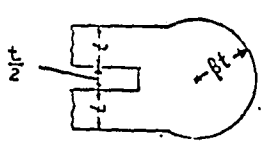

FIGURE 4.31b "PARALLEL" WELD DESIGN

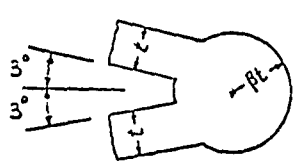

FIGURE 4.31c "INCLINED" WELD DESIGN

employed. This welding procedure resulted in a total angle of 6^{o} between the cones. This is indicated in Fig. 4.31c. The most difficult measurement to obtain for the experimental bellows was the shell thickness t. A scatter in these measurements using the shadowgraph is unavoidable due to the lack of sharpness in focusing. We used the average of five independent measurements, each with an independent focusing. Since the overall deflection is very sensitive to $\bar{t}$, this is the most critical measurement in the experiment. Obtaining a value of $\beta = 1.25$ and $\bar{t} = 0.0038$, we applied the method of Section 4.4.2 to obtain $n^* = 2$, $\alpha_1 = 0.86$, $\alpha_2 = 0.99$, and $n = 17$. We then generated the solution for an interior layer which yielded $\overline{\Delta}^{o} = 2.342 \times 10^{5}$. Applying equation (4.4.2-2), and using these values, we obtain $\overline{\Delta}_T = 7.893 \times 10^{6}$. If we then make use of equation (2.5-1b), we may convert this deflection into dimensional form to obtain $\Delta_T = 0.015"$. This leads to a theoretical flexibility of 0.068 in./lb.. The theoretical flexibility only differs from the experimental flexibility by 5.25%. This error can be accepted as being within the limits of the experimental measurement of $\bar{t}$. The theoretical deflection-load relation is indicated by the dotted line in Fig. 4.30.

A quantitative measure of the boundary layer's effect on the bellows' overall deflection is given by the relation:

$$\frac{n^* - \sum_{i=1}^{n^*} \alpha_i}{n} \qquad (4.5\text{-}1)$$

Application of equation (4.5-1) with the appropriate values of n*, n, and α_i shows that the effect of the boundary layer is to reduce the bellows' overall deflection by only 0.88%.

4.6 CONCLUSIONS

The general method developed in this study for the analysis of welded bellows:

i) Gives a fast and economical way of analyzing any welded bellows.

ii) Can be used to analyze accurately several (the actual number depends upon $\bar{t}$) layers directly.

iii) Can be applied to analyze accurately any number of layers using the "boundary layer method".

iv) Is applicable to welded bellows having any meridional shape whatsoever.

v) Can be easily modified to solve the problem of internal pressure loading; hence the problem of combined axial force loading and internal pressure loading can be solved by superimposing the solution of each separate problem.

BIBLIOGRAPHY

1. E. Reissner, "On the Theory of Thin Elastic Shells," Reissner Anniversary Volume: Contributions to Applied Mechanics (Ann Arbor, Mich.: J.W. Edwards, 1949), pp. 231-247.

2. J.L. Sanders, "Nonlinear Theories for Thin Shells," Quarterly of Applied Mathematics, Vol. 21, No. 1, 1963, pp. 21-36.

3. T.G. Beckwith and N.L. Buck, Mechanical Measurements, 3d ed. (Reading, Mass.: Addison-Wesley, 1964), Chapter 9.

4. J.W. Dally and W.F. Riley, Experimental Stress Analysis (New York: McGraw-Hill, 1965), Chapter 5.

5. Ibid., Chapter 14.

6. H. Wissler, "Festigkeitsberechnung von Ringflächenschalen," doctoral thesis, Zürich, 1916.

7. K. Stange, "Der Spannunzstand einer Kreisringschale," Ingenieur-Archiv, Vol. 2, Part 1, 1931, pp. 47-91.

8. R.A. Clark, T.I. Gilroy, and E. Reissner, "Stresses and Deformations of Toroidal Shells of Elliptical Cross Section," Journal of Applied Mechanics, Trans. ASME, Vol. 74, 1952, pp. 37-48.

9. R.A. Clark and E. Reissner, "On Axially Symmetric Bending of Nearly Cylindrical Shells of Revolution," Journal of Applied Mechanics, Trans. ASME, Vol. 78, 1956, pp. 59-67.

10. J.A. Haringx, "Design of Corrugated Diaphragms," Trans. ASME, Vol. 79, 1957, pp. 55-64.

11. H.J. Grover and J.C. Bell, "Some Evaluations of Stresses in Aneroid Capsules," Proceedings of the Society for Experimental Stress Analysis, Vol. 5, No. 2, 1948, pp. 125-131.

12. R.F. Dressler, "Bending and Stretching of Corrugated Diaphragms," Journal of Basic Engineering, Trans. ASME, Vol. 81, Series D, 1959, pp. 651-659.

13. A. Kalnins, "Analysis of Shells of Revolution Subjected to Symmetrical and Nonsymmetrical Loads," Journal of Applied Mechanics, Trans. ASME, Vol. 31, Series E, 1964, pp. 467-476.

14. G.A. Cohen, "Computer Analysis of Asymmetric Free Vibrations of Ring Stiffened Orthotropic Shells of Revolution," AIAA Journal, Vol. 3, 1965, pp. 2305-2312.

15. D. Bushnell, "Computer Analysis of Shell Structures," ASME Miscellaneous Papers, Vol. 1, 1969, 69-WA/PVP-13, pp. 1-16.

16. A. Kalnins and J.F. Lestingi, "On the Nonlinear Analysis of Elastic Shells of Revolution," Journal of Applied Mechanics, Trans. ASME, Vol. 34, Series E, 1967, pp. 59-64.

17. J.F. Lestingi and S. Brown, "Comparison of the Numerical Integration Technique and the Finite Element Method in the Analysis of Thin-Shell Structures," Second International Conference on Structural Mechanics in Reactor Technology, Vol. 5, Structural Analysis and Design, Part M: Methods for Structural Analysis; Reliability Analysis, Berlin, 1973, M 5/6, pp. 1-11.

18. J.F. Lestingi and L.E. Hulbert, "The Application of Linear and Nonlinear Thin Shell Theory in the Analysis of Formed and Welded Metallic Bellows," ASME Miscellaneous Papers, Vol. 5, 1972, 72-WA/PVP-3, pp. 1-9.

19. S. Timoshenko and S. Woinowsky-Krieger, Theory of Plates and Shells, 2d ed. (New York: McGraw-Hill, 1959), Chapter 16, Section 127.

20. Ibid..

21. Ibid., Section 128.

22. C.B. Biezeno and R. Grammel, Engineering Dynamics, Vol. II: Elastic Problems of Single Machine Elements (Princeton, N.J.: D. Van Nostrand, 1956), Part II, Section 13.

23. Ibid., Section 32.

24. R.W. Hamming, Numerical Methods for Scientists and Engineers, 2d ed. (New York: McGraw-Hill, 1973), Part II, Section 24.

25. M.J. Romanelli, "Runge-Kutta Methods for the Solution of Ordinary Differential Equations," Mathematical Methods for Digital Computers, A. Ralston and H.S. Wilf, eds. (New York: John Wiley & Sons, 1960), Vol. 1, pp.110-120.

26. System/360 Scientific Subroutine Package Version III, 5th ed. (New York: IBM, 1970).

27. E. Isaacson and H.B. Keller, Analysis of Numerical Methods, 5th ed. (New York: John Wiley & Sons, 1970), Chapter 8, Section 1.2.

28. K. Stange, op. cit..

29. R.A. Clark, T.I. Gilroy, and E. Reissner, op. cit..

30. H. Kraus, Thin Elastic Shells: An Introduction to the Theoretical Foundations and the Analysis of Their Static and Dynamic Behavior (New York: John Wiley & Sons, 1967), Chapter 4.

31. R.F. Dressler, "Hydraulic Resistance Effect Upon the Dam-Break Functions," Journal of Research of the National Bureau of Standards, Vol. 49, No. 3, 1952, pp. 217-225.

32. Lord Kelvin and P.G. Tait, Treatise on Natural Philosophy, Vol. 1, Part 2, 1883, p. 203.

33. K.O. Friedrichs and R.F. Dressler, "A Boundary-Layer Theory for Elastic Plates," Communications on Pure and Applied Mathematics, Vol. 14, 1961, pp. 1-33.

34. H. Kraus, op. cit..

35. H. Blasius, "Grenzschicten in Flüssigkeiten mit kleiner Reibung," Z. Math. u. Phys., Vol. 56, Part 1, 1908, pp. 1-37; Engl. trans., NACA TM 1256.

VITA

Nicholas Vasilios Kountouras was born in New York City on January 10, 1948. In September of 1964, Mr. Kountouras entered The City College of The City University of New York where he majored in mechanical engineering. Graduating cum laude with a Bachelor of Engineering degree in mechanical engineering in June of 1969, Mr. Kountouras was awarded The City College Engineering Alumni Graduate Scholarship. Receiving a Teaching Assistantship in September of 1969, Mr. Kountouras entered the Ph.D. Program in Civil Engineering at The City University of New York as a full-time student.

As a member of the instructional staff in the Civil Engineering Department of The School of Engineering of The City University of New York from 1970 to 1974, Mr. Kountouras continued his doctoral studies, and was awarded the Master of Engineering degree in civil engineering in February of 1971, and the degree of Doctor of Philosophy in civil engineering in September of 1974. Presently, Mr. Kountouras is Adjunct Assistant Professor of Civil Engineering at The City College of The City University of New York. Mr. Kountouras is a member of Pi Tau Sigma and Tau Beta Pi.